OPTIMIZATION OF THE RANDOM VIBRATION CHARACTERISTICS

OF VEHICLE SUSPENSIONS

by

ERICH KENNETH BENDER

S.B., Massachusetts Institute of Technology
(1962)

S.M., Massachusetts Institute of Technology
(1963)

M.E., Massachusetts Institute of Technology
(1966)

SUBMITTED IN PARTIAL FULFILLMENT

OF THE REQUIREMENTS FOR THE

DEGREE OF DOCTOR OF

SCIENCE

at the

MASSACHUSETTS INSTITUTE OF

TECHNOLOGY

June, 1967

Signature of Author .,
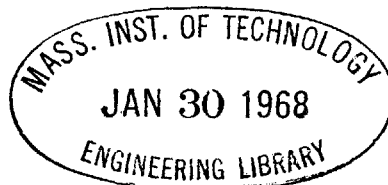   Department of Mechanical Engineering,
                    April 27, 1967

Certified by ......
                    / Thesis Supervisor,

Accepted by ....
           Chairman, Departmental Committee on Graduate
                    Students

OPTIMIZATION OF THE RANDOM VIBRATION CHARACTERISTICS

OF VEHICLE SUSPENSIONS

by

ERICH KENNETH BENDER

ABSTRACT

Some of the fundamental limitations and trade-offs regard-
ing the capabilities of vehicle suspensions to control random vi-
brations are investigated. The vehicle inputs considered are sta-
tistically described roadway elevations and static loading varia-
tions on the sprung mass. The vehicle is modeled as a two-degree-
of-freedom linear system consisting of a sprung mass, suspension
and an unsprung mass which is connected to the roadway by a spring.
The criterion used to optimize the suspension characteristics is
the weighted sum of rms vehicle acceleration and clearance space
required for sprung mass-unsprung mass relative excursions. Two ap-
proaches to find the suspension characteristics which optimize the
trade-off between vibration and clearance space are considered. The
first, based on Wiener filter theory, is used to synthesize the
optimum suspension transfer function. Mechanization of this function
is discussed. The second approach, using a computer parameter search,

consists of finding optimum parameter values for a fixed configuration suspension. Since the above optimization is without regard to the wheel-roadway interaction a constraint on vibration-clearance design charts is developed to insure that wheel hop is not excessive. The minimum rms force required to maintain adequate wheel-roadway contact is also established to provide an estimate for upper vehicle speed limitations. Some of the potential capabilities of a suspension which reacts to roadway irregularities before the vehicle reaches them are investigated. This preview control concept is studied for suspensions using Wiener filtering and for a suspension that may be easily mechanized. Finally, to illustrate the use of general design charts established in the first few sections of the thesis, a specific numerical example is carried out. The results of this thesis show that under certain circumstances active suspensions can substantially reduce the clearance space and sprung mass vibration levels over that obtainable by passive spring-shock absorber suspensions. For a given clearance space, preview control may be used to reduce vibration by as much as a factor of sixteen as compared with optimum non-preview suspensions.

Thesis Supervisor: Dean C. Karnopp
Title: Associate Professor of Mechanical Engineering

ACKNOWLEDGMENT

TABLE OF CONTENTS

LIST OF ILLUSTRATIONS

NOMENCLATURE

a $k_s/(k_v + k_s)$

A   Roadway spectral density amplitude

B   Coefficient (Appendix A)

c   Damping coefficient

C   Coefficient (Appendix A)

D   Coefficient (Appendix A)

E   Coefficient (Appendix A)

f_s Sprung mass natural frequency $(\omega_s/2\pi)$

f_u Unsprung mass natural frequency $(\omega_u/2\pi)$

F   Loading variation, Force

F_s Suspension Force

$\bar{F}$ $F/8\pi^2 \alpha M \sqrt{AVf_u^3}$

g   Gravitational constant

h   Suspension clearance space

H   Transfer function

I   Coefficient (Appendix A)

j $\sqrt{-1}$

k   Spring rate

k_{01} Unsprung mass spring rate

k_{12} Sprung mass spring rate

k_s Gain of preview controller

k_v Preview suspension spring rate

K   Feedback gain

L   Preview distance

m   Mass of unsprung mass

M   Mass of sprung mass

n   Constant

P   Penalty function

r   Mass ratio m/M

s   Laplace operator

t   Time

T   Preview time

V   Velocity

W   Synthesized suspension transfer function

W_p Preview synthesized suspension transfer function

W_w Synthesized transfer function for minimum rms suspension force

x,X   Roadway elevation; constant

x_s Roadway elevation at preview sensor

x_v Roadway elevation at vehicle

y,Y   Sprung mass position; constant

y_s Response of y to a step in x

z,Z   Unsprung mass position

α Clearance factor

β $\rho\omega_u^2$

γ ω_s/ω_u

$\Upsilon(t)$ Inverse transform of $\Gamma(s)/\Delta^-(s)$

-9-

Γ Synthesizing function

δ $z-y$

δ_o Static unsprung mass deflection due to vehicle weight

δ_p $x_v - y$

δ_w $z-x$

Δ Synthesizing function

ε Small quantity

ζ Damping ratio $c/2\sqrt{k_{12}M}$

ρ Lagrange multiplier or weighting factor

τ $\sqrt{2}\,\rho^{1/4}$

ϕ s/ω_u; s/ω_n in Section 5

Φ Power spectral density

ψ $\rho^{1/4}s$

ω Frequency

ω_o Spectrum level-off frequency

ω_n Preview suspension natural frequency $\sqrt{(k_v + k_s)/M}$

ω_s Sprung mass natural frequency $\sqrt{k_{12}/M}$

ω_u Unsprung mass natural frequency $\sqrt{k_{01}/m}$

Ω Wave number (rad./ft.)

SECTION I

INTRODUCTION

1.1 Trends in Ground Transportation

Present trends in ground transportation combine to make the suspension design problem ever more severe. Tendencies toward higher speed and lighter weight vehicles to travel over roadways which should have minimal maintenance and construction costs make ride (passenger comfort) and maneuverability requirements increasingly difficult to meet. Conventional spring and shock absorber suspensions become less and less practicable as increased demands are made on vehicle performance. It seems appropriate then to discuss briefly some of the ways in which speed, weight, and roadway maintenance requirements affect suspension characteristics and to outline the primary functions of a suspension system and the methods currently taken to meet such requirements. Once some of the significant problem areas have been delineated, several fundamental limitations and trade-offs involved in passive and active suspension system design will be studied in some depth. The emphasis of this thesis will be on optimization of the random vibration characteristics of vehicle suspensions.

Increasing vehicle speed for a given vehicle-roadway combination generally intensifies vehicle vibration which in turn downgrades both ride and maneuverability. It is fairly obvious, and has been shown empirically [1] *, that ride becomes worse with increasing vibration. The interaction between vibration and maneuverability or

---
*
Numbers in brackets designate references at the end of this thesis.

handling is a subject which, to the author's knowledge, has not received much study. Nevertheless, we can gain some qualitative insight into the vibration effects on maneuverability by considering an automotive vehicle turning on a rough surface. If the vibration level is sufficiently high, i.e., the road roughness and vehicle speed are great enough, the wheel-ground normal contact force multiplied by the sideways friction coefficient will frequently become less than the lateral centrifugal force. Thus considerable side slip will occur during these intervals resulting in poor steering response and increased tire wear.

Vibration caused by surface roughness is in fact one of the fundamental speed limitations to a great variety of vehicles. Ground unevenness often constrains off-the-road vehicles to a mere 5 mph [2], whereas vibrations of conventional rail trains may cause considerable passenger discomfort at a train speed of about 100 mph [1].

A desire for light-weight vehicles usually goes along with high acceleration and cruising speed requirements. As a vehicle body is made lighter, the supporting springs must be made correspondingly weaker in order to maintain roughly the same vibration isolation quality. However, softer springs result in larger deflections due to cargo variations. Thus a conventionally suspended light-weight vehicle must have a larger sprung mass (vehicle body)-unsprung mass (wheels + axles) clearance space and correspondingly higher center of gravity than a heavy vehicle. This, in turn, often results in undesirably larger roll angles due to cornering.

There is a trade-off between suspension and roadway quality for a given ride. A sophisticated suspension system for a vehicle

traveling over a rough roadway is generally required to provide passengers with a comfortable vibration environment. On the other hand, a simple suspension is usually adequate for a vehicle traversing a very smooth, well maintained, and correspondingly costly roadway. The Japanese Tokaido Line, for example, can operate trains at 160 mph only as a result of special roadbed construction and maintenance efforts [3, 4]. Consequently, there is an economic impetus to investigate suspension systems with increasingly better vibration isolation capabilities in order to minimize roadway capital and upkeep costs.

1.2 Suspension Requirements

Broadly speaking, the single requirement of a vehicle suspension is to control the vehicle motion in such a way as to maximize passerger comfort as the vehicle travels from point of origin to its destination. While this statement is probably valid, it is more useful in designing suspensions to be more specific. Thus, although suspensions must meet a variety of particular requirements according to specific system needs, the four distinct functions that are common to virtually all vehicle suspension systems are guidance, body force vector alignment, force insensitivity, and vibration isolation. The first, and perhaps most obvious, is guidance. A suspension must provide vehicle support and directional control. In order to perform the latter, wheel-ground contact must be firm or, as previously mentioned, considerable side slip may occur during turning maneuvers. Secondly, a suspension should align the least sensitive cargo axis (Cargo is used in the broad sense to include passengers.) with the resultant body force vector (arising from acceleration plus gravity). Since this axis is parallel to the spine of a seated or standing passenger [5, 6],

the vehicle should roll into a turn, as does a motorcycle. It should
not lean out of a turn, as is the case for most automotive and rail ve-
hicles. Thirdly, an ideal suspension is insensitive to externally ap-
plied forces. Thus cross winds, cargo weight variations, and contact
forces among various cars in a train should result in a minimum of ve-
hicle vibration. Finally, a suspension should provide maximum vibration
isolation; that is, motion of the cargo compartment resulting from
ground roughness should be minimal.

It is virtually impossible to optimize all of the four sus-
pension functions of guidance, body force vector alignment, force in-
sensitivity, and vibration isolation with a passive conventional spring-
shock absorber suspension due to the mutually antagonistic nature of
some of these functions. Guidance, as we shall see in Section 4, re-
quires a suspension that is neither very stiff nor very flexible in the
vertical direction in order to maintain good wheel-roadway contact.
Proper alignment of a passenger's spinal axis with the body force vector
cannot be achieved in a maneuvering conventional automotive or rail ve-
hicle where the roll axis is below the center of gravity. Consequently,
suspensions are often made fairly rigid to minimize roll. Force insen-
sitivity calls for a stiff suspension, whereas vibration isolation de-
mands a soft suspension. Thus each suspension requirement is only par-
tially met in practice. Furthermore, a suspension designer must con-
sider all of the suspension functions simultaneously, or optimization
of one may lead to unsatisfactory performance of another.

1.3 State of the Art

In an effort to build suspensions that will carry out the four
suspension functions in the best practical manner for any given set of

vehicle performance requirements, suspension designers have incorporated a variety of passive and active systems. Passive devices tend to have undesirable dynamic side effects while active systems have not generally found widespread use due to their inherent complexity and consequent high cost. A brief review of some current suspension system problems and practices pertaining to each fundamental suspension function will be given to provide a base for the study of suspension control of vibration.

Guidance is often a significant problem in the design of high performance automobiles and of rail vehicles that use flanged wheels. The suspensions of automotive vehicles with good handling qualities are designed to minimize side slip by providing proper suspension vertical stiffness and damping, as well as controlling changes in weight distribution and wheel camber angles resulting from cornering [7]. Rail vehicles with flanged wheels often exhibit severe hunting or self excited lateral oscillations. A considerable effort has been devoted to this problem over several decades [8 - 12].

A variety of passive and active roll control devices has been used to align the passenger spinal axis with the gravitational plus centripetal body force vector. Most common of these is the anti-roll bar. The base of this U-shaped bar is placed in a journal fastened to the underside of a car, parallel to and forward of the wheel axles in such a way that it has only rotational freedom of motion. The end of each leg of the U is pivoted to a point on the axle near the wheel. Thus the wheels are constrained to move together in the vertical direction; roll stiffness is consequently quite high. The principal disadvantages of this coupling is a degradation in vibration isolation. Furthermore, the

anti-roll bar provides only limited roll control. It prevents roll out of a turn but does not permit the vehicle to lean into a turn.

A passive roll control device, with somewhat superior performance to the anti-roll bar, which has been built for a high speed rail train [13] essentially consists of a linkage which places the roll center above the vehicle center of gravity. Thus proper banking is achieved with no reduction in vibration isolation. The principal disadvantage of this system is that as the car's center of gravity swings toward the outside of a turn the train could overturn more easily than if it were only equipped with an anti-roll bar.

Several types of active roll control servomechanisms have also been built and tested. A tricycle has been devised that leans into turns either by steering and center of gravity control like an ordinary motorcycle or underactive pendulous roll control [14]. A hydraulic vibration and roll controller for automotive types of vehicles has also been built and tested [15, 16]. This system automatically rolls the car body until the component of the gravitational vector along the lateral body fixed axis nulls the radial acceleration inertial force. The performance of these systems is, for all practical purposes, uncoupled from the other three suspension functions.

One of the most significant vehicle force disturbance generally arises from cargo weight variations. The suspension clearance needed for different static deflections corresponding to loaded and unloaded conditions of a simple spring-shock absorber suspension makes it necessary to place the vehicle center of gravity higher than would be necessary for a constant weight car body. It is, however, desirable to build

the vehicle as low to the ground as possible from a volume economy point of view and to minimize rolling and pitching moments. A simple remedy to this loading variation problem which has received some attention in the automotive industry [17, 18] is to provide an automatic height controller which applies a force to the car body proportional to the integral of the sprung mass-unsprung mass relative displacement. The force thus generated essentially balances any cargo variation without requiring clearance space above that necessary for dynamic excursions.

A great deal has been done to improve the vibration isolation function of vehicle suspensions. An almost endless list of combinations of automotive suspension geometries, spring, and damper designs could be made. One of the very few active vibration isolators is the aforementioned hydraulic vibration and roll control system [15, 16]. A force proportional to sprung mass acceleration is applied between the sprung and unsprung masses with a dynamic effect similar to increasing the vehicle body mass. Thus the vehicle natural frequency is lowered resulting in better roadway roughness filtering without the necessity of decreasing spring stiffness.

1.4 Optimization of Suspension Vibration Characteristics

There are requirements for research and development in virtually every aspect of suspension system design. The relationship between vehicle maneuverability and the wheel-roadway interaction is not well understood. Hunting is still a problem in rail vehicles. Prototype roll control devices have been built but still require further development. Aerodynamic forces cause noticeable motion of many types of automobiles.

Of course, isolation of passengers from vibration caused by roadway roughness is still a significant problem area.

Fortunately some of these problem areas may be studied almost independently of the others. Although there has been much development of vehicle suspensions to provide good vibration characteristics, there is a noticeable absence in the open literature of studies to determine fundamental vibration control capabilities of suspensions. Some related work has been done on the optimization of elementary vibration isolators [19, 20] and on optimizing the transient response of shock isolation systems [21, 22]; however, these studies do not apply directly to suspension vibration problems. In view of these considerations, this thesis will be concerned with some basic limitations of suspensions to control vehicle and wheel vibrations.

Until one devotes some thought to the fundamental limitations and hence optimum design of suspensions, it is not obvious exactly what a suspension should do with regard to vibration control. Initially one suspects that an ideal suspension would completely isolate the vehicle passenger compartment from variations in roadway height. This, however, would require a sprung mass-unsprung mass clearance space at least as great as the elevation difference between the lowest and highest points of the roadway over which the vehicle is to travel. It becomes evident that, for practical situations, the vehicle must move vertically over at least some hills and bumps. Just how much of this vertical vibration the vehicle must undergo depends on the amount of clearance space provided. The trade-off between vibration and clearance space is fundamental to every surface following vehicle ranging from conventional automobiles, trains, and off-the-road trucks and tractors to hydrofoil ships, ground

effect machines, and low flying terrain following military aircraft. The optimization of this trade-off will be central to the vibration control study which follows.

The scope of this study cannot encompass all of the vibration and dynamic aspects of vehicle suspensions. Vehicles are generally multi-degree-of-freedom, flexible, non-linear, three-dimensional systems subject to a variety of vibrational environments resulting in many output variables of interest. Rather than trying to incorporate all of these details which, at best, would result in a simulation of a particular vehicle, a simple dynamic model representative of vehicles that have unsprung masses (as contrasted to most ground effect machines, for example,) will be chosen. Thus, in Section 2 the environment, a vehicle dynamic model, and a mathematical formulation of criteria and constraints will be discussed. Section 3 will present methods of optimizing the vibration isolation characteristics of vehicles excited by random roadway disturbances and cargo weight variations. The problem of guidance will receive some attention in Section 4 where wheel-roadway dynamics will be discussed. Since a vehicle-roadway combination is one of the few systems in which the input can easily be known in advance, the benefits of a suspension system that can use such preview information, compared with one that cannot, will be investigated in Section 5. Use of the optimization design charts and procedures derived in the first five sections will be illustrated by an example in Section 6. Finally, Section 7 will summarize results as well as present conclusions and recommendations for further study.

SECTION 2

SYSTEM MODEL AND PERFORMANCE CRITERIA

Vehicles are generally very complicated dynamical systems which interact with their environment in a variety of ways. There are many response variables of interest, several of which still cannot be quantitatively measured. In order to study such a system, particularly with the intent of optimizing a design aspect, it is necessary to describe mathematically the important inputs, the vehicle dynamics, and measures of performance. In each of these descriptions some simplifications will be made to make the treatment tractable and to obtain meaningful quantitative results; however, the input, model, and criteria established in this section are felt to be representative of a broad range of vehicle systems. The results of this thesis should have general applicability and form a starting place for specific vehicle design.

2.1 Vehicle Disturbances

Four principal vehicle disturbances are body forces, aerodynamic forces, loading variations, and roadway roughness. Body forces and turbulent winds usually result in low frequency (0 - 5 Hz) rolling and pitching moments which should be adequately compensated for by some form of roll and pitch control device like those previously mentioned [13 - 16], for example. Wind gusts also cause yawing moments which may cause significant steering problems [23 - 25]. In addition to altering vehicle dynamics, loading variations place a requirement on clearance space. An amount of space equal to the maximum loading difference divided by the zero frequency suspension stiffness must be added to that needed for dynamic excursions unless automatic height control is provided.

Static loading variations range from about 15% of empty vehicle weight
for railroad passenger cars to a rated 500% for large earth haulers [26].
Roadway roughness is the disturbance which tends to make the largest
contribution to passenger discomfort. Therefore, let us consider a quan-
titative description of the statistics of roadway elevations.

Elevation spectra and profiles for a great variety of surfaces
have been measured [27 - 30]. Mean square elevation spectra for rail-
roads, aircraft runways, highways, a cow pasture and a very rough Bel-
gium block test track are shown in Figure 1. Most of these spectra were
computed from elevation data measured statically with a surveyor's level,
rod, and tape. A typical runway profile shown in Figure 2 [27] illustrates
the random nature of these inputs.

An analytical description of input spectra is necessary to fa-
cilitate response calculations. Boundary lines with a minus two slope
have been shown in Figure 1 to indicate the general nature of ground
spectra. It is remarkable that all of the spectra shown, ranging from
the smoothest rail through cow pastures to an extremely rough test track
may be approximated very well by a straight line fit of the form A/Ω^2
where the roughness parameter A has the extremely large range of 10^4
and where Ω is the spacial frequency or wave number. Thus, for purposes
of analyses the roadway spectrum is given by

$$\phi_{xx}(\Omega) = \frac{A}{\Omega^2} \tag{1}$$

or, as a time function, the spectrum becomes [31, 32]

$$\phi_t(\omega) = \frac{AV}{\omega^2} = \frac{AV}{s^2} \tag{2}$$

where s is the Laplace operator. Good results have, in fact, been obtain-
ed by using the A/Ω^2 approximation in analyzing the dynamics of a Boeing

WAVELENGTH , FT
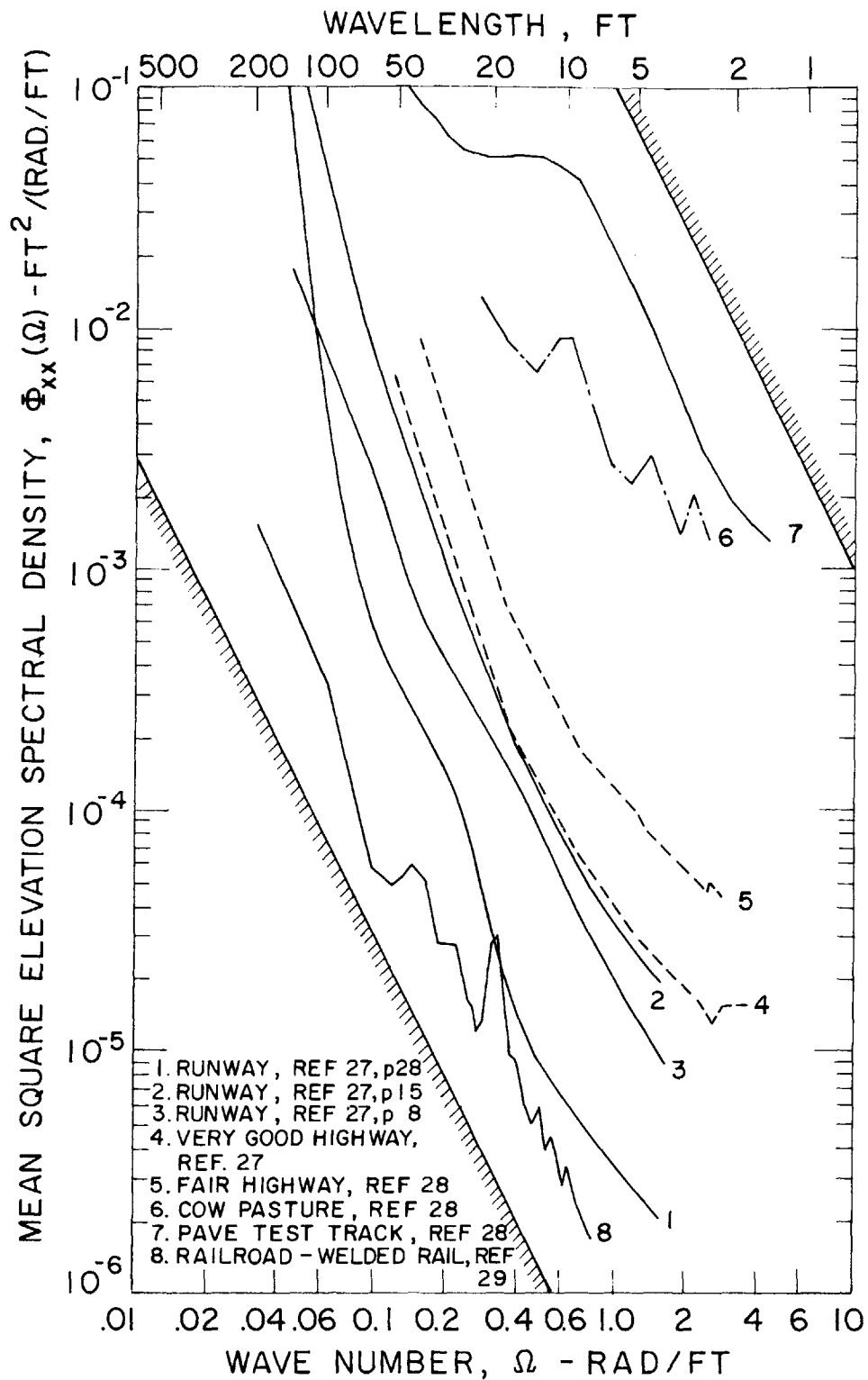
Figure 1. Representative Roadway Mean Square Elevation Spectral Densities
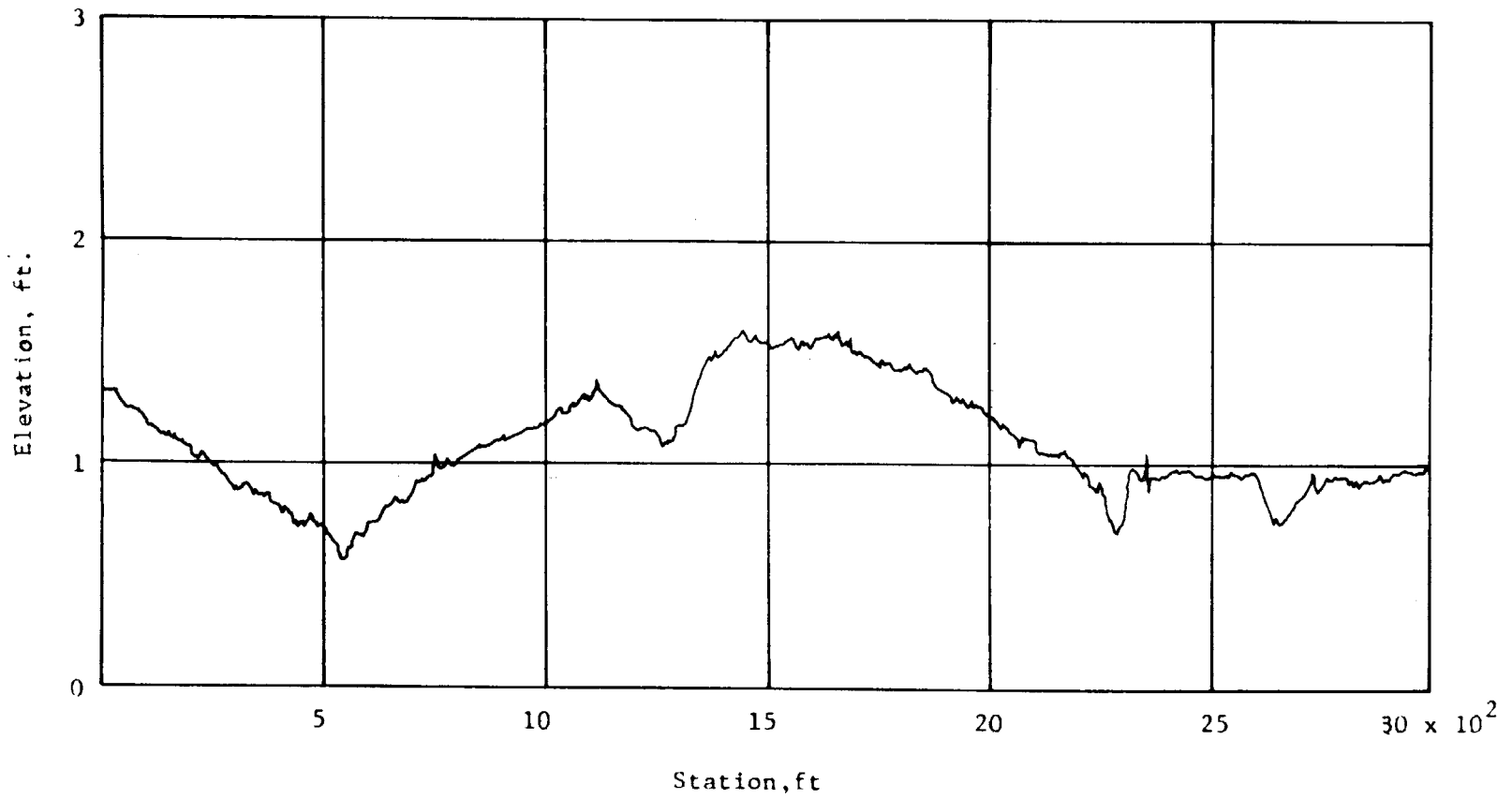
Figure 2. Typical Runway Profile

B-29 airplane [33]. In order to be confident that results are valid,
however, they must be only weakly dependent on the spectrum outside of
the measured range. At the low frequency end, A/Ω^2 becomes infinite,
whereas elevation spectra must level off due to the finite height of
roadways. This apparently occurs at a frequency below that which has
thus far been measured. Since the high frequency portion of the road-
way spectrum approximation extends mathematically to infinity, the num-
erator of the transfer function relating roadway displacement to a re-
sponse variable must be of the same order as, or lower than, that of the
denominator so that the computed mean square response will not be infinite.

Runways and highways are much more rigid than primary (wheels)
and secondary (spring-shock absorber) suspensions used to support vehi-
cles traversing these roadways. One can, therefore, assume, for the
purposes of examining vehicle dynamics, that such roadways are perfectly
rigid and the profiles, measured statically under no-load conditions, do
in fact represent the dynamic suspension disturbance. When suspension
system stiffness is not significantly less than that of the guideway, as
perhaps in the case of railroads where wheels are less elastic than rail-
roadbed configurations, it becomes necessary to know roadway stiffness
as a function of distance along the roadway. A perfectly smooth sur-
face with rigid and flexible regions would appear rough to a moving ve-
hicle.

2.2 **Vehicle Dynamics**

The vehicle model chosen for this study is shown schematically
in Figure 3. The rigid mass M represents the vehicle body or sprung
mass. The unsprung mass consisting of wheels, axles, etc., is idealized
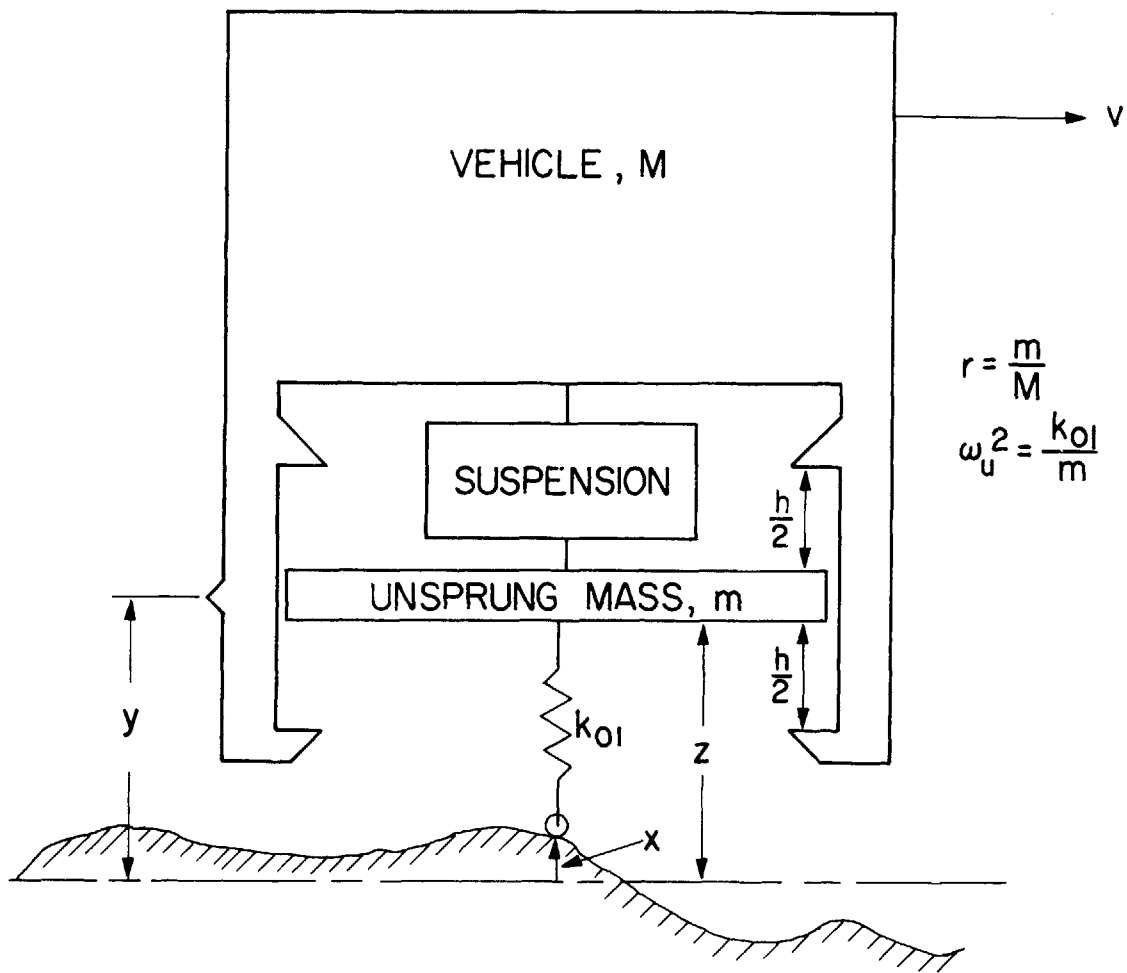
Figure 3. Vehicle - Roadway Configuration

as a mass m supported by a linear spring with stiffness or spring rate k_{01}. The suspension shown between the sprung and unsprung masses is the focal point for this thesis. The questions that we will try to answer are 1) What should the suspension elements be in order to optimize suspension vibration characteristics? and 2) If the elements are specified, what should their parameter values be for optimum performance?

2.3 Criteria and Constraints

Optimization of suspension system design must be based on pre-established performance criteria and constraints. Measures of random vibration that are useful in studying the trade-off between vibration and sprung mass-unsprung mass clearance space, as well as wheel-roadway dynamics, need to be established. Other design considerations, such as reliability and maintainability or the quantitative evaluation of capital and operating costs, are applicable to later, more detailed design stages than to this basic study.

Human discomfort should be minimized when passenger vehicles are designed. Vibration is probably the only source of discomfort which can be controlled by the suspension system. However, broad-band vibration in the audible and sub-audible frequency range usually makes the largest contribution to passenger discomfort. There are basic differences in both effects and mechanics between low frequency vibrations which shake all or part of the human body and high frequency acoustical vibrations which cause auditory annoyances. Hence, problems in each frequency range are quite different and may usually be treated separately, superposing the end results. This study will consider only the low end of the vibration spectrum.

Unfortunately, an accurate quantitative measure of human discomfort to random vibration is not currently available. Most investigators in the field of human vibration sensitivity have carried out their experiments by sinusoidally vibrating subjects in seated, standing, or lying positions on rigid shake platforms. Most data are presented as curves of constant discomfort on acceleration versus frequency plots [34 - 39]. Generally an increased sensitivity appears in the neighborhood of 5 - 10 Hz while sensitivity decreases above 100 Hz. The relation of these data to the realistic situation where a passenger is seated on a soft chair with his feet on a carpeted floor and vibrated in a random way is indeed tenuous. One might be tempted to multiply the seat acceleration spectrum by a weighting factor based on frequency sensitivity curves and use the rms of this product as a measure of discomfort. Since this approach is not valid in determining acoustical discomfort [40], there is no reason to believe it should work for discomfort arising from low frequency vibrations. A small group of researchers have suggested a correlation between power input to a passenger and discomfort [41 - 43]. This theory, while promising, is based on one set of data for physically fit young males that have been subjected to rather severe vibration environments. Therefore, basing a discomfort criterion for a general vehicle study for these results does not seem altogether justifiable.

Rather than trying to hypothesize a discomfort weighting function of unknown validity that would account for increased sensitivity in the neighborhood of 5 - 10 Hz or base a study on a preliminary "absorbed power" criterion, it was thought meaningful and advisable to use rms acceleration as a measure of vibration within the scope of this study. This

simple measure weighs all frequencies equally and seems adequate for the broad, fundamental study attempted in this thesis. The only frequency range where equal acceleration weighting differs greatly from sinusoidal response curves might be above 100 Hz in the acoustical region. This does not pose a problem since the spectral content for the systems considered in this thesis lies almost entirely in the sub-audible range.

One of the important suspension design parameters is the clearance space h between the sprung and unsprung masses. It is desirable to make this space as small as possible from a volume economy point of view and to minimize rolling and pitching moments arising from vehicle maneuvers. On the other hand, it is necessary to provide enough clearance for static deflections due to vehicle loading variations F and for dynamic excursions arising from vehicle motion over a rough road. Figure 4 shows that the sprung mass is centered in the clearance space at half of the expected maximum load. The sprung mass equilibrium position will move up or down a distance F/2k under full load and no load conditions where k is the zero frequency suspension stiffness. (An automatic height control system makes k infinite.) The remaining clearance space h/2 - F/2k at each end of the static excursion range is required for dynamic excursions.

Since dynamic excursions of the sprung and unsprung masses relative to each other will occasionally be large as a result of the random nature of roadway inputs, the probability of bottoming can only be made infrequent, not zero. There are two generally accepted means of computing bottoming occurrences. The first is to determine the expected frequency at which the dynamic relative excursion would exceed the

VEHICLE , M

DYNAMIC EXCURSION
PROBABILITY DENSITY

$h/2 - F/2k$

δrms

m

EQUILIBRIUM POSITION
FOR LOAD F

$h/2$

UNSPRUNG MASS

EQUILBRIUM POSITION
FOR LOAD F/2

m

EQUILBRIUM POSITION
FOR NO LOAD

$h/2$

$h/2 - F/2k$
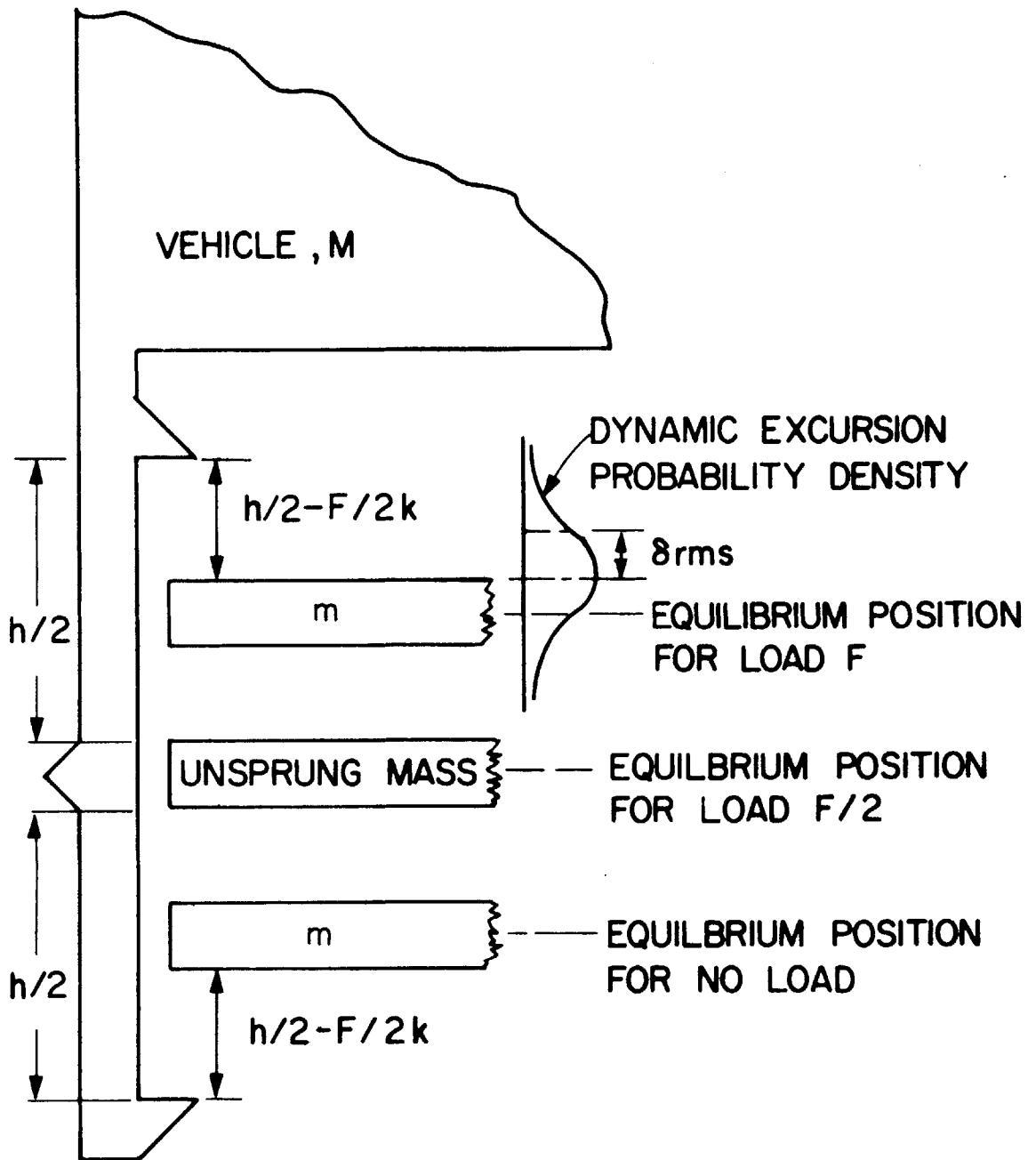
Figure 4. Suspension Deflection Quantities

allowed clearance space if no limiting bumpers were present [44, 45]. The second is to calculate the proportion of time the dynamic excursion would be greater than the clearance space, again in the absence of bumpers [46]. The implication in each method is that bottoming occurs so rarely that the system behavior is essentially unaltered by the excursion limits. This assumption seems well founded for our purposes. Since both schemes appear to be equally valid, the latter will be used for this study, mainly for reasons of convenience. Bottoming can be made infrequent by allowing clearance space needed for dynamic excursions equal to several times (by a factor of α) the rms relative dynamic displacement. Thus

$$h/2 - F/2k = \alpha\delta_{rms} \tag{3}$$

Since there are indications that the roadway elevation distribution is gaussian [47], the parameter α should be about 3 to keep the sprung mass from bottoming at least 99.9% of the time. Nevertheless, bottoming will occasionally occur so a smoothly increasing stiffness near excursion limits or a similar approach is required in practice to provide adequate shock isolation.

The constraint placed on suspension systems to be studied here is that the wheel remain in contact with the ground nearly all of the time. This is necessary to provide proper guidance and to minimize wear [48, 49]. By comparing the rms dynamic displacement of the wheel center with respect to the roadway with the static deflection due to the vehicle weight, it is possible to determine the degree of wheel-roadway contact. If the rms dynamic excursion is less than 1/3 or 1/4 of the static deflection, then we can assume the wheel stays on the road a sufficient proportion of time. On the other hand, if the rms wheel-road displacement is greater than about 1/3 to 1/2, considerable wheel hop will probably occur.

SECTION 3

OPTIMUM VIBRATION CONTROL

Two approaches to linear system design will be used to deter-
mine systems which are optimum with respect to the vibration-clearance
trade-off. The first method, developed from work begun by Wiener [50]
and pursued by others [51], consists of synthesizing a vehicle suspen-
sion system transfer function. By considering variables that are easily
measured and filtered, one may subsequently devise a hardware configura-
tion for active systems that will perform according to the optimum syn-
thesized suspension characteristics. Although this approach leads to
a system that is the absolute optimum for the linear model chosen, the
hardware mechanization of the optimum transfer function might be unduly
complicated. Hence it is desirable to see how well one can do with a
less sophisticated system. The second method, which is essentially
analytical, is used to determine the optimum parameter values of any
passive or active linear suspension system whose configuration (trans-
fer function) and input statistics are specified.

The steps involved in synthesizing or analyzing the suspen-
sion systems which optimize the vibration-clearance trade-off are simi-
lar. First, a penalty or cost function, P, is formed which is a linear
combination of the rms acceleration, $\ddot{y}_{rms}$, and clearance space, h, re-
quired for dynamic plus static sprung mass-unsprung mass relative dis-
placement. Thus

$$P = \rho\ddot{y}_{rms} + h = \rho\ddot{y}_{rms} + 2\alpha\delta_{rms} + F/k \qquad (4)$$

where ρ is a weighting factor of Lagrange multiplier.

When the synthesis is used, F/k will be neglected for two reasons. First, there will probably be sufficient flexibility in choosing parameters so that we may make k arbitrarily large. (This assumption is borne out later.) Secondly, any sophisticated suspension will no doubt employ an automatic height controller which will make the steady state displacement due to static force variations zero.

The weighting factor ρ is used to generate vibration-clearance trade-off curves. The procedure is to choose a value of ρ and compute the system parameters in such a way that the sum of clearance space plus ρ times the rms acceleration minimizes the penalty functional P. At the computed minimum value of clearance, $\ddot{y}_{rms}$ is a minimum and vice versa. By varying ρ a locus of such points generates an optimum trade-off curve.

3.1 Synthesis of Optimum Suspensions

3.1.1 Derivation

An optimum suspension transfer function is synthesized by essentially expressing $\ddot{y}_{rms}$ and δ_{rms} in Equation (2) in terms of the roadway input spectrum, transfer functions relating δ to the roadway input and an unknown transfer function W(s) defined (see Figure 5) in terms of the Laplace operator s as

$$W(s) \overset{\Delta}{=} \frac{\ddot{Y}}{X} (s) \tag{5}$$

The suspension is restricted to one which applies forces only between the sprung and unsprung masses, thereby eliminating from consideration suspensions that might use aerodynamic control surfaces, extra masses as vibration absorbers, and so forth. Starting with the model shown in Figure 3, the equations of motion for the unsprung mass m and
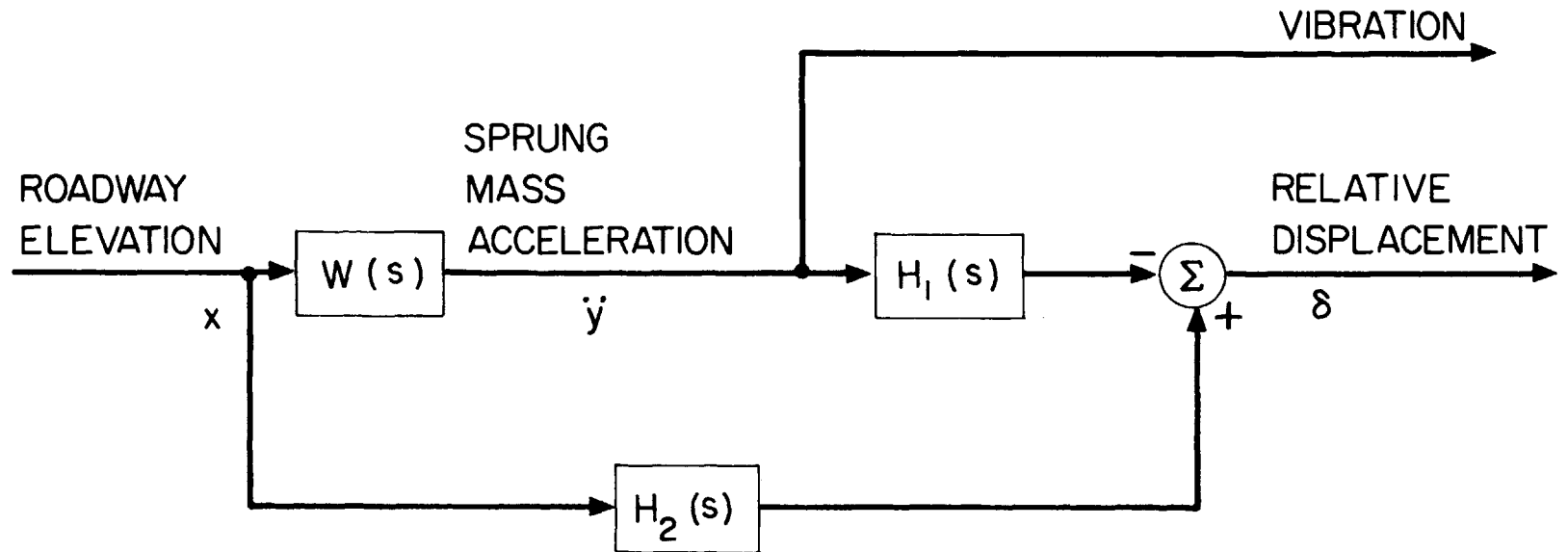
Figure 5. Block Diagram Showing the Relation of Vibration and Relative
Displacement to the Roadway Elevation

-33-

sprung mass M are

$$-F_s + k_{01}(X-Z) = ms^2Z$$

$$F_s = Ms^2Y \tag{6}$$

The force, F_s, exerted by the suspension on each mass may be eliminated from these equations. Noting that $\ddot{Y}(s) = W(s)X(s)$ and $\delta = z - y$, the relative displacement $\delta(s)$ is

$$\delta(s) = \left\{ \frac{1}{(\frac{s}{\omega_u})^2 + 1} - \frac{[(1+1/r)(\frac{s}{\omega_u})^2 + 1]}{s^2[(\frac{s}{\omega_u})^2 + 1]} W(s) \right\} X(s) \tag{7}$$

where $\omega_u = \sqrt{k_{01}/m}$ is the unsprung mass natural frequency and r is the mass ratio m/M. Upon comparing Equation (7) with the block diagram in Figure 5, we see that

$$H_1(s) = \frac{(1+1/r)(\frac{s}{\omega_u})^2 + 1}{s^2[(\frac{s}{\omega_u})^2 + 1]} \tag{8}$$

$$H_2(s) = \frac{1}{(\frac{s}{\omega_u})^2 + 1} \tag{9}$$

The solution for the optimum $W(s)$, found by the variational calculus (see Reference 51, Chapter 7, for details), is

$$W(s) = \frac{\left[\frac{\Gamma(s)}{\Delta^-(s)}\right]_+}{\Delta^+(s)} \tag{10}$$

where

$$\Gamma(s) = 2\pi H_1(-s)H_2(s)\Phi_t(s) \tag{11}$$

$$\Delta(s) = 2\pi[H_1(s)H_1(-s) + \rho]\Phi_t(s) \tag{12}$$

The plus and minus superscripts of Δ (s) in Equation (10) indicate that only poles and zeros of Δ (s) in the left-half plane and right-half plane, respectively, are to be retained. Similarly, the plus subscript outside the bracketed term in Equation 10 designates the component of that term that has all its poles in the left-half plane. This spectral factorization is performed to insure that W(s) is physically realizable. From Equations (2), (8), and (12), the expression for Δ is

$$\Delta(\phi) = \frac{2\pi AV}{\omega_u^6} \frac{\beta\phi^8 + 2\beta\phi^6 + [\beta + (1 + 1/r)^2]\phi^4 + 2(1 + 1/r)\phi^2 + 1}{\phi^6(\phi^2 - 1)^2} \qquad (13)$$

where

$$\phi = \frac{s}{\omega_u} \qquad ; \qquad \beta = \rho\omega_u^2$$

The numerator and denominator of the right-hand side of the above equation for $\Delta(\phi)$ are factored to form $\Delta^-(\phi)$ and $\Delta^+(\phi)$. Since the numerator is of eighth order, its roots are evaluated numerically on a digital computer. A partial fraction expansion of $\Gamma(s)/\Delta^-(s)$ is made, and only terms with poles in the left-half plane are retained. Finally, the optimum transfer function is found. (See Appendix A for the derivation of the following expression and the evaluation of its parameters.)

$$W(\phi) = \frac{\omega_u^2\phi^2[(B + 1)\phi^2 + C\phi + 1]}{\sqrt{\beta}\ \phi^4 + 2\sqrt{\beta}\ D\phi^3 + \sqrt{\beta}\ E\phi^2 + 2\sqrt{\beta}\ I\phi + 1} \qquad (14)$$

The optimum vibration-clearance trade-off curve is determined by computing the rms accelerations and relative excursions corresponding to the above expression for $W(\phi)$ for a range of weighting factors, ρ. The general equation for finding the rms of a response variable C to an

input R is

$$C_{rms} = \left[\frac{1}{j} \int_{-j\infty}^{j\infty} \frac{C}{R}(s)\frac{C}{R}(-s)\Phi_{RR}(s)ds \right]^{1/2} \tag{15}$$

where $\Phi_{RR}(s)$ is the power spectral density of R. If C/R (s) multiplied by the factor of $\Phi_{RR}(s)$ whose roots lie in the left-half plane is a ratio of polynomials of order 10 or less, $C_{rms}^2 / 2\pi$ may be found tabulated [51] in terms of the parameters of C/R (s) and $\Phi_{RR}(s)$.

From Equations (2), (14), and (15) the expression for the rms acceleration $\ddot{y}_{rms}$, non-dimensionalized by the roadway roughness A, vehicle speed V, and unsprung mass natural frequency in Hz, f_u, is

$$\frac{\ddot{y}_{rms}}{4\pi^2 \sqrt{AVf_u^3}} = \left[\frac{1}{2\pi j} \int_{-j\infty}^{j\infty} \frac{W(\phi)}{\phi} \cdot \frac{W(-\phi)}{-\phi} \cdot d\phi \right]^{1/2} \tag{16}$$

With the help of tabulated algebraic expressions for the above integral [51], the acceleration becomes

$$\frac{\ddot{y}_{rms}}{4\pi^2 \sqrt{AVf_u^3}} = \left\{ \frac{(B + 1)^2(2\sqrt{\beta} EI - \sqrt{2} D) + (C^2 - 2B - 2)2\sqrt{\beta}I + 2\sqrt{\beta}D}{8\beta (\sqrt{\beta} DEI - D^2 - \sqrt{\beta} I^2)} \right\}^{1/2} \tag{17}$$

where B, C, D, E, and I are evaluated in Appendix A. Similarly, (see Appendix B) the clearance space $h = 2\alpha\delta_{rms}$ is given by

$$\frac{h}{2\alpha} \sqrt{\frac{f_u}{AV}} = \left\{ \frac{\sqrt{\beta} - (B+1)(1+1/r)^2 2D + [2\sqrt{\beta} D - C(1+1/r)]^2 2\sqrt{\beta}(DE-I)}{8(\beta DEI - \sqrt{\beta}D^2 - \beta I^2)} \right\}^{1/2} \tag{18}$$

The vibration-clearance space trade-off for the optimum synthesized suspension corresponding to a given mass ratio r is found as follows:

Choose a value of β, compute B, C, D, E, and I (see Appendix A) and then
find the rms acceleration and the clearance space from the above two
equations. Increment β and repeat the whole procedure. The points on a
vibration-clearance plot thus found define a curve which is a lower
bound to the performance of suspensions which are linear, do not use
preview information, and apply equal forces to the unsprung and sprung
masses. This optimum trade-off curve is shown for $r = 0.1$ in a design
chart (Figure 6) along with curves for passive, fixed configuration
systems. Before we discuss these other curves in Section 3.2, let us
consider how the suspension described by Equation (14) could be mechan-
ized.

3.1.2 Mechanization of Synthesized Suspension

There are various control system configurations with transfer
functions which can be made to match the transfer function of Equation
(14) which has been mathematically synthesized. The procedure followed
here is to consider variables which are easily measured and filtered to
generate a control force command signal (see Figure 7). Accelerometers
may be used to measure unsprung and sprung mass accelerations. Each
signal may be filtered by a function of the form $(K_a + K_v/s)$ and then
summed to form a command signal. Amplifier and servomechanism dynam-
ics need to be considered in a specific design study but are neglected
in this preliminary treatment. In addition, forces proportional to
unsprung mass-sprung mass relative displacement and velocity may be
generated either passively by springs and shock absorbers or actively
by a variety of transducers, amplifiers, and actuators. Thus the con-
trol force is assumed to be of the form

$$F_s = (cs + k_{12})(z - y) - K_{sa}s^2 y - K_{sv}sy + K_{ua}s^2 z + K_{uv}sz \qquad (19)$$
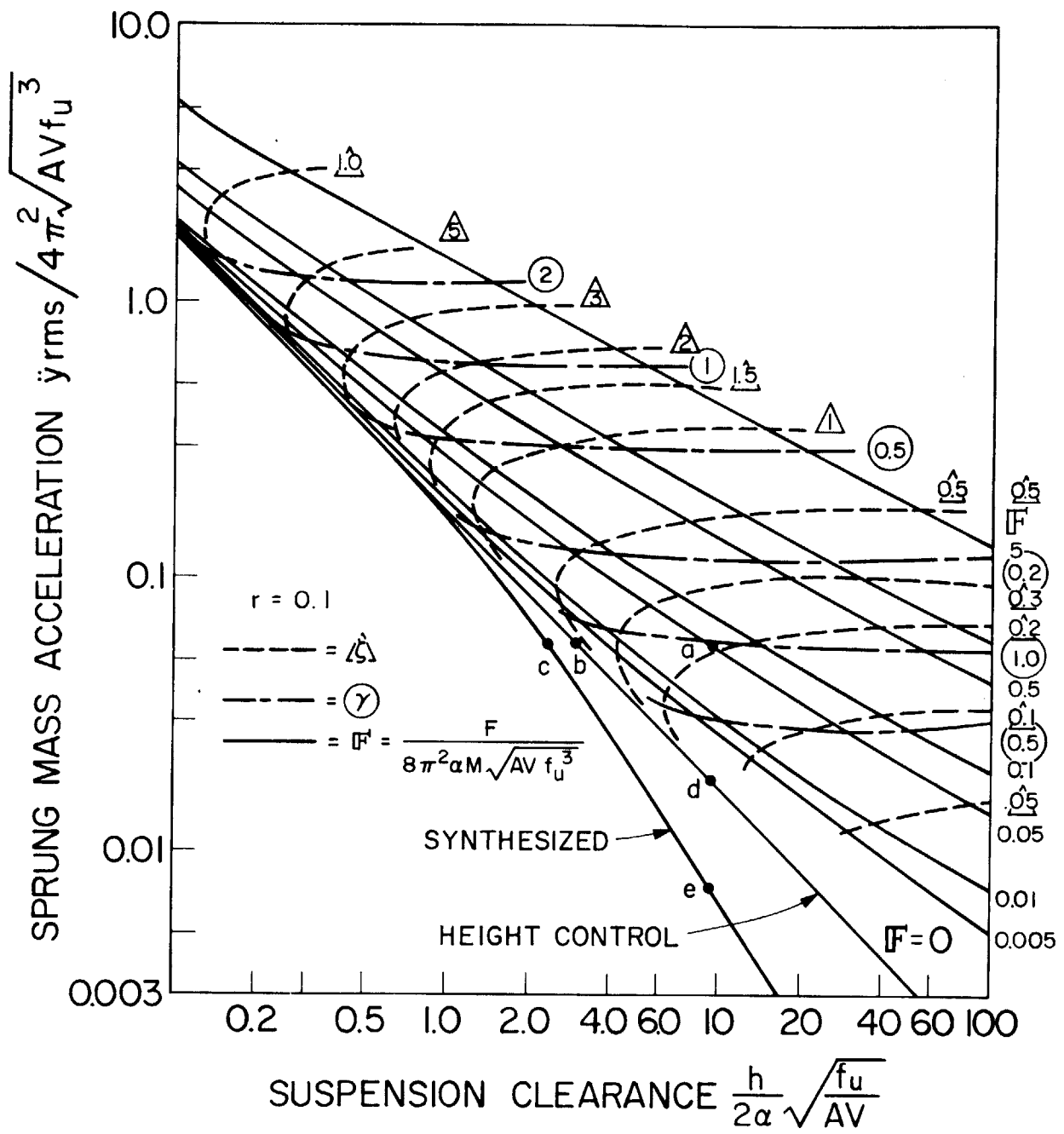
Figure 6. Acceleration - Suspension Design Chart

ACCELEROMETER

$$K_{sa} + \frac{K_{sv}}{s}$$

SPRUNG

MASS

M

k_{1Z} C

ACTUATOR

COMMAND SIGNAL

SERVO
AMPLIFIER

ACCELEROMETER

$$K_{ua} + \frac{K_{uv}}{s}$$

UNSPRUNG MASS m

k_{01}
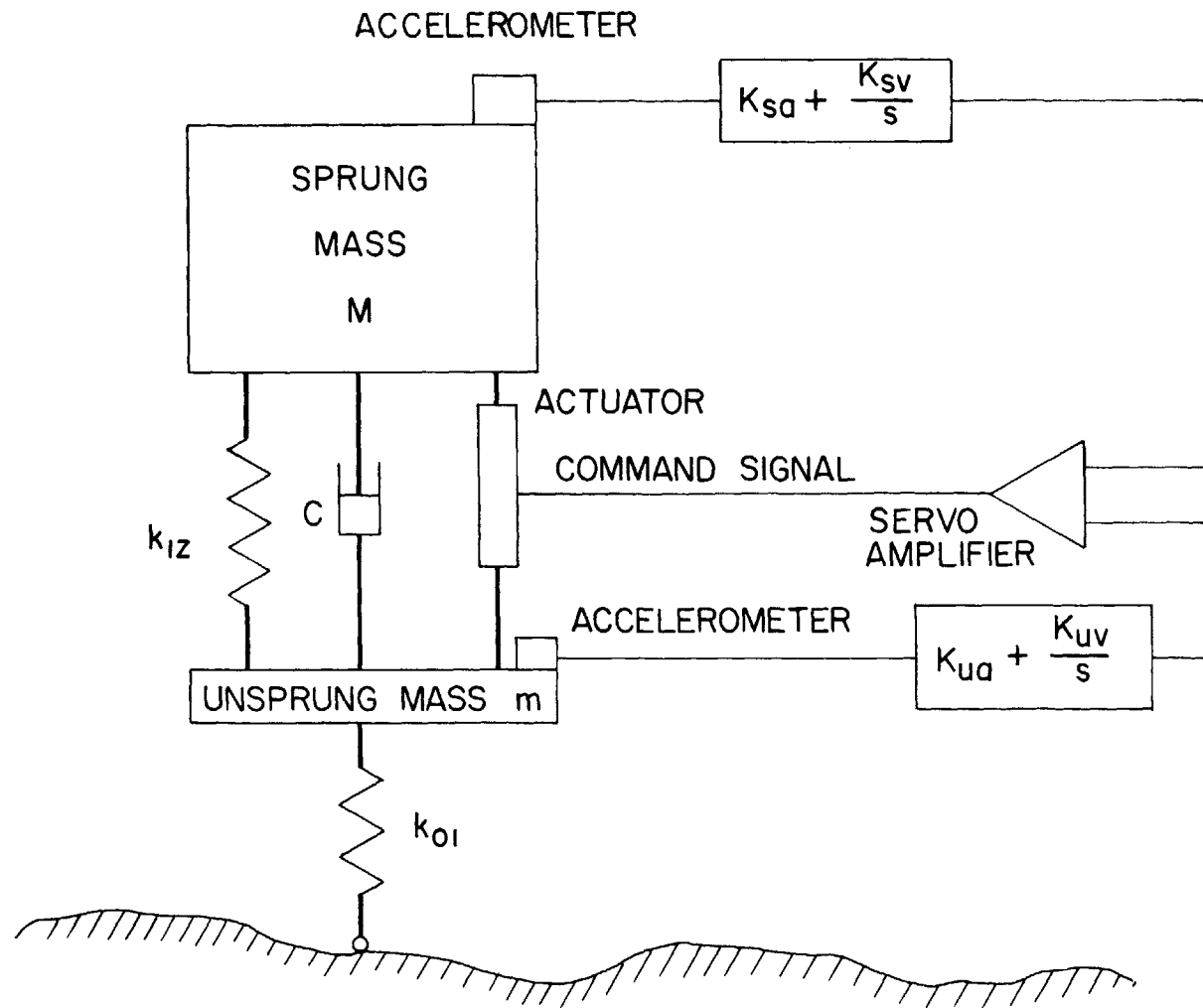
Figure 7. Schematic Diagram of Active Suspension

where the nomenclature is defined in Figure 7. From the above and from Equation (6), the transfer function relating sprung mass acceleration to roadway elevation is

$$\frac{\ddot{y}(\phi)}{x(\phi)} = \frac{\omega_u^2 \phi^2 [\frac{rK_{ua}}{\gamma^2 m} \phi^2 + (\frac{2\zeta}{\gamma} + \frac{r}{\gamma^2 m\omega_u} K_{uv})\phi + 1]}{\gamma^{-2}(1 + \frac{K_{sa}}{M} + \frac{K_{ua}}{m})\phi^4 + [\frac{2\zeta(1+1/r)}{\gamma} + \frac{K_{sv}}{\gamma^2 M\omega_u} + \frac{K_{uv}}{\gamma^2 m\omega_u}]\phi^3}$$

$$+ (\gamma^{-2} + \frac{K_{sa}}{\gamma^2 M} + 1 + 1/r)\phi^2 + (\frac{2\zeta}{\gamma} + \frac{K_{sv}}{\gamma^2 M\omega_u})\phi + 1$$

$$\circ \ \circ \ \bullet \ (20)$$

where $\gamma^2 = k_{01}M/k_{12}m$; $\zeta = c/2 \sqrt{k_{12}M}$.

The block diagram for the general active suspension system described by Equation (20) and used in Section 6 for an analog computer simulation is shown in Figure 8.

The active suspension system can be made optimum by equating coefficients of like power of ϕ in the numerators and in the denominators of Equations (14) and (20). There is some redundancy of parameters. For example, K_{uv} can be zero and γ or K_{sa} chosen arbitrarily. If γ is arbitrary, the spring stiffness k may be made as large as hardware limitations permit in order to minimize the effects of externally applied vehicle forces. In order to realize optimum suspension performance, it is essential that the actuator force depends in part on unsprung mass acceleration.

The non-dimensional equations relating the parameters used in the active suspension described by Equation (20) to the coefficients of ρ
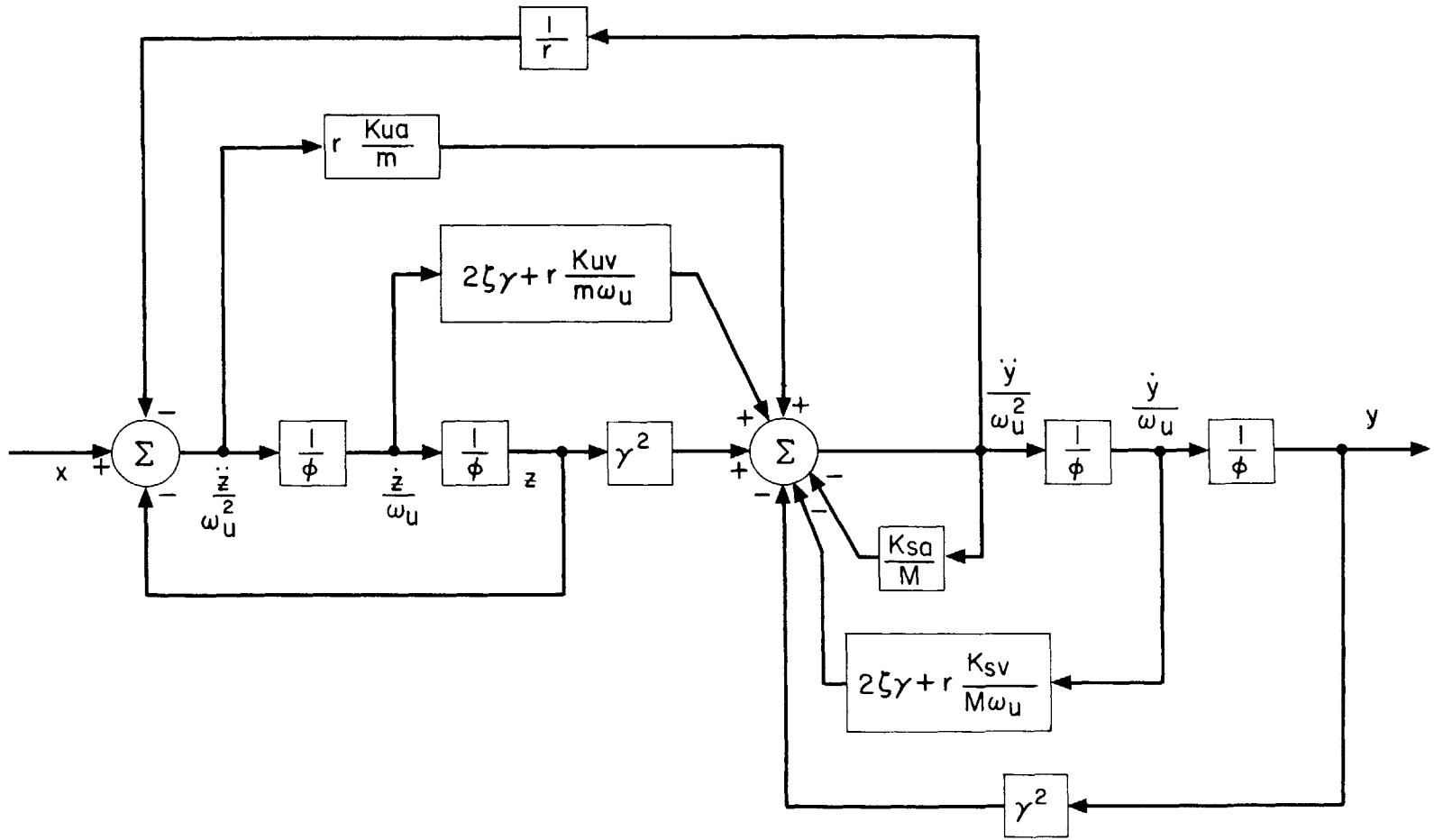
Figure 8. Active Suspension System Block Diagram

In the optimum synthesized transfer function for $K_{uv} = 0$ are:

$$\gamma = \left[\frac{1 + K_{sa}/M}{\sqrt{\beta} - B(1+1/r)} \right]^{1/2}$$

$$\frac{K_{ua}}{m} = \gamma^2 (B + 1)/r$$

$$\zeta = \frac{1}{2} \gamma C$$

$$\frac{K_{sv}}{M\omega_u} = 2\sqrt{\beta}\ D\ \gamma^2$$

(21)

Since it is desirable to build as simple a system as possible, let us choose K_{sa} equal to zero to minimize the number of feedback variables. The parameters γ, K_{ua}/m, ζ, and $K_{sv}/M\omega_u$ are computed from the above equations and plotted in Figure 9.

In a rather lengthy theoretical synthesis study such as this, one often wonders if results (the design chart, Figure 6, and optimum parameter chart, Figure 9) are valid. To confirm the above results, a parameter search optimization was performed. The rms acceleration $\ddot{y}_{rms}$ and relative displacement δ_{rms} were expressed in terms of the system parameters γ, K_{ua}/m, ζ, and $K_{sv}/M\omega_u$ from Equations (2), (7), (15), and (20) and substituted into the expression for the penalty function P (Equation (4) with $F = 0$). P was then minimized for several values of the weighting factor ρ by a hill climbing type of digital computer parameter search program (see Appendix C). The results of this independent optimization procedure confirm those found by the synthesis method.

3.1.3 Sensitivity Analysis

In addition to determining the optimum parameter values from Figure 9, it is desirable to examine the roots of the synthesized system
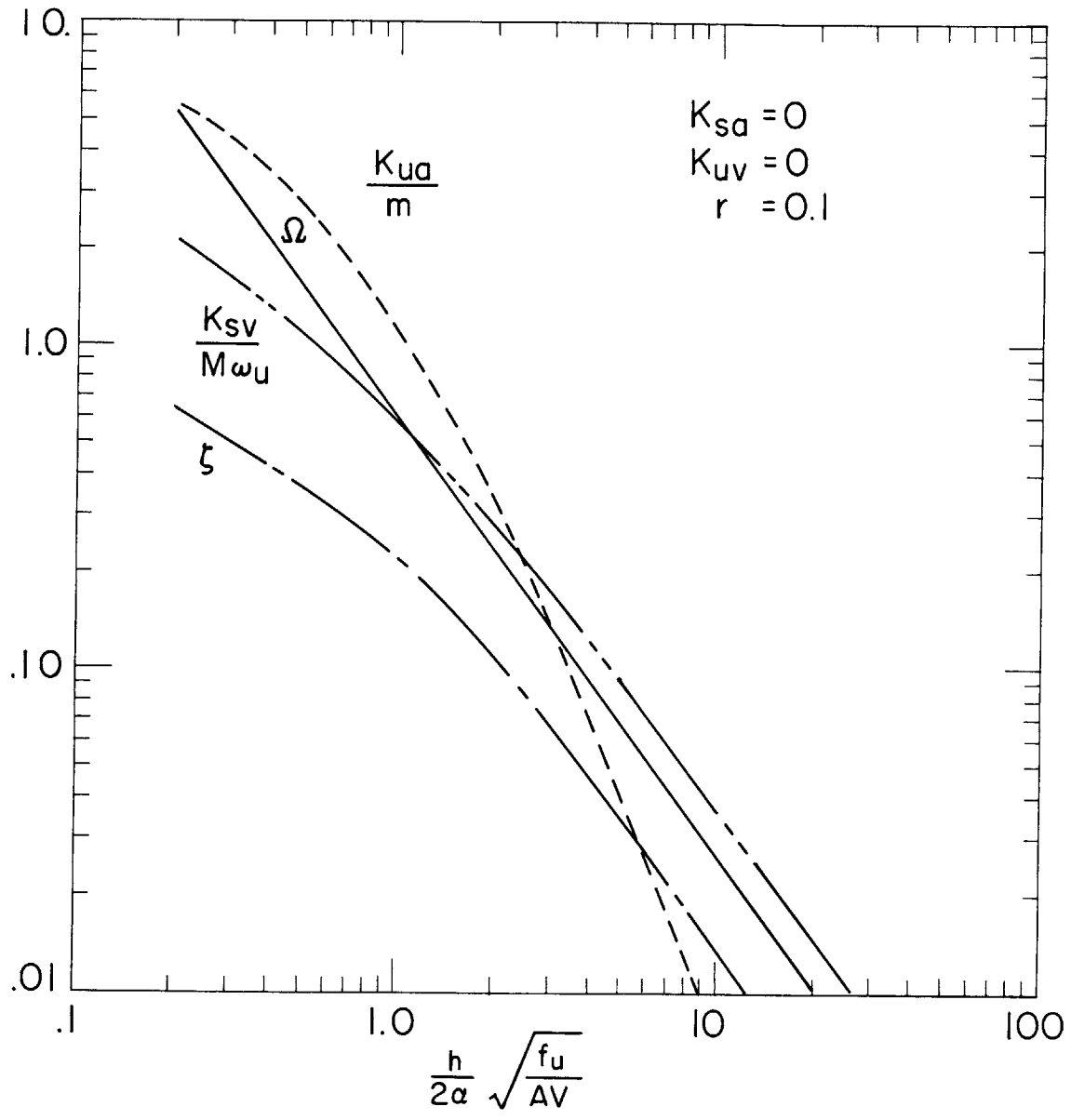
Figure 9. Optimum Active System Parameter Values

characteristic equation. The roots indicate system resonant frequencies and damping ratios that should be known before any complete system design is undertaken. In practice it is not generally possible to build a system with the precise parameter values specified by an initial design study. Consequently, one should be aware of the sensitivity of system performance to deviations in values of parameters from the optimum. It is especially important to determine the effects of parameter variations on stability.

Each of the roots of the characteristic equation for the optimum synthesized system depends only on the weighting factor β. We may therefore plot the poles of the optimum transfer function (Equation 20) as a function of β. The root locus shown in Figure 10 was found by computing the coefficients of the synthesized system characteristic equation and extracting the roots with the aid of a digital computer program. It should be emphasized that this root locus is not the conventional type where only one gain is varied. Here all gains are varied according to the above parameter computation scheme. It may be seen that at very low and very large values of β, corresponding to high and low acceleration levels, there will be very lightly damped system poles. (A physical interpretation of this will be given in Section 4.1.) These poles might be a problem if they occur at frequencies near other structural resonant frequencies not accounted for in our preliminary investigation. In addition, one might think that a small change in parameter values from the optimum could shift these poles into the right-half plane, making the system unstable.

A sensitivity analysis was performed to determine the percentage that parameters (the mass ratio r and those specified by Figure 9)

would have to be varied in order to make the system unstable. First, to
find destabilizing directions, each parameter was incremented plus and
minus 10% while the other parameters were held fixed at their optimum
values. This was done both for large ($\approx 10^6$) and small (≈ 1.0) values of
β. Once the destabilizing directions were found by this method the roots
of "worst case" combinations were found for several percentage parame-
ter variations. The results were somewhat surprising in two respects.
First, the fractional distance a pole shifted toward the right half
plane is approximately the same at any of the three points in Figure 10
where the roots approach the imaginary axis. Thus there does not seem
to be any greater tendency for poles near the right half plane to become
unstable than for poles further from the imaginary axis. Secondly, it
was found that every parameter could be varied as much as 50% in the de-
stabilizing direction without causing instability. Therefore, one
would not expect severe stability problems in using the optimum parame-
ters of Figure 9 to mechanize vehicle systems that reasonably fit the
model chosen for this investigation (Figure 7).

3.2 Analytical Optimization of Fixed Configuration Suspensions

When the analytical approach is used to determine optimum sus-
pension parameter values, $\ddot{y}_{rms}$ and h are expressed algebraically in terms
of suspension characteristics, roadway statistics, and vehicle loading
functions. The penalty or cost function P (see Equation (4)) may be mini-
mized, holding ρ constant, in one of two standard ways. If the expression
for P is not particularly complicated, one may take partial derivatives
of P with respect to each suspension parameter, set each expression equal
to zero, and solve the resulting simultaneous algebraic equations for the
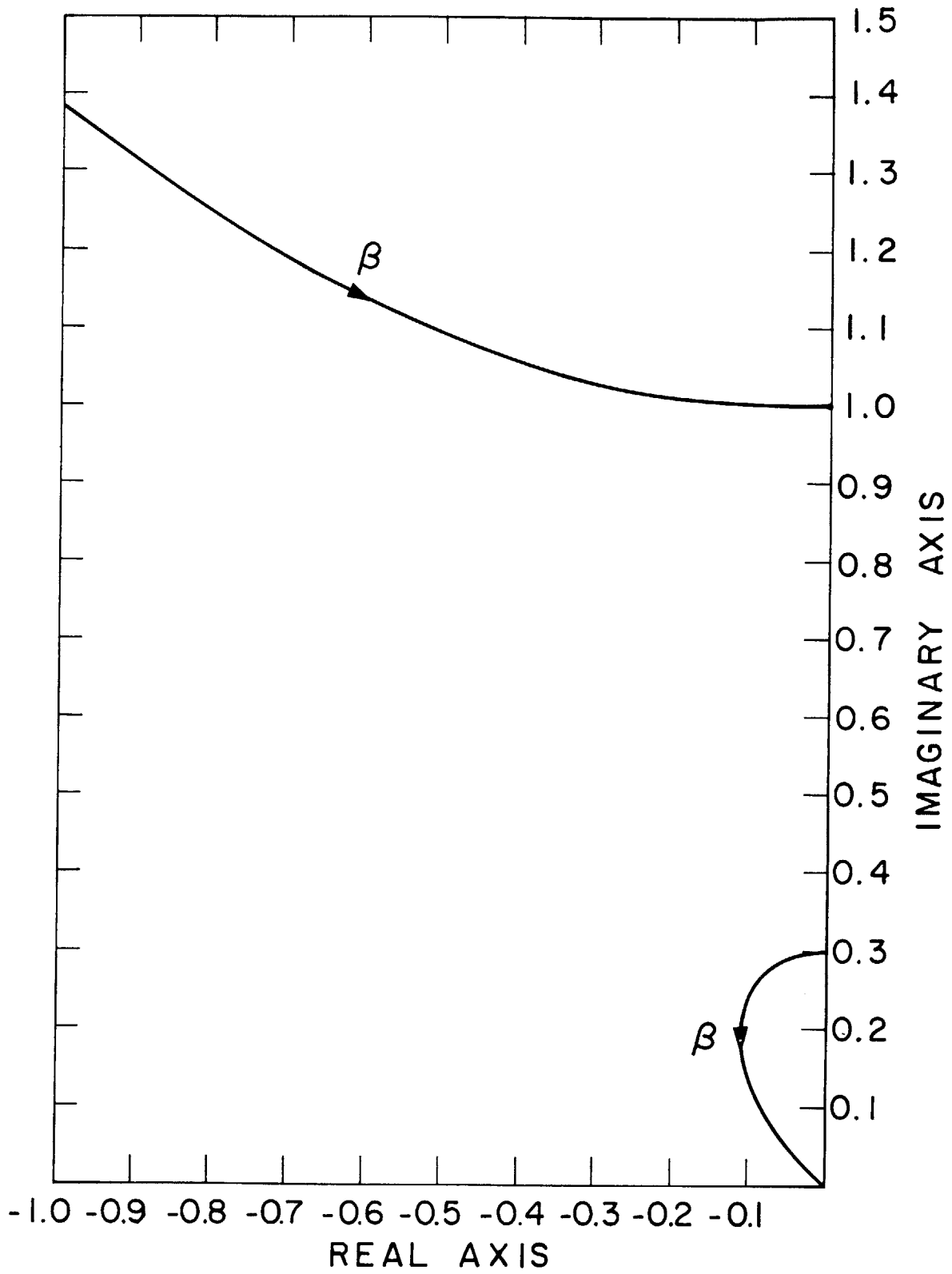
Figure 10. Roots of Optimum Synthesized Transfer Function

optimum parameter values. On the other hand, the expression for P is

often so lengthy that a closed form algebraic solution is not feasible.

In this case, a computer parameter search is appropriate. When optimum

parameters are found, $\ddot{y}_{rms}$ and h, computed using these values, define

a minimum trade-off curve on the vibration-clearance plane.

The above procedure is demonstrated by developing the trade-off

curves for the simple passive spring-shock absorber suspension of a ve-

hicle moving with velocity V (Figure 3 where "suspension" is a parallel

spring and damper). The transfer functions relating sprung mass accelera-

tion and sprung mass-unsprung mass relative excursion to roadway eleva-

tion are

$$\frac{\ddot{y}}{x}(\phi) = \frac{\omega_u^2 \phi^2 (2\zeta\gamma\phi + \gamma^2)}{\phi^4 + 2\zeta\gamma(1+1/r)\phi^3 + [\gamma^2(1+1/r)+1]\phi^2 + 2\zeta\gamma\phi + \gamma^2} \tag{22a}$$

$$\frac{\delta}{x}(\phi) = \frac{\phi^2}{\phi^4 + 2\zeta\gamma(1+1/r)\phi^3 + [\gamma^2(1+1/r)+1]\phi^2 + 2\zeta\gamma\phi + \gamma^2} \tag{22b}$$

The corresponding rms values for a roadway input spectrum of the form

AV/s^2 are found from Equations (15) and (22) as

$$\frac{\ddot{y}_{rms}}{4\pi^2\sqrt{AVf_u^3}} = \sqrt{r\zeta\gamma + \frac{(1+r)\gamma^3}{4\zeta}} \tag{23a}$$

$$\delta_{rms}\sqrt{\frac{f_u}{AV}} = \sqrt{\frac{r+1}{4\zeta\gamma}} \tag{23b}$$

Since $h = 2\alpha\delta_{rms} + F/k$, we may write the penalty function P in terms of

the above expressions for non-dimensional acceleration, clearance space,

and force variation as

$$P = \rho \sqrt{r\zeta\gamma + \frac{(1+r)\gamma^3}{4\zeta}} + \sqrt{\frac{r+1}{4\zeta\gamma} + \frac{F/(8\pi^2\alpha M \sqrt{AV f_u^3})}{\gamma^2}} \qquad (24)$$

The two algebraic equations obtained by differentiating P with respect to ζ and γ were intractable unless $F = 0$. For this case it was found that P is minimum for $\zeta = \infty$, $\gamma = 0$. This may be seen by rewriting P for $F = 0$ as follows

$$P = \rho \sqrt{r\zeta\gamma + \frac{(r+1)\gamma^4}{4\zeta\gamma}} + \sqrt{\frac{r+1}{4\zeta\gamma}} \qquad (25)$$

If we consider $\zeta\gamma$ as a single variable, then we can see from Equation (25) that γ must be zero in order to minimize P. The product $\zeta\gamma$ depends on the value of ρ. We may now write only for $F = 0$:

$$\frac{\ddot{y}_{rms}}{4\pi^2\sqrt{AVf_u^3}} = \sqrt{r\zeta\gamma}$$

$$\frac{h}{\alpha}\sqrt{\frac{f_u}{AV}} = \sqrt{\frac{r+1}{4\zeta\gamma}} \qquad (26)$$

Eliminating $\zeta\gamma$ from Equation (26) gives the equation for the optimum trade-off between acceleration and clearance for $F = 0$

$$\left(\frac{\ddot{y}_{rms}}{4\pi^2\sqrt{AVf_u^3}}\right)\left(\frac{h}{\alpha}\sqrt{\frac{f_u}{AV}}\right) = \frac{1}{2}\sqrt{r(1 + r)} \qquad (27)$$

Equation (27), rewritten in dimensional form, may be interpreted physically

$$\ddot{y}_{rms}\frac{h}{\alpha} = \frac{\pi AVk_{01}}{\sqrt{M}}\sqrt{1 + \frac{m}{M}} \qquad (28)$$

Equation (28) shows that to optimize the acceleration-clearance trade-off, a vehicle should be built with a light unsprung mass, heavy sprung

mass, and soft tires. Qualitatively this is nothing new; however, Equation (28) expresses this idea quantitatively for optimum conditions.

The interpretation of the result $\zeta = \infty$, $\gamma = 0$ is that there is no spring, only a damper between the sprung and unsprung masses. This, of course, is impractical but only because there will be a finite force variation on any vehicle in addition to gravity, both of which were assumed zero. The damping coefficient C may be computed from Equation (26) for any selected value of acceleration or clearance space by noting that $\zeta\gamma = C/2\omega_u M$.

When there are variations in force on the vehicle, a digital computer parameter search to find optimum values of ζ and γ is used. The results of a straightforward hill climbing type of search (see Appendix C) are shown in Figure 6. There are trade-off curves for several values of force variations. Also plotted are lines of constant ζ and γ which give the optimum acceleration and clearance for the different values of force variation.

3.3 **Use of Design Chart**

Let us consider qualitatively how to use Figure 6 as a design chart. (A more detailed numerical example illustrating the use of this chart and a few more to be derived in Section 4 will be presented in Section 6.) A suspension with minimum clearance space for a given vibration level would be based on several parameter values. In particular, numerical values for the rms vehicle vibration, $\ddot{y}_{rms}$, the roughness of the road, A, over which the vehicle would travel, the operating speed, V, the unsprung mass natural frequency, f_u, and the expected vehicle loading variation, F, would be required. If the non-dimensional acceleration were 0.056 and the non-dimensional force variation were 0.05,

point "a" on Figure 6 would correspond to optimum spring-shock absorber design conditions. The damping ratio ζ would be 0.2; the natural frequency ratio γ would be 0.1; and the design clearance could be computed from the abscissa. Point "b" indicates that a long time constant automatic height control system would allow clearance space reduction by a factor of 3. If this clearance space were unsatisfactory, a small additional reduction could be achieved using a system corresponding to point "c". Further clearance space reduction for a linear system which applies a force only to sprung and unsprung masses and does not use preview information is not possible.

On the other hand, if a predetermined amount of clearance space were available, we could easily compute and compare the rms acceleration levels corresponding to a passive system, one incorporating automatic height control, and finally the optimum linear system (points "a", "d", and "e", respectively). Figure 6 shows that an optimum synthesized system provides considerable acceleration reduction compared to an automatic height controller. This is in contrast to the slight improvement of point "c" over point "b".

SECTION 4

WHEEL-ROADWAY INTERACTION

In Section 3 we found active and passive suspension systems
that are optimum with respect to the vibration-clearance trade-off.
Whether these optimum systems represent satisfactory designs depends
on other criteria not accounted for in the original penalty or cost
function. Chief among these is the criterion that wheels maintain
nearly continuous contact with a roadway. The relation between wheel-
roadway dynamics and other dynamic and economic factors of interest
such as maneuverability, traction, and wear are not clear. However,
it is certain that each of these qualities will be adversely affected
by any appreciable loss of wheel-ground contact. By restricting the
rms dynamic deflection $\delta_{w,rms}$ of the wheels with respect to the road-
way to $1/\alpha_w$ of the static deflection δ_o of the unsprung mass due to
vehicle weight, wheel roadway contact may be maintained for an accept-
able proportion of time. For $\alpha_w = 3$, for example, wheels should con-
tact the road for 99.9% of the time since roadway elevation probability
density functions tend to be gaussian [47].

In this section let us examine two aspects of wheel-roadway
contact. First, a method and appropriate chart will be developed for
determining the degree to which the wheels of systems described by the
vibration-clearance design chart (Figure 6) hold the road. Secondly,
we shall find the minimum rms force required to hold the wheels of a
moving vehicle on the road. Since this force is generally applied to
the sprung mass (as contrasted to a vibration absorber, for example)

and increases with velocity, we will be able to determine upper speed

limits of a vehicle for any given rms sprung mass vibration level.

4.1 Design Chart Constraint

We may test whether or not optimum suspensions are satisfac-

tory in regard to unsprung mass excursions relative to the roadway by

first computing the static deflection of the unsprung mass, δ_o, and then

the rms dynamic deflections, $\delta_{w,rms}$ for any particular design. If δ_o is

greater than $\delta_{w,rms}$ by a factor of three or more, for example, we may

tentatively assume that a wheeled vehicle would possess adequate wheel-

roadway contact. On the other hand, if δ_o is not three or more times

larger than $\delta_{w,rms}$, we may either include $\delta_{w,rms}$ in the penalty function

(Equation (4)) and proceed with a more complicated analysis than pre-

sented here or try to modify the optimum system to have good, though

not optimum, vibration, clearance space, and wheel-roadway characteristics.

The static deflection of the unsprung mass is easily computed

as the weight of both sprung and unsprung masses divided by the stiff-

ness k_{01}. Thus

$$\delta_o = \frac{(m+M)g}{k_{01}} \tag{29}$$

where g is the gravitational constant. For a mass ratio m/M of 0.1 the

static deflection in feet is

$$\delta_o = 9.0/f_u^2 \tag{30}$$

where f_u is the unsprung mass natural frequency in Hz.

The rms dynamic excursion is found from the transfer function

relating roadway elevation to δ_w and the roadway mean square elevation

spectral density. The transfer function for δ_w, derived for the general

active suspension system (Figure 7), is

$$\frac{\zeta_w}{x}(\phi) = \cfrac{\phi^2 \quad \left(1+ \frac{K_{sa}}{M} + \frac{K_{ua}}{m}\right)\phi^2 + \left[2\ \zeta\gamma(1+1/r)+\frac{K_{sv}}{M\omega_u}\right]\phi + \gamma^2(1+1/r)}{\left(1+ \frac{K_{sa}}{M} + \frac{K_{ua}}{m}\right)\phi^4 + \left[2\zeta\gamma(1+1/r)+\frac{K_{sv}}{M\omega_u} + \frac{K_{uv}}{m\omega_u}\right]\phi^3 \atop +\left[\gamma^2(1+1/r)+1+\frac{K_{sa}}{M}\right]\phi^2+\left(2\zeta\gamma+\frac{K_{sv}}{M\omega_u}\right)\phi+\gamma^2}$$

(31)

From the above and Equations (2) and (15) the wheel-roadway rms dynamic excursion is computed for the optimum systems specified by Figure 6. The results are plotted in Figure 11 as a function of the non-dimensional design clearance.

The shape of the curves in Figure 11 may be explained from physical reasoning. The suspensions corresponding to the left-hand side of Figure 11 are designed for small clearance and are consequently quite stiff. Thus, as clearance space becomes smaller, the sprung and unsprung masses become more nearly locked together as one unit atop the undamped spring represented by k_{01}. This system approaches a single-degree-of-freedom lightly damped oscillator which exhibits considerable relative excursions when excited by a random input. At the right-hand side of Figure 11, $\delta_{w,rms}$ again increases with distance from the central minimum. In this case, however, systems are designed for very low acceleration levels, hence small force transmissibility. As the suspension forces become ever lower, the unsprung mass becomes increasingly isolated from the sprung mass and behaves like a lightly damped resonant oscillator.

The procedure for testing whether any particular optimum system satisfies the unsprung mass dynamic excursion constraint is now
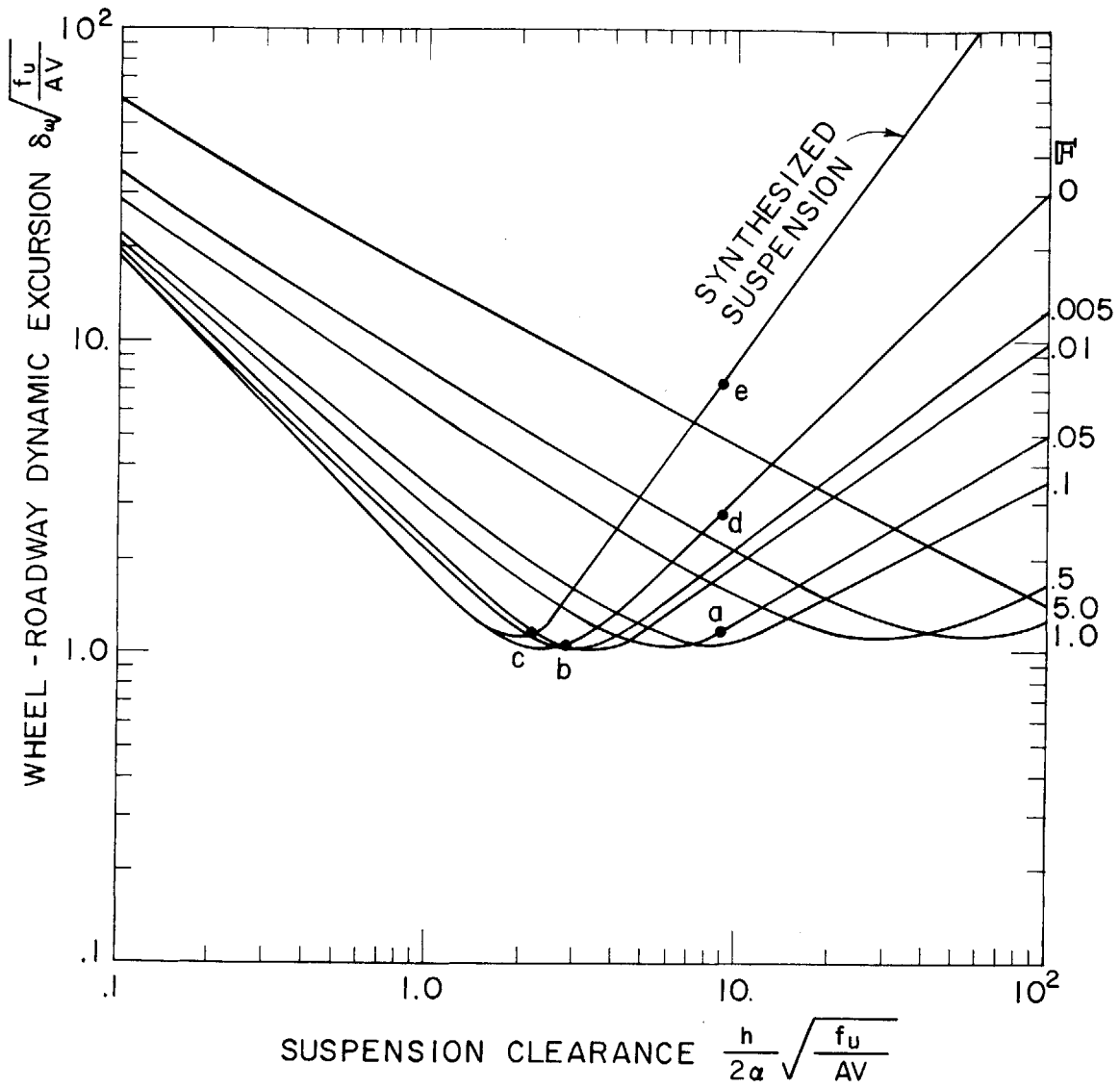
Figure 11. Wheel – Roadway Excursion for Optimum Suspensions Specified by Figure 6

straightforward. First, compute the static deflection from Equation (29). Then find from Figure 11 the value of $\delta_{w,rms} \sqrt{f_u/AV}$ (hence $\delta_{w,rms}$) which corresponds to the same trade-off curve and clearance space used in the optimum suspension design chart. Finally compare $\delta_{w,rms}$ with δ_o to determine if unsprung mass motion is excessive.

4.2 Minimum RMS Sprung Mass Force

One of the fundamental speed limitations to vehicles using conventional extremely lightly damped wheels arises from the time varying force required to maintain nearly continuous wheel-road contact. If there were no external forces applied to a wheel, modeled as a single-degree-of-freedom undamped oscillator excited by random roadway elevations, wheel-roadway excursions would be so large that the wheel would bounce a great deal. Since the time varying forces that must be applied to the wheel to keep it on the ground are also applied to the sprung mass (for suspensions that do not incorporate devices such as vibration absorbers), it seems appropriate to attempt to find the minimum rms force, hence rms sprung mass acceleration, required to maintain wheel road contact.

The procedure used here to find the lowest value of rms force needed to provide adequate wheel-road contact consists mainly of synthesizing the transfer function relating roadway elevation to suspension force which minimizes the weighted sum of the rms suspension force applied to the wheel plus the rms wheel-roadway dynamic excursion. Thus there is a trade-off between suspension force and wheel-road excursion in much the same way as there is a trade-off between sprung mass acceleration and sprung mass-unsprung mass relative excursion as discussed in

Section 3. By letting the rms excursion for this optimum wheel-road system be as large as is compatible with road holding requirements ($1/\alpha_w$ of the static displacement) the force is minimal. We will therefore find the characteristics of the linear system that can hold the wheels of a vehicle on the road with minimum sprung mass vibration without regard to sprung mass-unsprung mass clearance space.

The equation of motion for an unsprung mass m excited by roadway elevation variations x and a suspension force F_s is

$$F_s + k_{01}(x-z) = m\ddot{z} \tag{32}$$

where k_{01} is the wheel stiffness and z is the wheel displacement. Noting that the wheel-road relative excursion δ_w is defined by $\delta_w = x-z$ the solution for δ_w in terms of F_s and wheel parameters is

$$\delta_w = \frac{\phi^2}{\phi^2+1} x - \frac{F_s/k_{01}}{\phi^2+1} \tag{33}$$

By analogy to the block diagram, Figure 5, in Section 3 with F_s/k_{01}, δ_w and the synthesized wheel-roadway transfer function $W_w(s)$ replacing $\ddot{y}$, δ_9 and $W(s)$, respectively, we find that

$$H_1(\phi) = \frac{1}{\phi^2+1}$$

$$H_2(\phi) = \frac{\phi^2}{\phi^2+1} \tag{34}$$

From Equations (2), (11), (12), and (34) the expressions for $\Gamma(\phi)$ and $\Delta(\phi)$ are

$$\Gamma(\phi) = - \frac{2\pi AV/\omega_u^2}{(\phi^2+1)^2}$$

$$\Delta(\phi) = -2\pi AV/\omega_u^2 \left[\frac{\phi^4+2\phi^2+1+1/\rho}{\phi^2(\phi^2+1)^2}\right] \tag{35}$$

The numerator of the bracketed term of the above equation may be factored in two stages. First

$$\phi^4 + 2\phi^2 + 1 + 1/\rho = (\phi^2 + 1 + j/\sqrt{\rho})(\phi^2 + 1 - j/\sqrt{\rho}) \tag{36}$$

Then the roots of each of the above bracket terms are found so that $\Delta(\phi)$ is given by

$$\Delta(\phi) = -2\pi\rho AV/\omega_u^2 \; \frac{(\phi+b+cj)(\phi+b-cj)(\phi-b+cj)(\phi-b-cj)}{\phi^2(\phi^2+1)^2} \tag{37}$$

where

$$b = (1+1/\rho)^{1/4} \sin\left[\frac{1}{2}\tan^{-1}(1/\sqrt{\rho})\right]$$

$$c = (1+1/\rho)^{1/4} \cos\left[\frac{1}{2}\tan^{-1}(1/\sqrt{\rho})\right] \tag{38}$$

Upon factoring $\Delta(\phi)$ into terms, each of which contains roots on opposite sides of the imaginary axis, we have

$$\Delta^+(\phi) = \frac{\rho(\phi+b+cj)(\phi+b-cj)}{\phi(\phi^2+1)}$$

$$\Delta^-(\phi) = -\frac{2\pi AV/\omega_u^2(\phi-b+cj)(\phi-b-cj)}{\phi(\phi^2+1)} \tag{39}$$

Consequently, the expression for $\Gamma(\phi)/\Delta^-(\phi)$ is

$$\frac{\Gamma(\phi)}{\Delta^-(\phi)} \quad \frac{\phi}{\phi(\phi^2+1)(\phi-b+cj)(\phi-b-cj)} \tag{40}$$

If we find that part of the partial fraction expansion of $\Gamma(\phi)/\Delta^-(\phi)$ that has only poles in the left-half plane and divide by $\Delta + (\phi)$, the optimum synthesized transfer function is given by

$$W_w(\phi) = \frac{[(\sqrt{1+1/\rho} - 1)\phi + 2b]}{\phi^2 + 2b\phi + \sqrt{1+1/\rho}} \tag{41}$$

There are now essentially three steps to find the minimum rms force $F_{s,rms}$, required to hold the wheels of a moving vehicle on the ground.

First, the rms wheel-roadway dynamic excursion $\delta_{w,rms}$ is found. Then by equating $\delta_{w,rms}$ to $1/\alpha_w$ of the static wheel deflection δ_o, an expression containing the weighting factor ρ and various system parameters is derived. The value of ρ that satisfies this equation corresponds to the minimum rms suspension force. Consequently, the last step is to find the rms force in terms of ρ and solve for $F_{s,rms}$.

From Equations (2), (15), (33), and (41) and noting that $F_s/k_{01} = W_w(s)X(s)$, the expression for $\delta_{w,rms}$ is

$$\delta_{w,rms} = \left[\frac{AV \ (\sqrt{1+1/\rho} \ +4b^2)}{f_u \ 4b \ \sqrt{1+1/\rho}} \right]^{1/2} \tag{42}$$

By equating α_w times the above equation to the expression for the static wheel deflection (Equation (29)), we get

$$\frac{AVf_u^{3}}{(1+1/r)^2 g^2} \ \frac{\alpha_w^2 (2\pi)^4 (\ \sqrt{1+1/\rho} \ + 4b^2)}{4b \ \sqrt{1+1/\rho}} = 1 \tag{43}$$

In a manner completely similar to the derivation of Equation (42), the expression for $F_{s,rms}$ divided by the sprung plus unsprung mass weight $(m + M)g$ is found to be

$$\frac{F_{s,rms}}{(m+M)g} = \left\{ \frac{AVf_u^{3}}{(1+1/r)^2 g^2} \ \frac{(2\pi)^4 [(\sqrt{1+1/\rho} \ -1)^2 \sqrt{1+1/\rho} \ + 4b^2]}{4b\sqrt{1+1/\rho}} \right\}^{1/2} \tag{44}$$

We can compute and plot $F_{s,rms}/(m + M)g$ as a function of the parameter AVf_u^{3}/g^2 for several values of r by using an iterative technique to solve Equation (43) for ρ and then by solving Equation (44) for $F_{s,rms}/(m+M)g$. The results of this analysis for $\alpha_w = 3$, illustrated in Figure 12, show how $F_{s,rms}/(m+M)g$, hence the minimum sprung mass vibration, increases with roadway roughness, vehicle speed, and unsprung mass natural frequency.

$$\frac{F_{rms}}{(M+m)g}$$

10^1

10^0

10^{-1}

10^{-2}

10^{-3}

10^{-4}

m/M = 0.30

m/M = 0.20

m/M = 0.10

m/M = 0.05

10^{-4} 10^{-3} 10^{-2} 10^{-1}

$$\frac{f_u^3 \, AV}{g^2}$$

M

F

SUSP

F

m

k

$\alpha = 3$

$$f_u^2 = \frac{k/m}{(2\pi)^2}$$
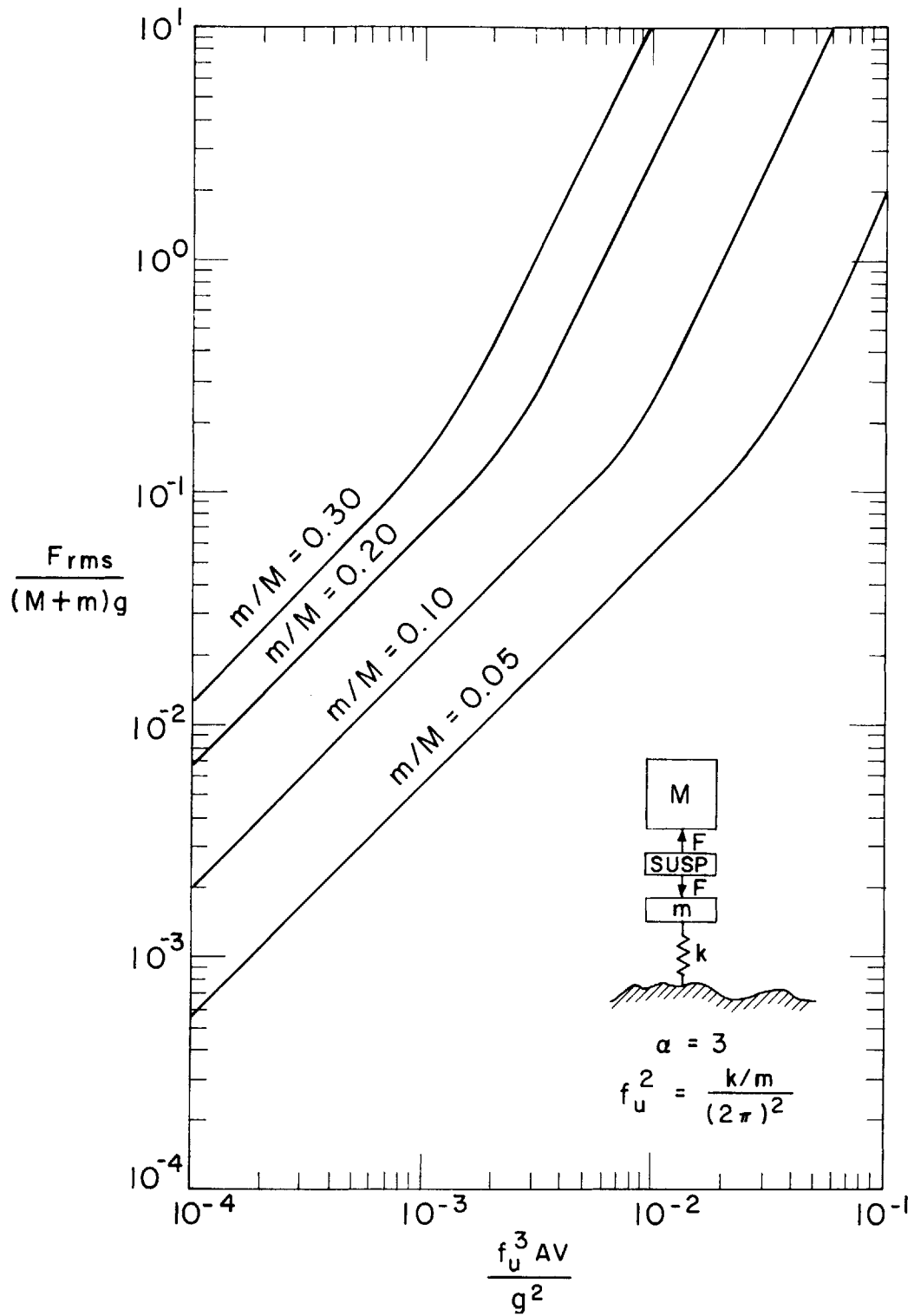
Figure 12. Minimum RMS Force Required to Maintain Wheel – Roadway Contact 99.9% of the Time

The benefits of light weight unsprung masses are also apparent.

The curves in Figure 12 represent ultimate speed limitations because of sprung mass vibration only for an unsprung mass modeled as a linear single-degree-of-freedom undamped system and for a linear suspension which applies equal forces to both unsprung and sprung masses. Damping, present in all real wheels, tends to make the results illustrated in Figure 12 conservative. Nevertheless, several steps may be taken to reduce the suspension force required to maintain adequate wheel-road contact if vehicle acceleration is excessive. First, since the rms suspension force is approximately proportional to the cube of the unsprung mass natural frequency, f_u, a considerable sprung mass vibration reduction may be brought about by a moderate decrease in f_u. Secondly, a vibration absorber may be used to reduce the forces applied to the sprung mass. Finally, for vehicles in a tunnel, an overhead suspension system, which might reduce vehicle vibration, could also be used to preload the main suspension thereby permitting large wheel-road excursion (hence small rms force) without loss of wheel-road contact.

SECTION 5

OPTIMUM LINEAR PREVIEW CONTROL

As anyone who has driven an automobile on very foggy days and
on clear days may verify, the accuracy with which a driver can keep his
vehicle at the center of a lane for a given speed depends, among other
things, on his visibility of the roadway ahead of the car. Certainly a
measure of tracking error (i.e., deviation of the vehicle from the cen-
ter of the lane) would decrease monotonically with increasing visibility
but would reach a finite value even for infinite visibility. Thus al-
though information regarding the roadway path ahead of a vehicle is sig-
nificant in controlling an automobile, for long distances such data ap-
parently provides diminishing returns as the preview distance lengthens.

There is a strong similarity between the function of a human
operator to steer a vehicle along a winding road and the function of a
suspension to guide a vehicle over the vertical part of a roadway profile.
In this section we shall investigate some of the fundamental limitations
and trade-offs pertaining to vehicle suspensions that are capable of
utilizing data on the roadway profile ahead of a vehicle. First, a ve-
hicle model (different from that used in Section 3) and optimum synthe-
sized suspension that does not use preview control will be established.
In order to find ultimate performance capabilities, the optimum system
transfer function and corresponding accelerations and relative displace-
ments will be found for a system that has infinite roadway preview.
Finite preview suspension systems will be studied to determine how vi-
bration and clearance space improvements depend on preview distance.

Finally, mechanization of preview suspension systems will be considered.

The vehicle model used for this study is a single-degree-of freedom rigid mass connected to the roadway by massless suspension elements. Unfortunately, the mathematics in this section are sufficiently lengthy to justify a preliminary study of only the simplest of systems. The model is, however, broadly representative of the fundamental suspension problem of guiding a vehicle over a road with a minimum of vibration and clearance space. Schematically, Figure 13 shows both the vehicle-suspension-roadway configuration and the block diagram relating roadway elevation to vehicle acceleration and to vehicle-roadway clearance space. The roadway elevation at the preview sensor, x_s, is viewed as the input to the synthesized suspension $W_p(s)$. The vehicle acceleration $\ddot{y}$ is integrated twice to give displacement y which is subtracted from the roadway elevation x_v under the vehicle to give vehicle-roadway relative excursion δ_p. The roadway elevation under a moving vehicle x_v is the same as that at the sensor position but delayed by a time T equal to the distance L of the sensor in front of the vehicle divided by the vehicle velocity V.

5.1 Zero Preview

The transfer function and vibration clearance trade-off curve for the case of zero preview (L = 0) are useful bases against which to compare similar results for finite and infinite preview suspension. From Equations (2), (11), and (12) the expressions for the synthesizing functions $\Gamma(s)$ and $\Delta(s)$ are derived by noting from Figures 5 and 13b that $H_1(s) = 1/s^2$ and $H_2(s) = 1$. Thus
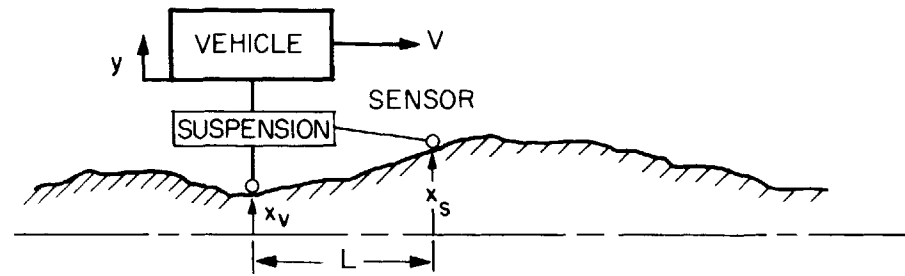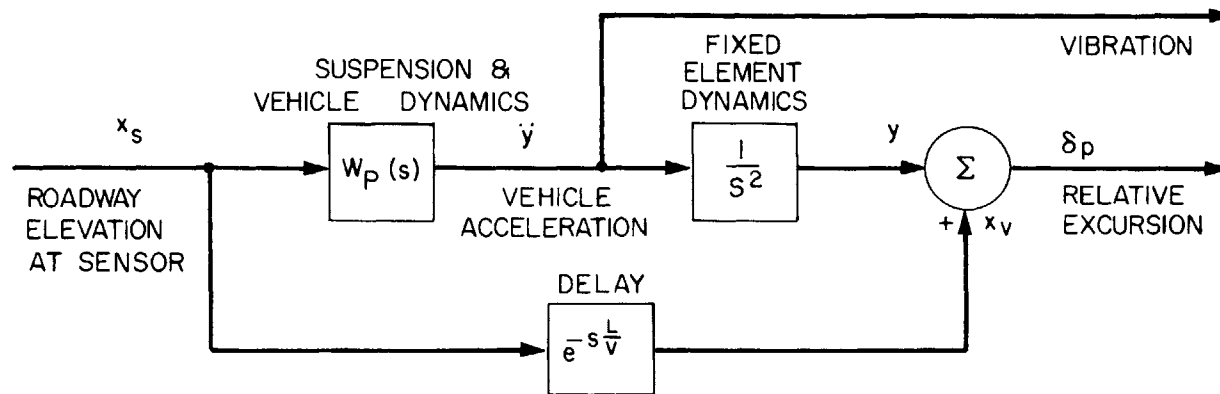
Figure 13. Preview Suspension System   a) Schematic   b) Block Diagram

$$\Gamma(s) = \frac{2\pi AV}{s^4} \tag{45}$$

$$\Delta(s) = 2\pi AV \frac{(\rho s^4 + 1)}{s^6} \tag{46}$$

$\Delta(s)$ may be factored into parts each of which contains only poles and zeroes in the right and left half planes as follows:

$$\Delta^-(s) = \frac{2\pi AV}{s^3}[\rho^{1/4}s - \frac{1}{\sqrt{2}}(1+j)][\rho^{1/4}s - \frac{1}{\sqrt{2}}(1-j)] \tag{47}$$

$$\Delta^+(s) = \frac{1}{s^3}[\rho^{1/4}s + \frac{1}{\sqrt{2}}(1+j)][\rho^{1/4}s + \frac{1}{\sqrt{2}}(1-j)] \tag{48}$$

When $\Gamma(s)/\Delta^-(s)$ is expanded in a sequence of partial fractions, the only term with poles in the left half plane is $1/s$. Consequently, $[\Gamma(s)/\Delta^-(s)]_+ = 1/s$ and, from Equations (10) and (48), the synthesized suspension transfer function $W_p(s)$ is

$$W_p(s)_{L=0} = \frac{s^2}{\rho^{1/2}s + \sqrt{2}\rho^{1/4}s + 1} \tag{49}$$

The rms vehicle acceleration $\ddot{y}_{rms}$ and relative excursion $\delta_{p,rms}$ are found from Equations (2) and (49), Figure 13, and the tables corresponding to Equation (15) [51]. Thus

$$\left(\frac{\ddot{y}^2_{rms}\rho^{3/4}}{2\pi AV}\right)_{L=0} = \frac{\sqrt{2}}{4} \tag{50}$$

$$\left(\frac{\delta^2_{p,rms}}{2\pi AV\rho^{1/4}}\right)_{L=0} = \frac{3\sqrt{2}}{4} \tag{51}$$

The weighting constant ρ may be eliminated from Equations (50) and (51)

to give the equation expressing the optimum zero preview vibration-clearance trade-off

$$\left(\frac{\ddot{y}_{rms}}{\sqrt{2\pi AV}}\right)\left(\frac{\delta_{rms}}{\sqrt{2\pi AV}}\right)^3_{L=0} = \frac{3\sqrt{3}}{8} \tag{52}$$

5.2 Infinite Preview

No system is likely to need or would be capable of utilizing profile information on the roadway very far (e.g., a one-hour travel time) in advance of the vehicle. However, the transfer function and trade-off curve for an infinite preview system are much easier to compute than those for a finite preview suspension and, in addition to giving ultimate performance limitations, present some interesting results not obtainable from finite preview considerations. Therefore, we may solve the Wiener-Hopf integral equation without regard to physical realizability restrictions (i.e., allow infinite preview). The Wiener-Hopf equation may be given by [51]

$$\Gamma(\tau) = \int_{-\infty}^{\infty} W_p(t)\Delta(\tau-t)dt \tag{53}$$

Multiplying each side of Equation (53) by $e^{-s\tau}$ and integrating over τ gives

$$\int_{-\infty}^{\infty} \Gamma(\tau)e^{-s\tau}d\tau = \int_{-\infty}^{\infty} e^{-s\tau}d\tau \int_{-\infty}^{\infty} W_p(t)\Delta(\tau-t)dt \tag{54}$$

or

$$\int_{-\infty}^{\infty} \Gamma(\tau)e^{-s\tau}d\tau = \int_{-\infty}^{\infty} W_p(t)e^{-st}dt \int_{-\infty}^{\infty} \Delta(\tau-t)e^{-s(\tau-t)}d\tau \tag{55}$$

Thus

$$\Gamma(s) = W_p(s)\Delta(s) \tag{56}$$

From Equations (11), (12), and (56) the expression for the optimum suspension transfer function for infinite preview $W_p(s)_{L=\infty}$ is

$$W_p(s)_{L=\infty} = \frac{H_1(-s)H_2(s)}{H_1(s)H_1(-s)+\rho} \tag{57}$$

The very remarkable feature of Equation (57) is that $W_p(s)_{L=\infty}$ is independent of the input. Consequently, one might suspect that a finite preview suspension system with characteristics similar to Equation (57) is likely to perform very well even for input signals with quite different statistics from those for which the system was synthesized. Before discussing finite preview control, let us find the vibration-clearance trade-off corresponding to Equation (57).

Since Equation (57) was derived by relaxing physical realizability constraints, $H_1(s) = 1/s^2$ and $H_2(s) = 1$, thus

$$W_p(s)_{L=\infty} = \frac{s^2}{\rho s^4+1} \tag{58}$$

By noting that $Y(s) = W_p(s)_{L=\infty}X(s)$ the expression for the rms value of $\ddot{y}$ is found from Equations (2), (15), and (58) as

$$\left(\frac{\ddot{y}^2_{rms}\,\rho^{3/4}}{2\pi\,AV}\right)_{L=\infty} = -\frac{1}{2\pi j}\int_{-j\infty}^{j\infty}\frac{\psi^2}{(\psi^4+1)^2}\,d\psi \tag{59}$$

where $\psi = \rho^{1/4}s$

Equation (59) may be evaluated from Appendix D for $x = 0$ and $n = 2$. Thus

$$\left(\frac{\ddot{y}^2_{rms}\,\rho^{3/4}}{2\pi\,AV}\right)_{L=\infty} = \frac{\sqrt{2}}{16} \tag{60}$$

Similarly the rms relative excursion $\delta_{p,rms}$ found from Equations (2), (15), (58) and $\delta_p(s) = (1 - W_p(s)/s^2)X(s)$ is

$$\frac{\delta^2_{p,rms}}{2\pi AV\rho^{1/4}}\Bigg|_{L=\infty} = - \frac{1}{2\pi j}\int_{-j\infty}^{j\infty} \frac{\psi^6}{(\psi^2+1)^2}\, d\psi \tag{61}$$

Equation (61) may also be evaluated from Appendix D for $x = 0$ and $n = 6$ as

$$\left(\frac{\delta^2_{p,rms}}{2\pi AV\rho^{1/4}}\right)_{L=\infty} = \frac{3\sqrt{2}}{16} \tag{62}$$

When ρ is eliminated from Equations (60) and (62), the vibration-clearance trade-off is described by

$$\left(\frac{\ddot{y}_{rms}}{\sqrt{2\pi AV}}\right)\left(\frac{\delta_{p,rms}}{\sqrt{2\pi AV}}\right)^3 = \frac{3\sqrt{3}}{128} \tag{63}$$

Consequently, from the above and from Equation (52) the relation between vibration and clearance for infinite preview as compared with zero preview for a roadway spectrum proportional to $1/\omega^2$ is

$$\frac{(\ddot{y}_{rms}\delta^3_{p,rms})_{L=\infty}}{(\ddot{y}_{rms}\delta^3_{p,rms})_{L=0}} = \frac{1}{16} \tag{64}$$

Thus, infinite preview provides a remarkable improvement over zero preview suspensions. Now that the potential of preview suspensions has been demonstrated, let us consider how suspension system improvement depends on the distance L ahead of the vehicle that the roadway is sensed.

5.3 Finite Preview

The method for synthesizing the optimum suspension transfer function for the case when a vehicle can sense the preceding roadway for

a finite distance is similar to the steps taken for the zero preview situation. However, the delay shown in Figure 13b requires us to use a more rigorous and lengthy treatment. Until now we have merely divided double poles on the imaginary axis evenly into $\Delta^-(s)$ and $\Delta^+(s)$ when factoring $\Delta(s)$. Here, however, it is necessary to first shift any poles on the imaginary axis into the left or right half plane by very small amounts, ε_1 and ε_2 and then find limiting function values as ε_1 and ε_2 approach zero. Thus

$$\Phi_t(s) = \frac{AV}{(s+\varepsilon_1)(-s+\varepsilon_1)} \tag{65}$$

$$H_1(s) = \frac{1}{(s+\varepsilon_2)^2} \tag{66}$$

$$H_2(s) = e^{-sT} \tag{67}$$

From the above and Equations (11) and (12) the synthesizing functions $\Gamma(s)$ and $\Delta(s)$ are

$$\Gamma(s) = \frac{2\pi AV e^{-sT}}{(-s+\varepsilon_2)^2(s+\varepsilon_1)(-s+\varepsilon_1)} \tag{68}$$

$$\Delta(s) = \frac{2\pi AV(\rho s^4 - 2\,\varepsilon_2\rho s^2 + \rho\varepsilon_2^4 + 1)}{(s+\varepsilon_2)^2(s+\varepsilon_1)(-s+\varepsilon_2)^2(-s+\varepsilon_1)} \tag{69}$$

For very small ε_2 the four roots of the numerator of Equation (69) lie well off the imaginary axis. For convenience then, let us approximate this numerator by $2\pi AV(\rho s^4 + 1)$. Thus Equation (69) factors as follows:

$$\Delta^{-}(s) = \frac{2\pi AV[\rho^{1/4}s - \frac{1}{\sqrt{2}}(1+j)][\rho^{1/4}s - \frac{1}{\sqrt{2}}(1-j)]}{(-s+\varepsilon_2)^2 (-s+\varepsilon_1)} \tag{70}$$

$$\Delta^{+}(s) = \frac{[\rho^{1/4}s + \frac{1}{\sqrt{2}}(1+j)][\rho^{1/4}s + \frac{1}{\sqrt{2}}(1-j)]}{(s+\varepsilon_2)^2 (s+\varepsilon_1)} \tag{71}$$

Dividing Equation (68) by Equation (70) gives

$$\frac{\Gamma(s)}{\Delta^{-}(s)} = \frac{e^{-sT}}{(s+\varepsilon_1)[\rho^{1/4}s - \frac{1}{\sqrt{2}}(1+j)][\rho^{1/4}s - \frac{1}{\sqrt{2}}(1-j)]} \tag{72}$$

The inverse Fourier transform of $\Gamma(s)/\Delta^{-}(s)$ is a time function $\gamma(t)$ which generally has non-zero values for plus and minus t. The function $[\Gamma(s)/\Delta^{-}(s)]_{+}$ is the Fourier transform of $\gamma(t)$ for $t>0$. Thus far it has been possible to find $[\Gamma(s)/\Delta^{-}(s)]_{+}$ by expressing $\Gamma(s)/\Delta^{-}(s)$ in a partial fraction expansion and retaining only terms with poles in the left half plane. Since $\Gamma(s)/\Delta^{-}(s)$ in Equation (72) is a transcendental function, $[\Gamma(s)/\Delta^{-}(s)]_{+}$ is evaluated first by finding $\gamma(t)$ and then by taking the Laplace transform of $\gamma(t)$ which is identical in form to the Fourier transform of $\gamma(t)$ for $t>0$. Thus

$$\gamma(t) = \frac{1}{2\pi j} \int_{-j\infty}^{j\infty} e^{st} \frac{\Gamma(s)}{\Delta^{-}(s)} \, ds \tag{73}$$

From Equations (72) and (73)

$$\gamma(t) = \frac{1}{2\pi j} \int_{-j\infty}^{j\infty} \frac{e^{s(t-T)}}{(s+\varepsilon_1)[\rho^{1/4}s - \frac{1}{\sqrt{2}}(1+j)][\rho^{1/4}s - \frac{1}{\sqrt{2}}(1-j)]} ds \qquad (74)$$

Equation (74) is evaluated in two parts (see Figure 14a).
First, for a path of integration around the left half plane, correspond-
ing to $(t-T)>0$, $\gamma(t)$ is equal to the residue at $s = -\varepsilon_1$. Secondly, for
$(t-T)<0$, $\gamma(t)$ is equal to minus the sum of the residues at poles (a) and
(b) for a contour taken clockwise around the right half plane. The resi-
due at $-\varepsilon_1$ is

$$\text{Res}(-\varepsilon_1) = \frac{e^{-\varepsilon_1(t-T)}}{\rho^{1/2}\varepsilon_1^2 + \sqrt{2}\rho^{1/4}\varepsilon_1 + 1} \qquad (75)$$

Taking the limit as $\varepsilon_1 \to 0$ gives

$$\gamma(t) = 1 \qquad \text{For } (t-T)>0 \qquad (76)$$

By evaluating the residues of the poles at (a) and (b), $\gamma(t)$ for
$(t - T)<0$ becomes (see Figure 13b)

$$\gamma(t) = e^{(t-T)/\tau} \, 1[\cos(\frac{t-T}{\tau}) - \sin(\frac{t-T}{\tau})] \qquad \text{For } (t-T)>0 \qquad (77)$$

where $\tau = \sqrt{2}\,\rho^{1/4}$

The function $[\Gamma(s)/\Delta^-(s)]_+$ may now be evaluated by taking the Laplace
transform of $\gamma(t)$ as follows:

$$\frac{\Gamma(s)}{\Delta^-(s)}\bigg|_+ = \int_0^\infty \gamma(t)e^{-st} \, dt \qquad (78)$$

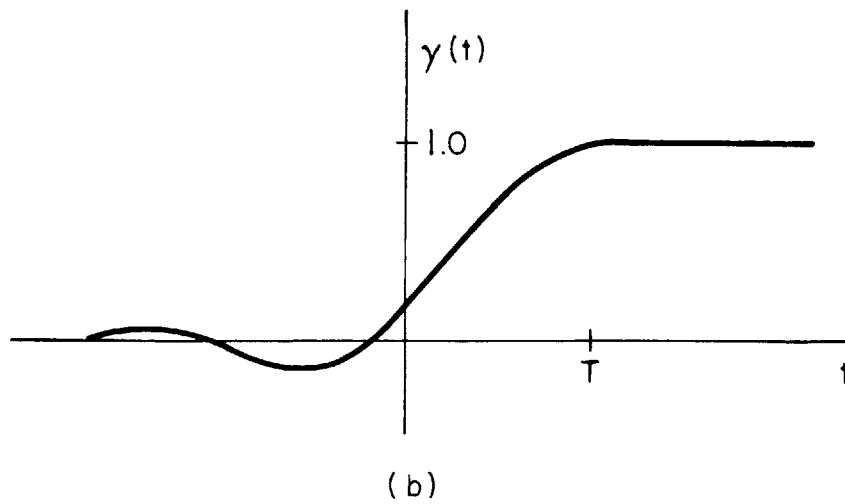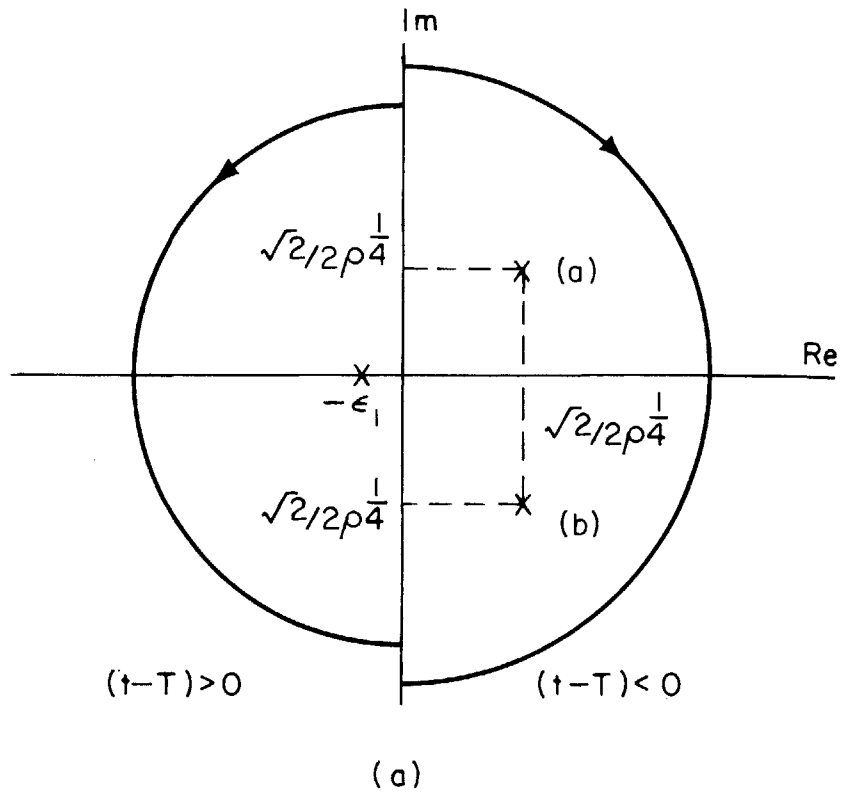From Equations (77) and (78) we have

(a)

(b)

Figure 14. a) Contour Integration of $\Gamma(s)/\Delta^-(s)$ b) Inverse Fourier
Transform of $\Gamma(s)/\Delta^-(s)$

$$\left[\frac{\Gamma(s)}{\Delta^-(s)}\right]_+ = \int_0^T e^{(t-T)/\tau}[\cos(\frac{t-T}{\tau})-\sin(\frac{t-T}{\tau})]e^{-st}dt + \int_T^\infty e^{-st}dt \qquad (79)$$

When the above integration is carried out and $[\Gamma(s)/\Delta^-(s)]_+$ is divided by $\Delta^+(s)$ (Equation (71)), the expression for the synthesized finite pre-view suspension transfer function $W_p(s)_{L=L_o}$ is

$$W_p(s)\Big|_{L=L_o} = \frac{s^2(A_1\rho^{1/2}s^2-\sqrt{2}A_2\rho^{1/4}s+1)}{\rho s^4 + 1} \qquad (80)$$

where $A_1 = e^{-T/\tau}(\cos T/\tau + \sin T/\tau)$

$\qquad A_2 = e^{-T/\tau}(\cos T/\tau)$

The rms acceleration and clearance may be found from Equation (80), and the relations indicated by Figure 13. Thus

$$\left(\frac{\ddot{y}^2_{rms}\rho^{3/4}}{2\pi AV}\right)_{L=L_o} = \frac{1}{2\pi j}\int_{-j\infty}^{j\infty} \frac{-\psi^2(A_1\psi^2 -\sqrt{2}A_2\psi + e^{-\psi T/\rho^{1/4}})}{(\psi^4 + 1)^2}$$

$$\frac{(A_1\psi^2 + \sqrt{2}A_2\psi + e^{\psi T/\rho^{1/4}})}{1} d\psi \qquad \ldots \quad (81)$$

When the numerator of the integrand in Equation (81) is reduced, there will be some terms of the form

$$\psi^n e^{-\psi T/\rho^{1/4}}/(\psi^4+1)^2.$$

By replacing ψ with $-\psi$ and appropriately adjusting integration limits, Equation (81) becomes

$$\left(\frac{\ddot{y}^2_{rms}\rho^{3/4}}{2\pi AV}\right)_{L=L_o} =$$

$$\frac{1}{2\pi j}\int_{-j\infty}^{j\infty} \frac{-A_1^2\psi^6-2A_1 e^{\psi T/\rho^{1/4}}+2A_2\psi^4+2\sqrt{2}A_2 e^{\psi T/\rho^{1/4}}\psi^3-\psi^2}{(\psi^4+1)^2} d\psi$$

$$\qquad \ldots \quad (82)$$

When Equation (82) is evaluated (see Appendix D), we have

$$\left(\frac{\overset{\cdot\cdot}{y}{}^2_{rms}\,\rho^{3/4}}{2\pi AV}\right)_{L=L_o} = \frac{\sqrt{2}}{16}\,(A_1{}^2+4A_1{}^2T/\tau+2A_2{}^2+1) \tag{83}$$

In an entirely similar manner the expression for the relative excursion is found as

$$\left(\frac{\delta^2_{p,rms}}{2\pi AV\rho^{1/4}}\right)_{L=L_o} = \frac{\sqrt{2}}{16}\,(3+3A_1{}^2-4A_1{}^2T/\tau+6A_2{}^2) \tag{84}$$

The trade-off curves between rms acceleration and clearance space ($h_p = 2\alpha\delta_{p,rms}$) are plotted in Figure 15 for several values of preview time (in seconds) along with curves for zero and infinite preview (Equations (52) and (63)).

The relationship between the benefits that may be brought about by preview control and preview time are not apparent from Figure 15. Consequently, let us pick a design point on the zero preview line ($h/2\alpha\sqrt{2\pi AV} = 0.4$, $\overset{\cdot\cdot}{y}_{rms}/\sqrt{2\pi AV} = 10.0$) and determine how $\overset{\cdot\cdot}{y}_{rms}$ may be reduced for constant h and AV, how h may be reduced for constant $\overset{\cdot\cdot}{y}_{rms}$ and AV, and how AV may be increased for constant $\overset{\cdot\cdot}{y}_{rms}$ and h. The results shown in Figure 16 indicate that substantial reductions in vibrations and clearance space may be brought about by using preview control. For a given vibration and clearance space a vehicle using preview control may travel up to four times faster or over a road four times rougher (as measured by A) than one without preview.

5.4 Step Responses

A great deal of insight into the nature of preview suspensions may be gained from the step response (y/x) plots of these systems. First,
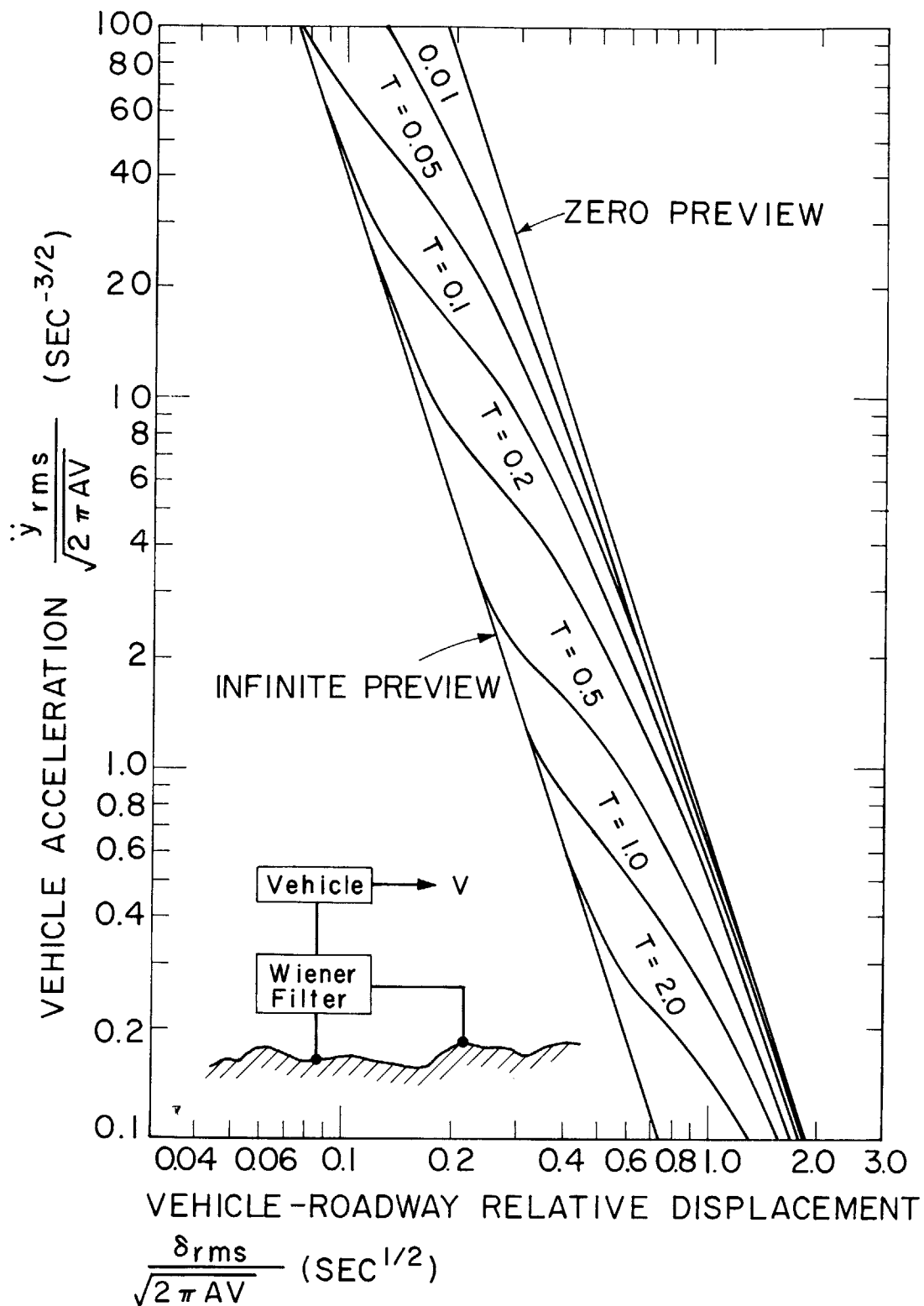
Figure 15. Vibration − Clearance Trade − Off for Synthesized Suspension for Several Values of Preview Time, T, (Seconds)
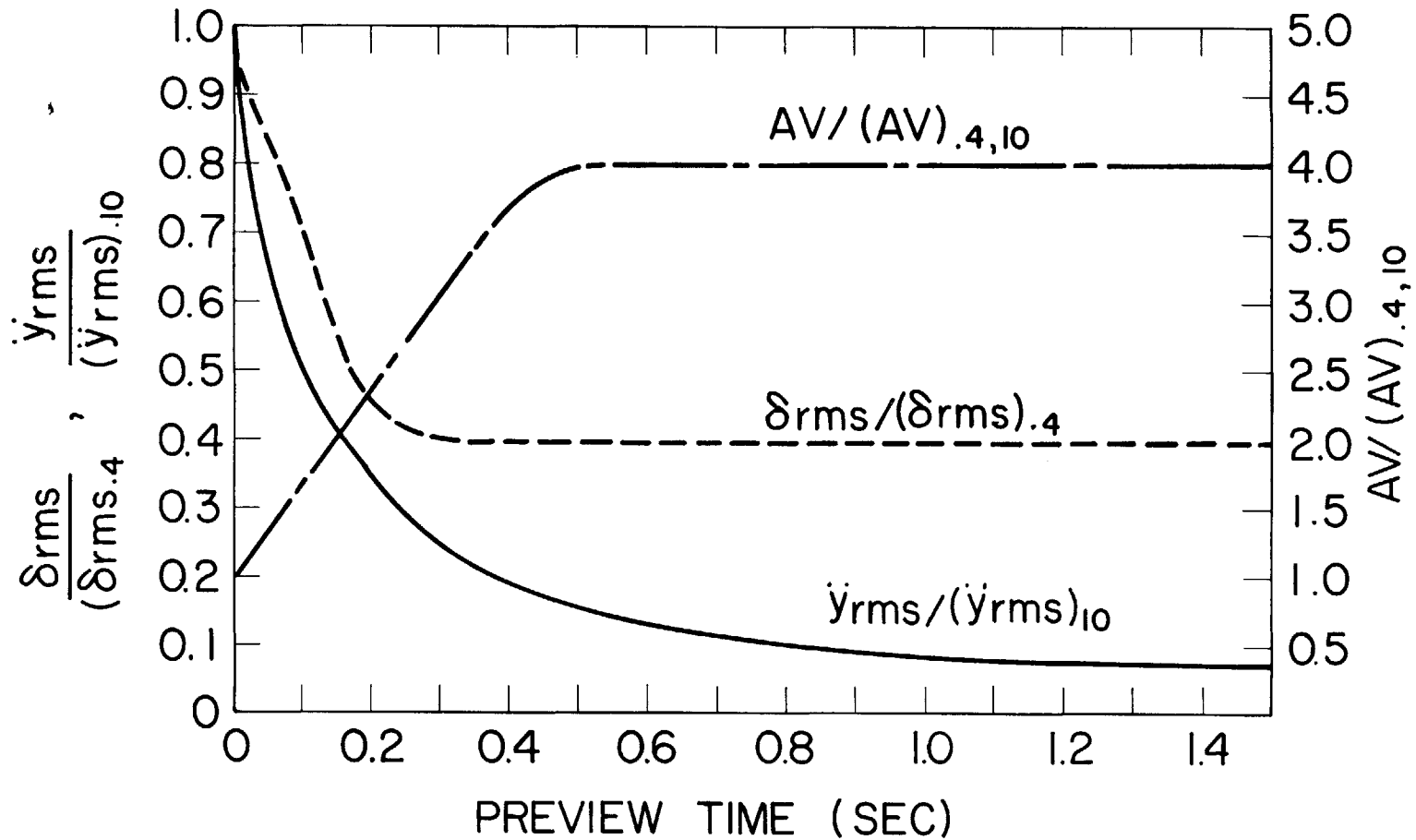
Figure 16. Example of Improvements in Speed Capabilities, Clearance Space, and Sprung Mass Acceleration as a Function of Preview Time for Synthesized Suspensions

because of the analogy between the integral square and mean square of response variables subjected respectively to step inputs and random inputs of the form AV/s^2 (see Appendix E) a qualitative comparison may be made among systems which operate with various preview times. Furthermore, step response plots facilitate a physical interpretation of the capabilities of preview systems which function with less acceleration and less relative excursion than optimum non-preview suspensions. Finally, step response plots provide hints for the development of systems which might be easily mechanized and which perform nearly as well as optimum synthesized preview suspensions.

The response of vehicle position y to a step in roadway elevation x_s is found from the definition of the inverse Fourier transform and the transfer function $W_p(s)$ (Equation (80)) by noting that $Y/X = W_p(s)/s^2$. Thus

$$y_s(t) = \lim_{\varepsilon \to 0} \int_{-j\infty}^{j\infty} \frac{A_1 \rho^{1/4} s^2 - \sqrt{2} \, A_2 \rho^{1/4} s + e^{-sT}}{(s+\varepsilon)(\rho s^4 + 1)} \, e^{st} \, ds \tag{85}$$

When the integration in the above equation is carried out, the step response $y_s(t)$ is found as

$$y_s(t) = \frac{1}{2} + \frac{1}{2} \frac{t-T}{|t-T|} [1 - e^{-\left|\frac{t-T}{\tau}\right|} \cos\left(\frac{t-T}{\tau}\right)]$$

$$- \frac{1}{2} e^{-\left(\frac{t+T}{\tau}\right)} [\cos\left(\frac{t-T}{\tau}\right) + 2\sin(t/\tau)\cos(T/\tau)] \tag{86}$$

Equation (86) is plotted in Figure 17 for several values of preview time T from the point of view of an observer at the vehicle. Thus preview time is the distance from $t/\tau = 0$ to the beginning of the response. The
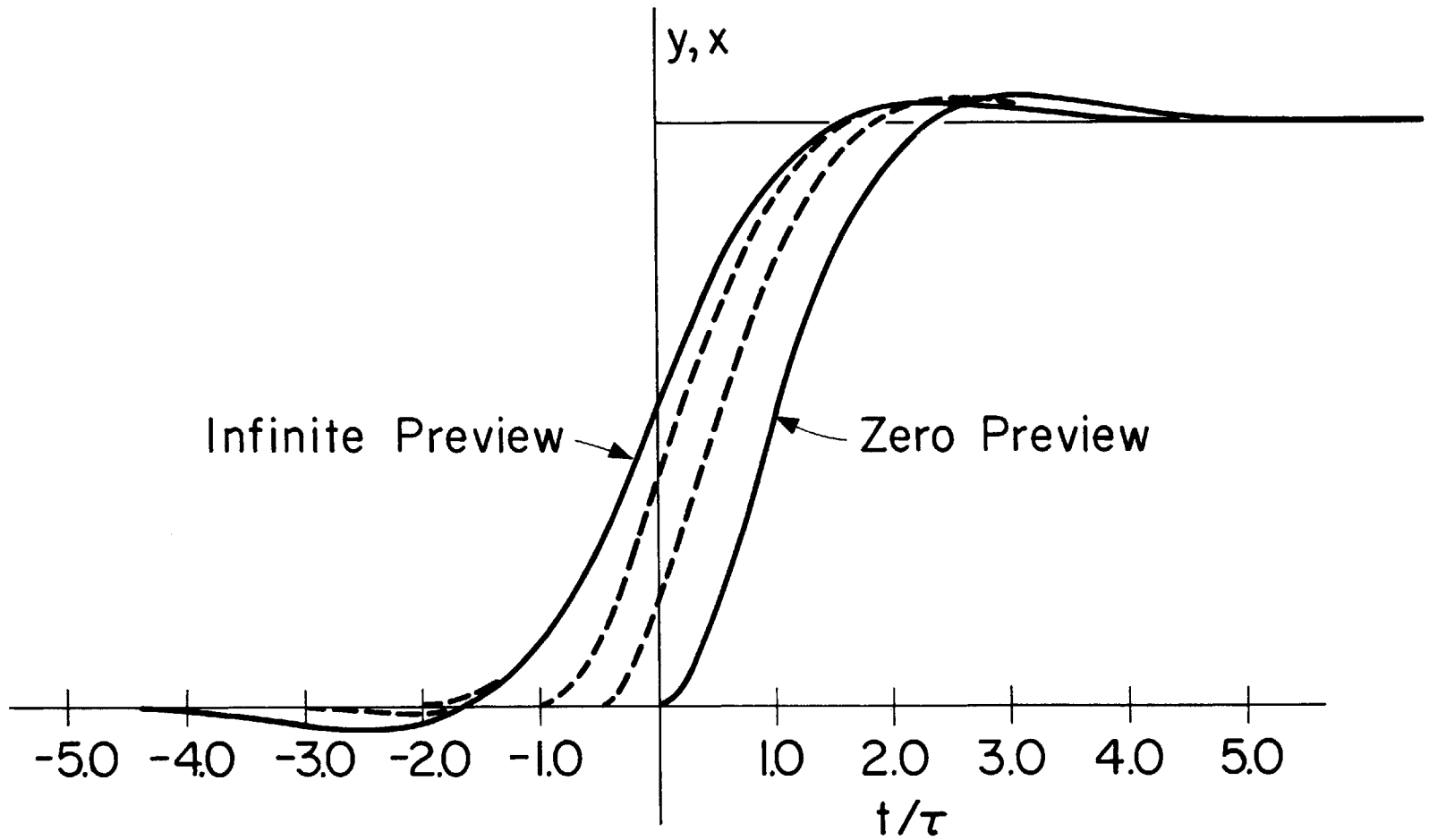
Figure 17. Synthesized Suspension Step Responses (y/x) for Several Values of Preview Time

non-dimensionalizing parameter $\tau = \sqrt{2}\, \rho^{1/4}$ may be thought of as a scaling factor. For example, when acceleration is to be small, ρ, hence τ, is large. Consequently, the step responses are more gradual than they would be if more importance were given to relative excursion.

Figure 17 shows how preview control improves both acceleration and relative excursion. Acceleration is proportional to the curvature (second derivative) of the plots in Figure 17 and relative excursion is proportional to the difference between the step and a response curve. The rms criterion weighs variables more heavily for large values than for small. Consequently, the zero preview step response shows that a large initial relative displacement and curvature will contribute to considerable rms excursion and acceleration. As longer preview time is used, response curves become more gradual and result in smaller relative displacement as the vehicle body responds to a step in roadway elevation before actually reaching it.

5.5 Mechanization

Mechanization of the transfer function for the optimum preview suspension (Equation (80)) is not at all straightforward. Since some of the poles of Equation (80) lie in the right half plane the system response first diverges then converges as illustrated by the infinite preview step response in Figure 17. Consequently, the approach taken here is to examine the step responses in Figure 17 and devise systems with similar responses.

The equation for infinite preview (Equation (58)) is identical in form to that for an infinite beam on an elastic foundation [52]. (The static deflection equation for a beam on an elastic foundation

may be derived by minimizing the weighted sum of the integral of curvature squared plus deflection squared which is analagous to minimizing the weighted sum of rms acceleration plus relative excursion.) Consequently, one suspects that the steady state behavior of a very long train such as that proposed by Edwards [53] might approach that of an optimum preview system. However, this is a very restricted case.

Let us determine the capabilities of the general but elementary model of the preview suspension system illustrated schematically in Figure 18. The vehicle, idealized as a rigid mass, is supported above the roadway by a suspension of stiffness k_v. The spring k_s represents a simple preview controller in which a force applied to the vehicle is proportional to the difference between the vehicle position, y, and elevation, x_s, of the roadway in front of the vehicle. Damping is proportional to vehicle velocity as shown by a damper attached to an inertial reference. In practice this form of damping could be approximated by generating a suspension force proportional to the integral of the output of a vehicle-mounted accelerometer.

The position transfer function Y/X for the system shown in Figure 18 is

$$\frac{Y}{X_s}(s) = \frac{k_s + k_v e^{-sT}}{Ms^2 + cs + k_v + k_s} \tag{87}$$

Equation (87), rewritten in terms of nondimensional variables is

$$\frac{Y}{X_s}(s) = \frac{a + (1-a)e^{-\phi\omega_n T}}{\phi^2 + 2\zeta\phi + 1} \tag{88}$$

where $\omega_n^2 = (k_v + k_s)/M$, $\zeta = c/2\sqrt{(k_v + k_s)M}$, $\phi = s/\omega_n$ and "a" which is a measure of distribution of stiffness between k_v and k_s is $k_s/(k_v + k_s)$.
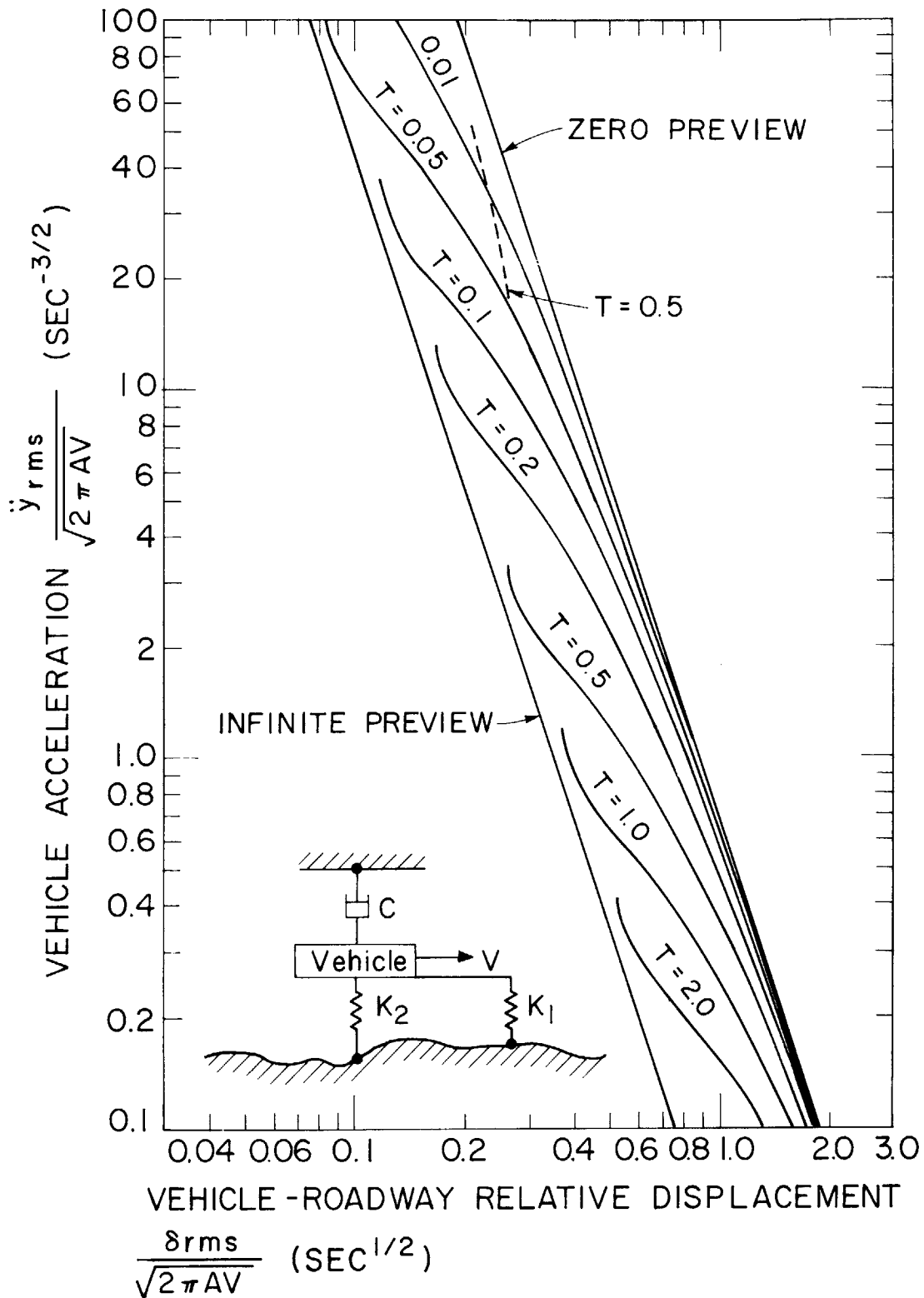
Figure 18. Vibration – Clearance Trade – Off for Simple Preview Suspension for Several Values of Preview Time, T, (Seconds)

From Equations (15), (65) (with $\epsilon_1 = 0$) and (88) the expression for the rms vehicle acceleration is

$$\frac{\ddot{y}^2_{rms}}{2\pi AV} = \frac{\omega_n^3}{2\pi j} \int_{-j\infty}^{j\infty} \frac{-\phi^2[1-2a+2a^2+a(1-a)e^{\phi\omega_n T}]}{(\phi^2+2\zeta\phi+1)(\phi^2-2\zeta\phi+1)} \, d\phi$$

$$+ \frac{\omega_n^3}{2\pi j} \int_{-j\infty}^{j\infty} \frac{-\phi^2 a(1-a)e^{-\phi\omega_n T}}{(\phi^2+2\zeta\phi+1)(\phi^2-2\zeta\phi+1)} \, d\phi \qquad \dots \ (89)$$

Equation (89) may be simplified by replacing ϕ with $-\phi$ in the second integral and appropriately adjusting limits of integration to give

$$\frac{\ddot{y}_{rms}}{2\pi AV} = \frac{\omega_n^3}{2\pi j} \int_{-j\infty}^{j\infty} \frac{\phi^2[-1+2a(1-a)(1-e^{\phi\omega_n T})]}{(\phi^2+2\zeta\phi+1)(\phi^2-2\zeta\phi+1)} \, d\phi \qquad (90)$$

When the above integral is evaluated (see Appendix F), the expression for rms acceleration is

$$\frac{\ddot{y}^2_{rms}}{2\pi AV} = \frac{\omega_n^3}{4\zeta} \left\{ 1+2a(1-a)[-1+e^{-\zeta\omega_n T}(\cos\sqrt{1-\zeta^2}\,\omega_n T \right.$$

$$\left. - \frac{\zeta}{\sqrt{1-\zeta^2}} \sin\sqrt{1-\zeta^2}\,\omega_n T)] \right\} \qquad (91)$$

The root mean square of the relative displacement of the vehicle with respect to the roadway is given by

$$\delta_p(s) = X_v(s) - Y(s) \qquad (92)$$

Thus, since $X_v(s) = X_s(s)e^{-sT}$

$$\frac{\delta_p(s)}{X} = \frac{(\phi^2+2\zeta\phi+a)e^{-\phi\omega_n T}-a}{\phi^2+2\zeta\phi+1} \qquad (93)$$

From Equations (15), (65), and (93), the expression for $\delta_{p,rms}$ is

given by

$$\frac{\delta^2_{p,rms} \, \omega_n}{2\pi AV} =$$

$$\frac{1}{2\pi j} \int_{-j\infty}^{j\infty} \frac{\phi^4 + 2(a-2\zeta^2)\phi^2 - 2a\phi^2 e^{\phi\omega_n T} + 4a\zeta\phi e^{\phi\omega_n T} + 2a^2(1-e^{\phi\omega_n T})}{(\phi+\epsilon_1)(\phi^2+2\zeta\phi+1)(-\phi+\epsilon_1)(\phi^2-2\zeta\phi+1)} \, d\phi$$

$$\dots \dots (94)$$

When the above integral is evaluated (see Appendix F), the expression for

$\delta_{p,rms}$ becomes

$$\frac{\delta^2_{rms}}{2\pi AV} = \frac{1}{4\zeta\omega_n} \{1 - 2(a-2\zeta^2) - 2a^2(4\zeta^2-1) + 2a[1-a$$

$$+ 4\zeta^2(1+a)]e^{-\zeta\omega_n T} \cos\sqrt{1-\zeta^2} \, \omega_n T + 2a\zeta[-1$$

$$+\zeta^2(1+a) - 3a]\frac{e^{-\zeta\omega_n T}}{\sqrt{1-\zeta^2}} \sin\sqrt{1-\zeta^2}\omega_n T\} - \frac{2a\zeta}{\omega_n} + a^2 T$$

$$\dots \dots (95)$$

The values of parameters a, ζ, and ω_n which optimize the trade-off between vibration and clearance space are found by minimizing $P =$ $\rho\ddot{y}_{rms} + \delta_{p,rms}$. The trade-off curves resulting from a digital computer parameter search (see Appendix C) are illustrated in Figure 18. These curves overlap the optimum synthesized trade-off curves shown in Figure 15 except near the infinite preview line. In this region the curves bend away from those corresponding to the synthesized suspension and terminate. At these end points a = 1.0 indicating that the spring beneath the vehicle has zero stiffness. Consequently, the step response, from the point of view of an observer on the vehicle, is that of a simple spring-mass-damper system but advanced by a time T. The only way a smaller

value of clearance may be obtained for this model is by having a relative-
ly flexible preview controller spring (small k_s) and a stiff suspension
spring (large k_v). This combination results in a system which allows
small clearance space only at the expense of very high acceleration levels.
The dotted curve for T = 0.5 seconds, shown in Figure 18, indicates this
aspect quantitatively. It is difficult to imagine a situation in which
such a system would be desirable since better performance may be achieved
with shorter preview times.

The presence of the discontinuity in trade-off curves is il-
lustrated by a contour plot (Figure 19) of P as a function of "a" and
ω_n for ζ = 0.7, and T = 0.5. The minimum at a = 1.0 corresponds to the
lower solid curve in Figure 18 whereas the minimum at a = .15 represents
the higher dotted line. The large value for the natural frequency ω_n
at the latter minimum explains the large acceleration levels found for
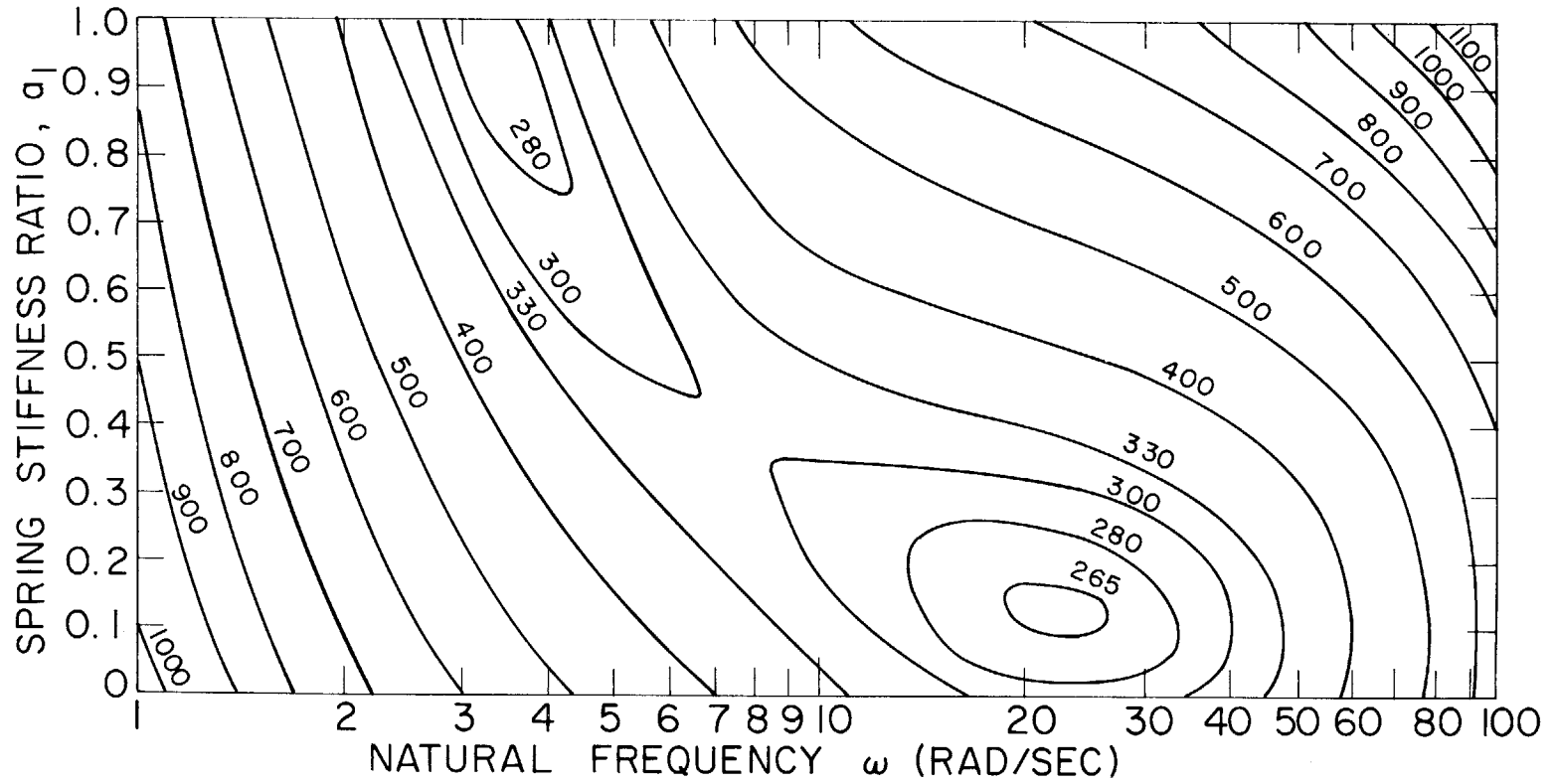the upper portion of the T = 0.5 seconds trade-off curve.

Figure   19.   Penalty Function Contour Plot for $\zeta = 0.7$ and $T = 0.5$ for Simple Preview Suspension

SECTION 6

NUMERICAL EXAMPLE

The preceding sections have presented rather general discussions of the optimization of the random vibration characteristics of vehicle suspensions. In order to illustrate the use of some of the suspension design charts (Figures 6, 10, and 11), a numerical example will be considered. First, a preliminary design of a conventional spring-shock absorber suspension will be carried out with the aid of Figure 6 for a high speed ground vehicle. Performance benefits that might be brought about by using automatic height control or synthesized suspensions will be examined. Figure 10 will be used to determine whether the suspensions thus far considered possess adequate road holding qualities. From Figure 11 we will establish a fundamental limitation to the primary design chart (Figure 6). Finally, the frequency responses, power spectral densities, and time responses to random roadway inputs will be found for several possible preliminary designs.

6.1 Use of Design Charts

The problem posed is to do a preliminary design study of a suspension system for a vehicle traveling 200 mph over a medium quality highway, $A = 2 \times 10^{-5}$ ft. First, in order to establish a design vibration level, let us compute the rms acceleration of an automotive type of vehicle going 70 mph over the same highway. For $\zeta = 0.5$, $r = 0.1$, $f_u = 10$ Hz, and $f_s = \sqrt{k_{12}/M} /2\pi = 1.5$ Hz the automobile sprung mass vibration, computed from Equation (23a) is about 5.5ft/sec^2.*

---

* Passengers would not feel this vibration level because seats filter much of the acceleration.

Let us suppose, for the high speed vehicle that $r = 0.1$, $f_u = 10$ Hz, α is equal to 3 to insure that bottoming occurs very infrequently and that loading variations are equal to 75% of the weight of the sprung mass. From this data, the nondimensional loading variations are

$$\ddot{y}_{rms}/4\pi^2\sqrt{AVf_u^3} = 0.056 \tag{96}$$

$$\mathbb{F} = F/8\pi^2\alpha M\sqrt{AVf_u^3} = 0.05 \tag{97}$$

Thus, in Figure 6 Equation (96) is satisfied at point "a" on the $\mathbb{F} = 0.05$ line and

$$(h/2\alpha)\sqrt{f_u/AV} = 9.0 \tag{98}$$

Therefore, the design clearance is

$$h = 1.31 \text{ ft.} \tag{99}$$

The design chart also shows that, at the design point "a", the optimum parameter values are

$$\zeta = 0.2$$

$$f_s = 1.0 \text{ Hz} \tag{100}$$

A 1.31 ft. suspension clearance seems rather large. If a low frequency automatic height control system were used to compensate for loading variations, $F/k = 0$ and the $\mathbb{F} = 0$ line applies. Point b in Figure 6 indicates that the suspension clearance would have to be only 5.25 inches if the same vibration level were maintained. Point c shows that the minimum possible clearance space is about 4.1 inches for the optimum synthesized suspension. Thus for this case an automatic height control suspension provides a suspension with nearly optimum performance.

If a 1.31 ft. suspension clearance is acceptable, then Figure 6 shows that active systems may be incorporated to reduce vibration and

provide a more comfortable ride. Points d and e indicate that an automatic height controller and optimum synthesized suspension may reduce sprung mass vibration by factors of 3 and 7 1/2, respectively. In this case, it appears that an optimum synthesized suspension offers a significant advantage over an automatic height controller which, in turn, is considerably more effective than a simple spring-shock absorber suspension.

Although the above discussion is valuable in comparing the vibration-clearance aspects of several suspensions, we must investigate further to determine whether the suspensions cited provide adequate wheel-road contact. From Equation (30), the static unsprung mass deflection δ_o is .09 ft. Since the rms relative wheel-roadway excursion δ_w should be at least three times smaller than δ_o, the maximum allowable value for δ_w is .03 ft. Thus

$$(\delta_w \sqrt{f_u/AV})_{max} = 1.4 \tag{101}$$

The points a - e in Figure 10 correspond to those in Figure 6. Only three points, "a", "b", and "c", fall below the 1.4 ordinate of Figure 9. Hence the suspensions corresponding to these points provide adequate wheel-road contact; whereas those suspensions corresponding to points d and e are unacceptable due to large wheel-roadway excursions.

Figure 11 may be used to determine the minimum possible vibration isolation capabilities of a linear suspension which maintains nearly continuous wheel-roadway contact. The numerical value of the abscissa, using the above high speed vehicle parameters, is

$$\frac{f_u^3 AV}{g^2} = 0.0058 \tag{102}$$

From Figure 11 the minimum rms suspension force is

$$\frac{F_{rms}}{(m+M)g} = 0.118 \qquad (103)$$

Since $\ddot{y}_{rms} = F_{rms}/M$, the minimum point on the ordinate of Figure 6 becomes

$$\frac{\ddot{y}_{rms}}{4\pi\sqrt{AVf_u^3}} = 0.043 \qquad (104)$$

Thus the largest vibration reduction from points a, b, and c that might be brought about is only 23%.

6.2 Investigation of Several Specific Systems

6.2.1 Frequency Responses and Power Spectral Densities

Of the five optimum systems, a-e, originally considered only three, a, b, and c, met the road holding constraint. The vehicle acceleration, sprung mass-unsprung mass relative excursion and the unsprung mass-roadway relative excursion frequency responses and power spectral densities for these three designs, illustrated in Figure 20, show at least two significant factors. First, as may be seen by comparing frequency responses and power spectral densities for each variable, the $1/\omega^2$ form of roadway elevation spectra causes considerably greater spectral content at the low frequency range than might be expected by merely inspecting frequency response plots. Secondly, active systems tend to attenuate or shift to higher frequencies the low frequency peak of the conventional spring-shock absorber suspension.

6.2.2 Analog Computer Simulation

An analog computer simulation of the five suspensions a-e was performed in order to check the above theoretical derivations and to
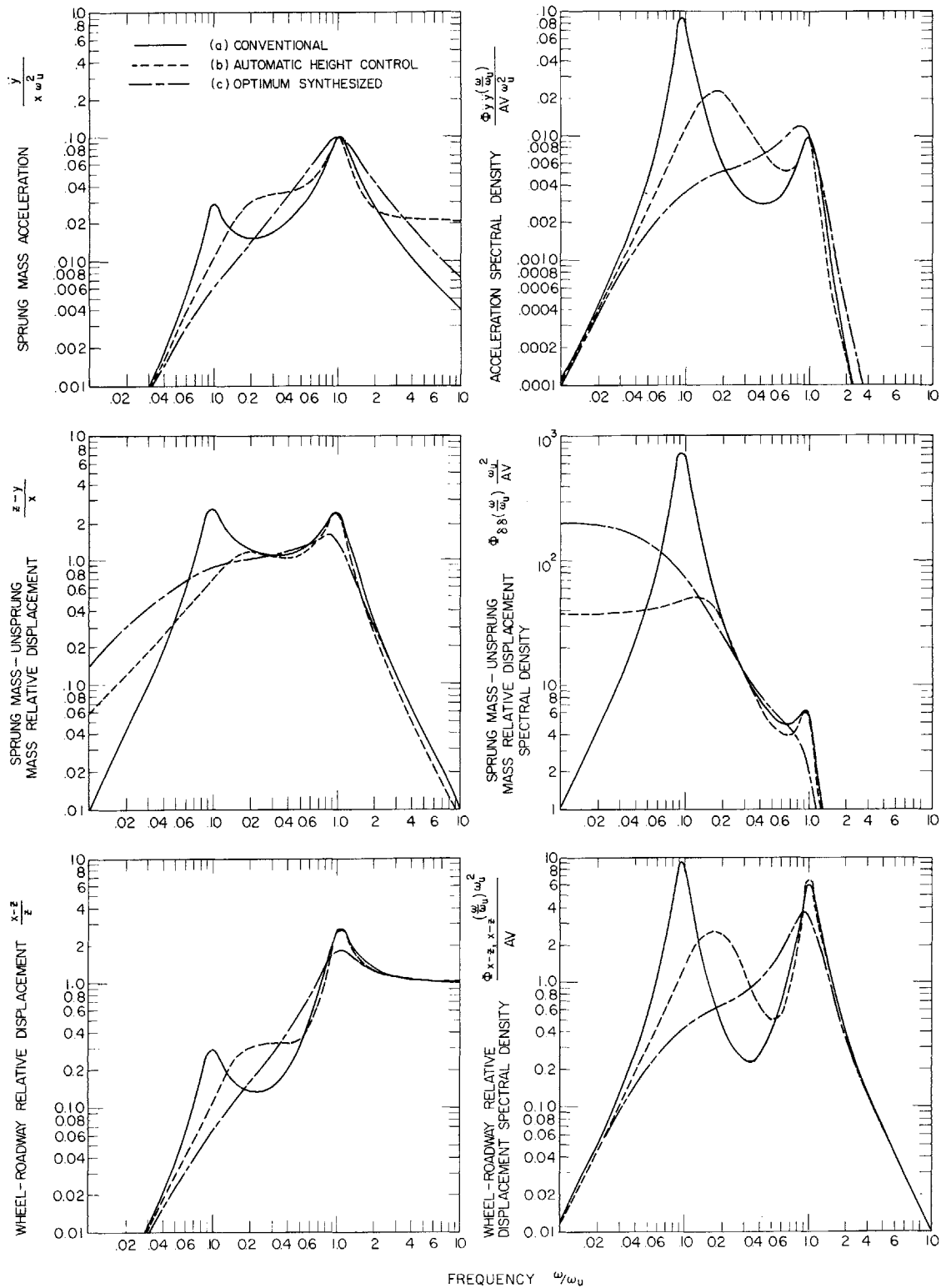
Figure   20.   Acceleration, Sprung Mass - Unsprung Mass Excursion, and
                Wheel - Roadway Excursion Frequency Responses and Power
                Spectral Densities Corresponding to Systems a, b. and c
                in Figure 6

examine time responses. A random noise signal, filtered to have approximately the same spectral shape as that of a measured roadway, was used to simulate a roadway input. The roadway, unsprung mass and sprung mass positions were displayed along with sprung mass acceleration. It was found that computer measurements and theory correlated very well.

Although theoretical computations were based on a roadway spectrum described by $\frac{AV}{\omega^2}$ it is necessary, due to finite computer amplitude ranges, to use for simulation purposes a noise function whose spectrum levels off at low frequencies. Figure 21 shows the empirically determined noise signal rms spectrum along with the rms roadway spectrum (proportional to $1/\omega$). Above the level-off frequency, ω_o (about 15 Hz), agreement between theory and experiment is very good. Vehicle dynamics were time scaled (shifted to high frequencies) so that the portion of the input spectrum below ω_o contributes little to system response. The error caused by low frequency spectrum level-off was computed as a function of ω_o/ω_u for each suspension simulated.

The example shown in Figure 22 is a plot of error due to low frequency level-off as a function of ω_o/ω_u for the conventional spring-shock absorber suspension ($\gamma = .1$, $\zeta = .2$). In this case $\omega_o/\omega_u = .03$ resulting in 7% and 4% error in measuring rms displacements and accelerations respectively. These deviations were accounted for in comparing theoretical with simulated results.

The time traces of several response variables shown in Figure 23 are in roughly the same positions as points a-e in Figure 6. In descending order in each oscilloscope photograph are sprung mass (y), unsprung mass (z) and roadway (x) vertical positions as well as sprung
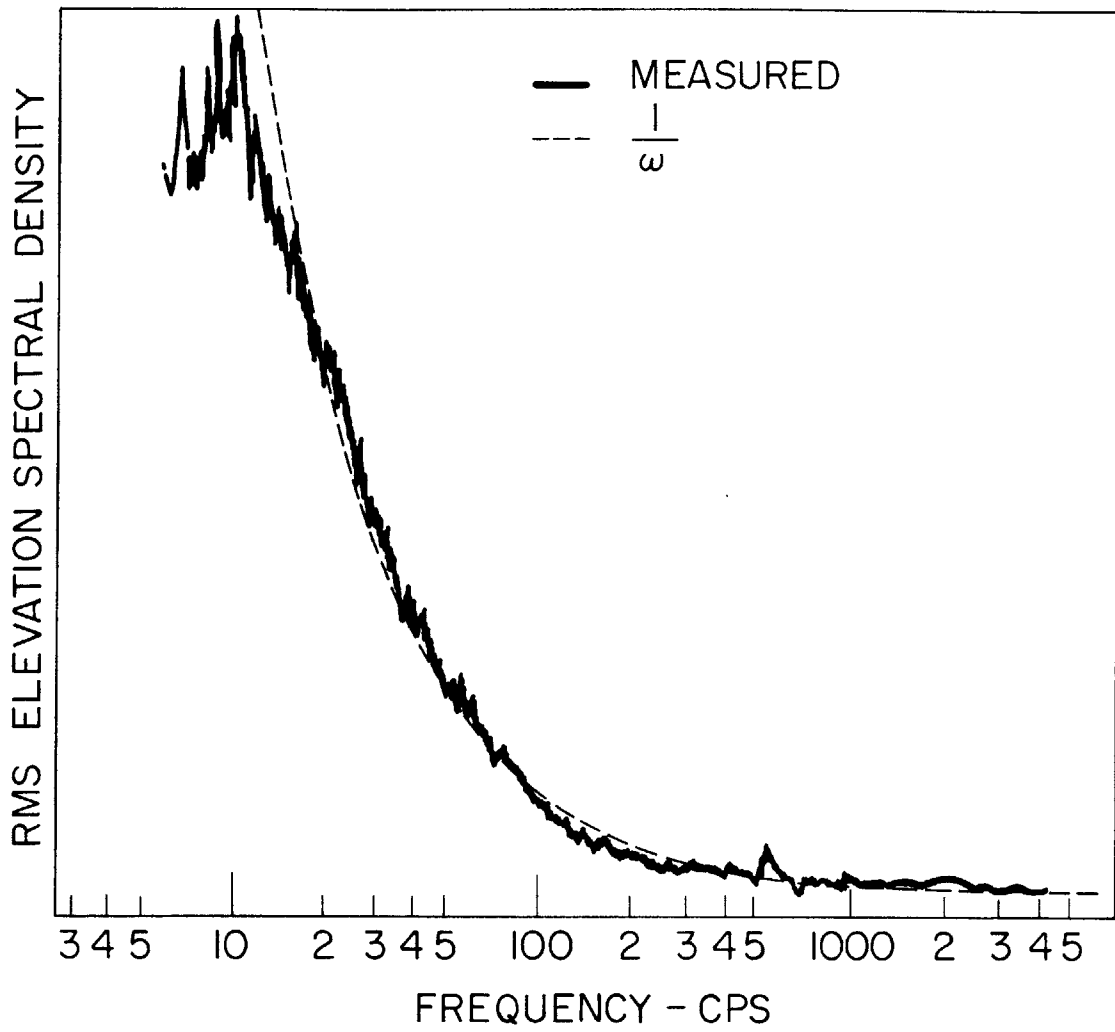
Figure   21.   Simulated Roadway RMS Elevation Spectral Density
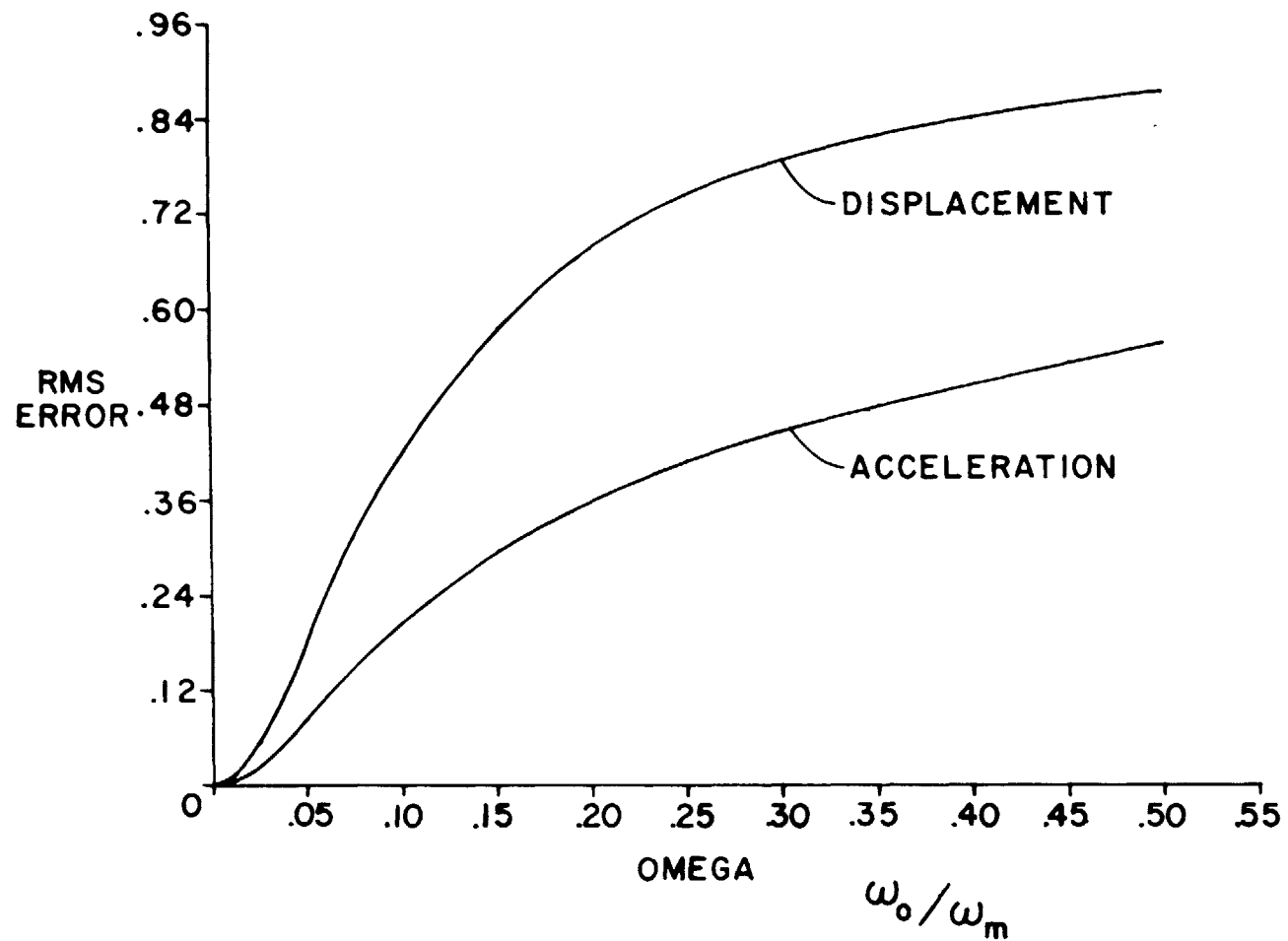
Figure 22. Error Due to Simulated Spectrum Low Frequency Level - Off
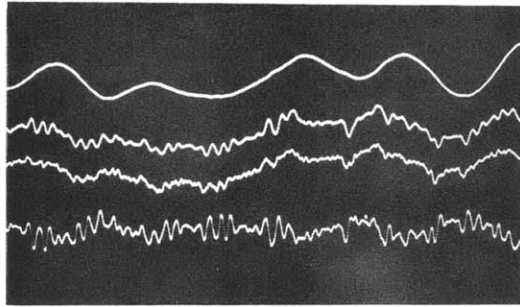
a) Conventional Passive Suspension

$$\frac{\ddot{y}_{rms}}{4\pi^2 \sqrt{AVf_u^3}} = 0.056 \;\; ; \;\; \frac{h}{2\alpha}\sqrt{\frac{f_u}{AV}} = 9.0$$
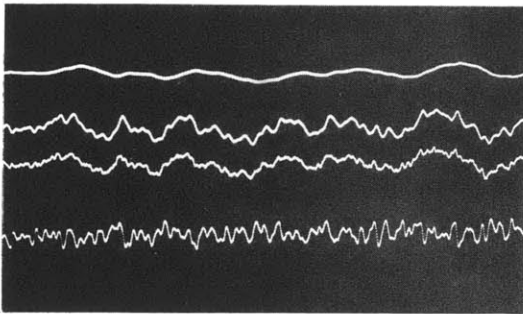
b) Automatic Height Control

$$\frac{\ddot{y}_{rms}}{4\pi^2 \sqrt{AVf_u^3}} = 0.056 \;\; ; \;\; \frac{h}{2\alpha}\sqrt{\frac{f_u}{AV}} = 2.28$$
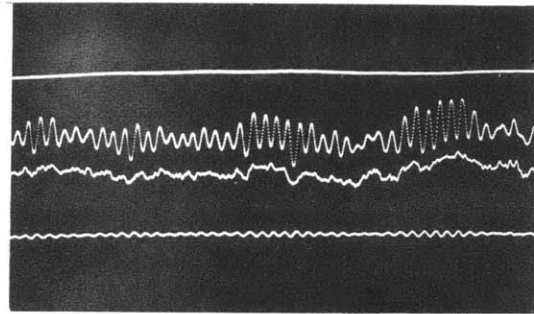
d) Automatic Height Control

$$\frac{\ddot{y}_{rms}}{4\pi^2 \sqrt{AVf_u^3}} = 0.017 \;\; ; \;\; \frac{h}{2\alpha}\sqrt{\frac{f_u}{AV}} = 9.0$$
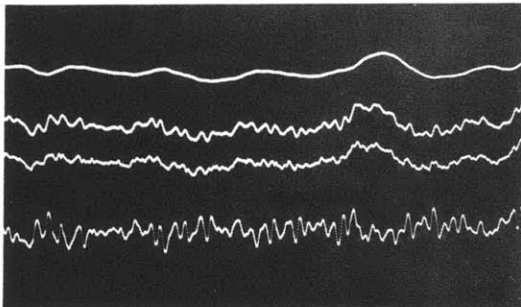
c) Optimum Synthesized Suspension

$$\frac{\ddot{y}_{rms}}{4\pi^2 \sqrt{AVf^3}} = 0.056 \;\; ; \;\; \frac{h}{2\alpha}\sqrt{\frac{f_u}{AV}} = 2.24$$
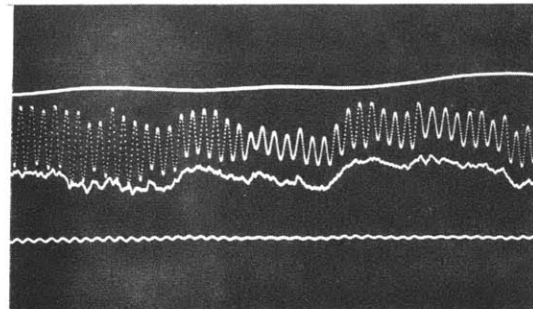
e) Optimum Synthesized Suspension

$$\frac{\ddot{y}_{rms}}{4\pi^2 \sqrt{AVf_u^3}} = 0.007 \;\; ; \;\; \frac{h}{2\alpha}\sqrt{\frac{f_u}{AV}} = 9.0$$

Figure 23.   Time Traces of Input and Response Variables Corresponding to Systems a – e in Figure 6. In descending order in each oscilloscope photograph are sprung mass, unsprung mass, and roadway vertical positions as well as sprung mass acceleration.

mass acceleration $(\ddot{y})$.

The top picture (Figure 23a), representing a conventional passive suspension, shows that the sprung mass does not follow the low frequency region of the unsprung mass very well. Figures 23 b and c, corresponding to active systems, illustrate increasing improvement in relative displacement requirements while maintaining similar sprung mass acceleration levels. The other two sets of traces (Figures d and e) show that in attempting to reduce vehicle accelerations, suspension forces become too small to adequately damp unsprung mass oscillations.

SECTION 7

RESULTS, CONCLUSIONS, AND SUGGESTIONS FOR FURTHER STUDY

7.1 Results and Conclusions

The intent of this thesis has been to examine some of the fundamental vibration control capabilities of vehicle suspensions. In order to formulate an optimization procedure, system disturbances, vehicle dynamics, and performance criteria were established in an analytically tractable but in a physically meaningful form. Two approaches to the minimization of the trade-off between vehicle vibration and the sprung mass-unsprung mass clearance space were investigated. First, using Wiener filter techniques, an optimum suspension configuration was synthesized. Secondly, the analytical optimization of some fixed configuration suspensions was treated. The results of these optimization procedures consist mainly of a chart (Figure 6) to be used as a starting point in the design of vehicle suspension systems. This chart shows the optimum trade-off between vibration and clearance space for passive suspensions subject to several values of loading variation. The passive suspension parameters are given in Figure 6 and the parameters for a synthesized system using easily measurable feedback variables are given in Figure 9.

Since the above optimization was carried out without regard to the interaction between the wheels and roadway, a graph (Figure 10) was developed as a constraint to the vibration-clearance trade-off chart. This graph shows that vehicles with very stiff or very flexible suspensions are likely to be unacceptable because of excessive wheel hop. The

minimum rms force required to hold the wheels of a moving vehicle on the roadway was also established to provide an estimate of upper speed limitations. It was found (see Figure 11) that vibration increases nearly linearly with AVf_u^3/g^2*

An active suspension system for a vehicle represents one of the few types of controls in which the input may easily be known before reaching the plant (i.e., the vehicle). The potential capabilities of a system using this preview information were found both for a suspension using optimum Wiener filtering and for a suspension that may be mechanized in a straightforward manner. The principal results of this section are that preview control may be used to reduce vibration by as much as a factor of sixteen over that for a non-preview suspension and that a simple preview system may be made to perform nearly as well as a synthesized system.

Finally, in order to illustrate the use of design charts established in the first few sections of the thesis, a numerical example was carried out. For the case considered, synthesized and height control systems showed substantial reductions over a spring-shock absorber suspension in clearance required for a given vibration level. However, the road holding constraint imposed on the unsprung mass prevented a significant reduction in vibration at constant clearance space.

---

* A is a roadway roughness parameter; V is the vehicle velocity; f_u is the unsprung mass natural frequency in Hz and g is the gravitational constant.

7.2 Further Study

This thesis represents part of the first of a logical sequence of steps that probably ought to be taken in designing mechanical suspension systems with optimum performance characteristics. The first step in suspension system design, namely research, is a fertile and broad region which requires further work ranging from theoretical system analysis to the investigation of components and materials with superior characteristics to those presently in use. Development (design, prototype construction, and testing stages), or the practical implementation of the results of research, may proceed along a great variety of paths. Below are discussed some fruitful areas for suspension research and development related to this thesis.

The same type of analysis and synthesis that was carried out in this thesis may be performed on more complicated models than have been used here. Models that include sprung mass damping, roll, and pitch modes would be appropriate. Although the optimum suspension synthesis procedure would become exceedingly difficult for high order systems with constraints (Additional constraints imply trade-offs among more variables.), digital computer parameter search techniques could probably be devised which would more readily handle complicated systems with several constraints.

Two constraints that might be imposed on a fixed configuration parameter search program are that the relative excursion of a wheel with respect to the roadway and that the response of an automatic height control system to a change in vehicle loading should be acceptable. The wheel-roadway rms excursion $\delta_{w,rms}$ would be determined from Equations

(2), (5) and a transfer function $\delta_{w,rms}(s)/X(s)$ in terms of suspension parameters. In order to insure that the response of an automatic height control system is sufficiently rapid, a measure of recovery from a step in loading such as $\int_0^\infty \delta^2(t)\, dt$ might be used. Thus only combinations of parameters which satisfy these constraints would be acceptable. Since a minimum in parameter space might be separated by unacceptable regions from the starting point of a search, a computer routine which examines a great range of points [54] might be more appropriate than the hill climbing type of program shown in Appendix C.

Non-linear aspects of suspension system design provide an area for considerable research. Certainly the stiffness of a spring in a passive suspension should increase near excursion limits to provide adequate shock isolation. Perhaps the damping coefficient should also increase in these regions. The optimization of such non-linear component characteristics for vehicle suspensions remains to be done [55]. Modulation of parameters may be carried out at high frequencies [56] or by low frequency adaptive systems [57] to provide vibration control. Dynamic programming [58] may be used to determine optimum trajectories over rough surfaces, hence optimum non-linear vibration-clearance trade-off curves. This approach might be applied most practically to terrain following aircraft or to hydrofoil ships in heavy seas.

Although a considerable amount of data has been accumulated on the statistics of roadway elevation along the direction of vehicle travel, measurements of cross-level and elasticity of certain roadways are needed. Cross-level (the angular elevation variations about a roadway center

line) spectra are required to predict vehicle roll vibration. Unpaved surfaces and railroad track are likely to be less rigid than the wheels of off-the-road vehicles and of railroad trains. Consequently, stiffness variations, particularly in jointed track, which contribute to vehicle vibration ought to be determined.

There seems to be a reasonable analytic basis from which to develop an active suspension for a specific vehicle-roadway system. In addition to providing vibration isolation, such a design could control roll and pitch, as well as deflections due to loading variations. Many elements (e.g., actuators, accelerometers, and power supplied) would be common to each of these functions. The features of a high speed of response hydraulic servomechanism might be compared with those of a lower frequency pneumatic suspension. Even the use of electromagnetic actuators may be feasible under certain conditions [59].

In conclusion, it may be seen that this thesis provides part of the framework from which to develop suspension systems with greater capabilities than those currently in use. There are areas of suspension system research which require further study. Nevertheless, the results of enough research are probably available so that active suspension systems may be designed to enhance the performance of a wide variety of vehicles. The methods discussed here are applicable to the design of a great variety of vehicles such as low speed off-the-road vehicles, high speed guided vehicles, terrain following aircraft, and hydrofoil ships.

REFERENCES

1. Batchelor, G. H., "Determination of Vehicle Riding Properties," Railway Gazette Vol. 117, 1962, Part I, July 20, pp. 69-72; Part II, July 26, pp. 97-100; Part III, August 3, pp. 129-131; Part IV, August 10, pp. 158-160, 164.

2. Bogdanoff, J. L. and F. Kozin, "On the Statistical Analysis of the Motion of Some Simple Vehicles Moving on a Random Track," Land Locomotion Laboratory Report RR20, LL65, November, 1959.

3. Kitaoka, H., "Track Irregularities", Japanese Railway Engineering, Vol. 7, No. 3, September, 1966, pp. 11-13.

4. Matsudaira, T., "How High Can Train Speed Be Increased?" Japanese Railway Engineering, Vol. 7, No. 2, June, 1966, pp. 4-7.

5. Carstens, J. P. and D. Kresge, M.D., "Literature Survey of Passenger Comfort Limitations of High Speed Ground Transports," United Aircraft Corporation Research Lab. Report D-910353-1, July 26, 1965.

6. Goldman, D. E. and H. E. Von Gierke, "The Effects of Shock and Vibration on Man," Naval Medical Research Institute, Lecture and Review Series No. 60-3, January, 1960.

7. Langer, B. F. and Shamberger, J. P., "Lateral Oscillations of Rail Vehicles," ASME Trans., Vol. 57, 1935, pp. 471-493.

8. Bergman, W., "Basic Nature of Vehicle Understeer-Oversteer," SAE Paper 957B, January, 1965.

9. Cain, B. S., "Safe Operation of High-Speed Locomotives," ASME Trans. Vol. 57, 1935, pp. 471-480.

10. Cain, B. S., "Vibration of Rail and Road Vehicles," Pitman Publishing Corp., New York, 1940.

11. de Pater, A. D., "The Approximate Determination of the Hunting Movement of a Railway Vehicle by Aid of the Method of Krylov and Bagolgubov," Applied Science Research, Section A, Vol. 10, 1961, pp. 205-228.

12. Koffman, J. L., "Vibrational Aspect of Bogie Design," The Institution of Locomotive Engineers, Journal, Volume 47, Part No. 6, 1957, Paper No. 580, pp. 549-634.

13. Shatz, R. H. and T. R. Wheaton, "The United Aircraft Turbine Motor Train and its Suspension," SAE Paper 660333, April, 1966.

14. Li, Y. T., "Stability and Controlability of Vehicles for High Speed and High Traffic Permeability," SAE Paper 660024, January, 1966.

15. Hanna, C. R. and W. O. Osbon, "Vehicle Ride Stabilization by Inertia Control," Proc. of the National Conference on Industrial Hydraulics, Vol. XV, October 19-20, 1961, Sherman Hotel, Chicago, Illinois.

16. Osbon, W. O., L. R. Allen, Jr., and A. R. Wilhelm, "Active Suspension Systems for Automotive Military Vehicles," Scientific Paper 65-1D1-HYDRA-P1, Westinghouse Research Laboratories, Pittsburgh, 1965.

17. Hansen, K. H., J. F. Bertsch, and R. E. Denzer, "1958 Chevrolet Level Air Suspension," SAE Trans. Vol. 66, 1958.

18. Dilman and Love, "Chrysler Torsion-Aire Suspension," SAE Preprint No. 79, March, 1957.

19. Bender, E. K., "Optimum Linear Control of Random Vibrations," to be published in the 1967 JACC Proceedings.

20. Larin, V. B., "Analytical Design of a Vibration Isolation System for Equipment Mounted on Moving Objects," Prik Ladnaza Mekhania, AN USSR, Vol. 3, 1966 (in Russian).

21. Kriebel, H. W., "A Study of the Practicality of Active Shock Isolation" Ph.D. Thesis, Stanford University, May, 1966.

22. Liber, T., and E. Sevin, "Optimal Shock Isolation Synthesis," Presented at 35th Symposium of Shock and Vibration, October 25-28, 1965, New Orleans, Louisiana.

23. Bohne, Q. R., "Power Spectral Densities in Ground Wind Drag Analyses," ARS Journal, Vol. 32, No. 2, February, 1962, p. 227-33.

24. Lay, W. E. and Lett, P. W., "Wind Effects on Car Stability," SAE Transactions, Vol. 61, 1953, p. 608-622.

25. Hara, T., "High Speed Rolling Stock Aerodynamical Problems," Quarterly Report, Railway Technical Research Institute, Japanese National Railways, October, 1963.

26. Moreno, E. F., and E. A. Domes, "A Unique Concept in Off-Highway Trucks," SAE Paper S420, April, 1965.

27. Thompson, W. E., "Measurements and Power Spectra of Runway Roughness at Airports in Countries of the North Atlantic Treaty Organization," NACA TN 4304, July, 1958.

28. Craggs, A., "The Assessment of Pave Test Track Loads Using Random Vibration Analysis," found in "Advances in Automobile Engineering," Vol. 7, Part 3, ed. by G. H. Tidbury, Pergamon Press, London, 1965.

29. Gilchrist, A. O., "A Report on Some Power-Spectral Measurements of Vertical Rail Irregularities," British Railway Research Department, Derby, England, August, 1965.

30. Walls, J. H., Houbolt, J. C. and Press, H., "Some Measurement and Power Spectra of Runway Roughness," NACA TN 3305, November, 1954.

31. Bender, E. K., D. C. Karnopp, and I. Paul, "On the Optimization of Vehicle Suspensions Using Random Process Theory," to be published in the Proceedings of the 1967 Transportation Engineering Conference.

32. Chang, S. S., "Synthesis of Optimum Control Systems," McGraw-Hill, New York, 1961.

33. Houbolt, J. C., Walls, J. H. and Smiley, R. F., "On Spectral Analysis of Runway Roughness and Loads Developed During Taxiing," NACA TN 3483, July, 1955.

34. Jacklin, H. and G. J. Liddell, "Riding Comfort Analysis," Purdue University Engineering Exp. Station Bulletin No. 44, Lafayette, Indiana, 1933.

35. Zeller, W., "Masseinheiten Fur Schwingungsstarke und Schwing Empfindungsstarke," ATZ Jahrg. 51, Nr. 4, 1949.

36. Parks, D. L. and F. W. Snyder, "Human Reactions to Low Frequency Vibration," Technical Report D3-3512-1, The Boeing Co., Wichita, Kansas, AD 261 330, July, 1961.

37. Janeway, R. N., "Passenger Vibration Limits," SAE Journal, August, 1948.

38. Meister, F. J., "Die Empfindlich des Menschen gegen Erschutterungen," Forschung auf dem Gebiete des Ingenieurwesens, Vol. 7, No. 3, May/June, 1953.

39. Postlethwait, F., "Human Susceptibility to Vibration," Engineering, Vol. 157, January 28, 1944.

40. Beranek, L. L., "Acoustics," McGraw-Hill, New York, 1954.

41. Pradko, F., R. A. Lee, and V. Kaluza, "Theory of Human Vibration Response," ASME Paper No. 66-WA/BHF-15, November, 1966.

42. Pradko, F., and R. A. Lee, "Vibration Comfort Criteria," SAE Paper No. 660139, January, 1966.

43. Pradko, F., T. R. Orr, and R. A. Lee, "Human Vibration Analysis," SAE Paper No. 650426, May, 1965.

44. Crandall, S. H., and Mark, W. D., "Random Vibration in Mechanical Systems," Academic Press, New York, 1963.

45. Himelblau, H., and L. M. Keer, "Space Requirements for Simple Mechanical Systems Excited by Random Vibration," J. Acoustical Soc. Am. Vol. 32, No. 1, January, 1960, pp. 76-80.

46. Skoog, J. A. and G. G. Setterlund, "Space Requirements for Equipment Items Subject to Random Excitation," J. Acoustical Soc. Am., Vol. 31, No. 2, February, 1959, pp. 227-32.

47. Rapin, P., "Une Application a l'automobile de la Technique des Vibrations," Rev. Francaise de Mechanique, n. 7-8, 1963, pp. 27-34.

48. Clark, D. C., "A Preliminary Analysis of the Kinetic Behavior of Roads," CAL Report No. YM-1304-V-2, June 7, 1960.

49. Code, C. J., "Wheel Loads and Rail Failures," Railway Age, February 15, 1965.

50. Wiener, N., "Extrapolation, Interpolation, and Smoothing of Stationary Time Series," Technology Press, Cambridge, 1949.

51. Newton, G. C., L. A. Gould and J. F. Kaiser, "Analytical Design of Linear Feedback Controls," John Wiley & Sons, New York, 1961.

52. Den Hartog, J. P., "Advanced Strength of Materials," McGraw-Hill, New York, 1952.

53. Edwards, L. K., "High Speed Tube Transportation," Scientific American, Vol. 213, No. 2, August, 1965, pp. 30-40.

54. Karnopp, D. C., "Random Search Techniques for Optimization Problems," Automatica, Vol. 1, 1963, pp. 111-121.

55. Van Trees, H. L., "Synthesis of Optimum Nonlinear Control Systems," M.I.T. Press, Cambridge, Mass., 1962.

56. Oleson, S. K., and J. J. Eige, "Development of Automatically Hardening Shock Mounts," Stanford Research Institute, Menlo Park, California, September, 1963.

57. Draper, C. S., and Y. T. Li, "Principles of Optimalizing Control Systems," ASME publication, September, 1961.

58. Bellman, R., "Dynamic Programming," Princeton University Press, Princeton, 1957.

59. Mela, R. L., "Electromagnetic Suspension of Vehicles," Dynatech Report No. 460, June, 1964.

Appendix A

DERIVATION OF OPTIMUM SYNTHESIZED SUSPENSION TRANSFER FUNCTION W(s)

Some observations about $\Delta(\phi)$ may be made in order to facilitate its factorization into two parts that have all of their respective zeroes and poles on opposite sides of the imaginary axis. The roots of the numerator of $\Delta(\phi)$ are conjugate because each coefficient is real and are symmetrical about the imaginary axis since, in addition to being conjugate, only even powers of ϕ are present. Thus all eight complex numerator roots may be expressed in terms of only four parameters b_1, c_1, b_2, c_2 as shown in Figure A-1. Since the poles of $\Delta(\phi)$ lie directly on the imaginary axis, it is not clear how to factor them. We could shift the poles of $H_1(s)$ off the imaginary axis into the left hand side (the stable half) of the imaginary plane by a small amount, ε. Similarly

since $\phi(s) = -\dfrac{AV}{s^2}$ we could write $\phi(s) = \dfrac{AV}{(s+\varepsilon)(-s+\varepsilon)}$. Then half of the poles would lie in the left half plane and the other half would be found in the right half plane. Our final answer would be the limit as $\varepsilon \to 0$. As long as we remember that poles with no real parts are even in number and would be divided equally in a spectral factorization we may avoid the added detail of using ε and write

$$\Delta^-(\phi) = \frac{2\pi AV\sqrt{\beta}}{\omega_u^4} \; \frac{(\phi - b_1 - c_1 j)(\phi - b_1 + c_1 j)(\phi - b_2 - c_2 j)(\phi - b_2 + c_2 j)}{\phi^3(\phi^2 + 1)} \qquad (A.1)$$

$$\Delta^+(\phi) = \frac{\sqrt{\beta}}{\omega_u^2} \; \frac{(\phi + b_1 - c_1 j)(\phi + b_1 + c_1 j)(\phi + b_2 - c_2 j)(\phi + b_2 + c_2 j)}{\phi^3(\phi^2 + 1)} \qquad (A.2)$$

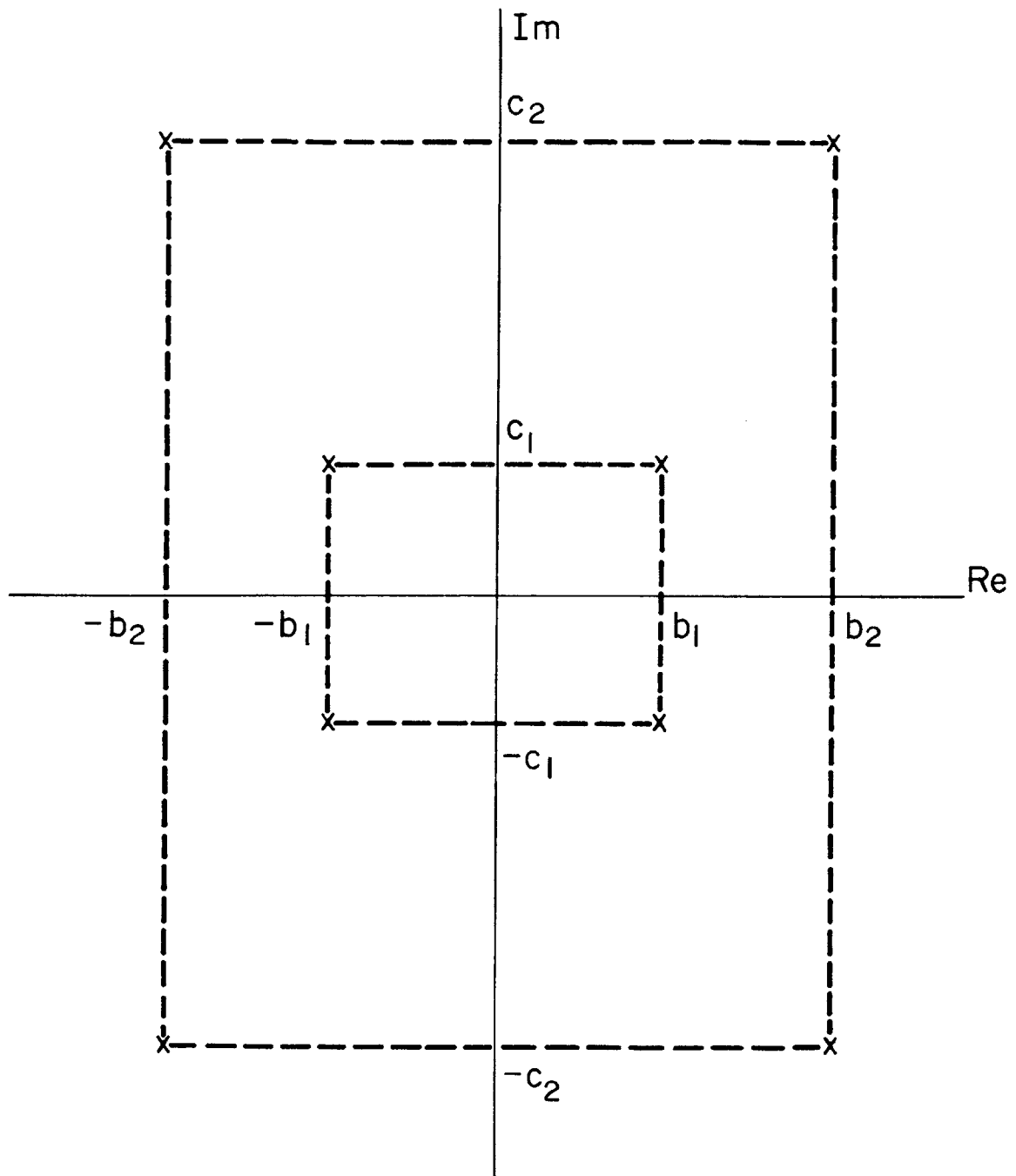Figure A-1.   Roots of an Optimum Synthesized Transfer Function W(s)

From the above and from Equations (2), (8), (9), and (11)

$$\frac{\Gamma(\phi)}{\Delta^-(\phi)} = \frac{(1+1/r)\phi^2 + 1}{\sqrt{\beta}\ \phi(\phi^2+1)(\phi-b_1-c_1j)(\phi-b_1+c_1j)(\phi-b_2-c_2j)(\phi-b_2+c_2j)} \tag{A.3}$$

A partial expansion of Equation (A.3) retaining only poles in the left half plane is

$$\frac{\Gamma(\phi)}{\Delta^-(\phi)} = \frac{A}{\phi} + \frac{B\phi + C}{\phi^2 + 1} \tag{A.4}$$

A, B, and C are evaluated from the above two equations

$$A = 1$$

$$B = \frac{p_1}{\sqrt{\beta}\ r(p_1^2 + p_2^2)}$$

$$C = \frac{p_2}{\sqrt{\beta}\ r(p_1^2 + p_2^2)} \tag{A.5}$$

where

$$p_1 = 1 - b_1^2 - c_1^2 - b_2^2 - c_2^2 - 4b_1b_2 + 1/\sqrt{\beta}$$

$$p_2 = 2[b_1 + b_2 - (b_1^2 + c_1^2)b_2 - (b_2^2 + c_2^2)b_1]$$

Finally, W(s) is Equation (A.4) divided by Equation (A.2)

$$W(s) = \frac{s^2[(B+1)\phi^2 + C\phi + 1]}{\sqrt{\beta}\ \phi^4 + 2\sqrt{\beta}\ D\phi^3 + \sqrt{\beta}\ E\phi^2 + 2\sqrt{\beta}\ I\phi + 1} \tag{A.6}$$

where

$$D = b_1 + b_2$$

$$E = b_1^2 + c_1^2 + b_2^2 + c_2^2 + 4b_1b_2$$

$$I = (b_1^2 + c_1^2)b_2 + (b_2^2 + c_2^2)b_1$$

The parameters b_1, c_1, b_2, c_2 are evaluated numerically by a digital computer program for a specified mass ratio value and weighting factor β. Figure A.2 shows the parameters b_1, c_1, b_2, c_2 and β plotted as a function of the non-dimensional acceleration $\ddot{y}/(4\pi^2\sqrt{AVf_u^3})$ which was computed from Equation (17) using these parameters for a value of $r = 0.1$. The graph is presented in this form for use in conjunction with the design chart, Figure 6.
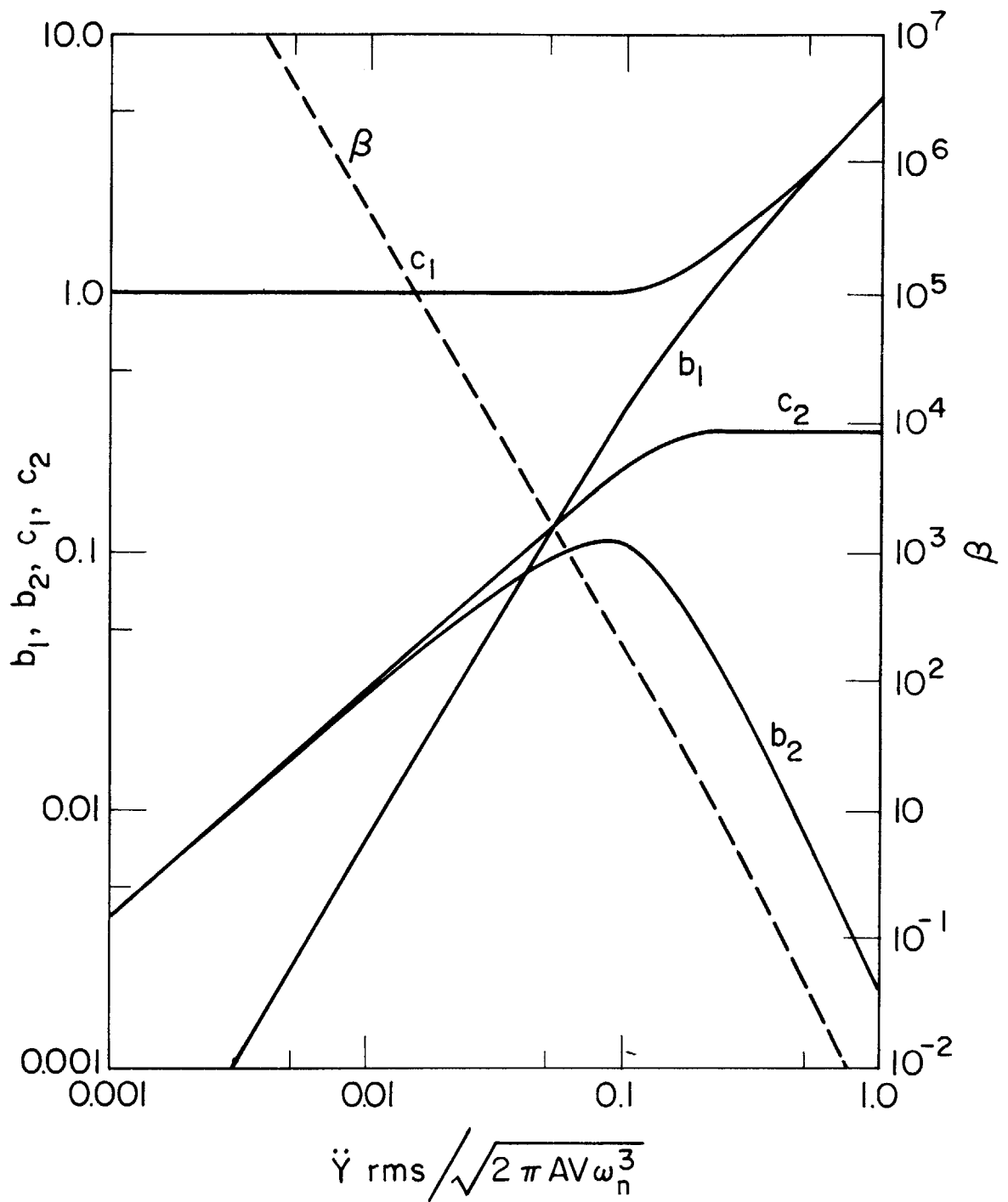
Figure A-2. Optimum Synthesized Suspension Parameters

APPENDIX B

DERIVATION OF EXPRESSION FOR CLEARANCE SPACE

FOR OPTIMUM SYNTHESIZED SUSPENSION

From Equation (7) for $\frac{\delta}{X}$ and Equation (14) for the optimum synthesized transfer function we have

$$\frac{\delta}{X}(\phi) = \frac{\phi}{\phi^2+1} \left\{ \frac{[\sqrt{\beta} - (B+1)(1+1/r)]\phi^3 + [2\sqrt{\beta} - c(1+1/r)]\phi^2 + [\sqrt{\beta} E - (B+2+1/r)]\phi + 2\sqrt{\beta} - I}{\sqrt{\beta} \, \phi^4 + 2\sqrt{\beta}D\phi^3 + \sqrt{\beta}E\phi^2 + 2\sqrt{\beta}I\phi + 1} \right\} \quad (B.1)$$

It looks as though δ_{rms} would be infinite due to the undamped roots in the denominator of the above equation. However, the solution for δ_{rms} evaluated from tables in Reference 51 is indeterminate (i.e. 0/0). Since δ_{rms} must be finite it looks as though the numerator of Equation (B.1) contains a $(\phi^2 + 1)$ factor. Let us consider the numerator in the brackets of the above equation factored into the following format

$$(\phi^2+1)(x\phi+y) = x\phi^3+y\phi^2+x\phi+y \quad (B.2)$$

If coefficients x and y in the right-hand side of the above equation may be made equal to the corresponding coefficients in Equation (B.1), then that equation does indeed contain $\phi^2 + 1$ in the numerator, and it may be cancelled with the same term in the denominator. In order to equate appropriate coefficients, it is necessary that the coefficients of ϕ^3 and ϕ as well as ϕ^2 and ϕ^0 be equal in Equation (B.1). Unfortunately, there does not seem to be any general way of showing whether or not this is true. Since it was found numerically for r = 0.1 that the coefficients of ϕ^3 and ϕ are equal, as are those for ϕ^2 and ϕ^0 and because of the above physical reasoning, let us assume $(\phi^2 + 1)$ can be factored

out of the numerator of Equation (B.1). Thus when rms excursion is evaluated from the simplified expression for $\frac{\delta}{x}(\phi)$ the expression for δ_{rms} is

$$\delta_{rms}\sqrt{\frac{f_u}{AV}} = \left\{ \frac{[\sqrt{\beta} - (B+1)(1+1/r)]^2 \ 2D + [2\sqrt{\beta}D - C(1+1/r)]^2 \ 2\sqrt{\beta} \ (DE-I)}{8(\beta DEI - \sqrt{\beta} \ D^2 - \beta I^2)} \right\}^{1/2}$$

(B.3)

APPENDIX C

MINIMIZATION PROGRAM

```
C  THIS PROGRAM, WRITTEN IN FORTRAN 4, IS USED TO MINIMIZE A FUNCTION OF
C  I VARIABLES B(I) USING A HILL CLIMBING TECHNIQUE. THE PROGRAM EVALUATES
C  A FUNCTION F IN THE MIDDLE OF A BOUNDED SECTION OF PARAMETER SPACE
C  THEN INCREMENTS EACH PARAMETER PLUS AND MINUS 10 PERCENT OF ITS MAXIMUM
C  RANGE, EVALUATING THE FUNCTION AT EACH STEP. WHENEVER A VALUE OF THE
C  FUNCTION IS FOUND THAT IS LESS THAN THE STARTING VALUE, FO, THE PROGRAM
C  CONTINUES FROM THE NEW POINT. WHEN A POINT IN PARAMETER SPACE IS
C  REACHED SUCH THAT THE FUNCTION VALUE CORRESPONDING TO THAT POINT IS
C  LESS THAN THE VALUES OF THE FUNCTION CORRESPONDING TO THE POINTS
C  DETERMINED BY PLUS AND MINUS INCREMENTS OF EACH PARAMETER THE INCREMENT
C  OR JUMP SIZE IS REDUCED BY A FACTOR OF TEN AND THE SEARCH PROCESS IS
C  CONTINUED. THE PROGRAM GIVEN HERE IS FOR THREE PARAMETERS AND EIGHT
C  ITERATIONS. HOWEVER, IT MAY BE EASILY CHANGED FOR OTHER NUMBERS OF
C  PARAMETERS AND ITERATIONS. THE BOUNDS ON THE PARAMETER SPACE ARE
C  GIVEN BY A(J) = BMAX(J), C(J) = BMIN(J). THE SUBROUTINE SHOOT IS FOR
C  THE FIXED CONFIGURATION PREVIEW CONTROL OPTIMIZATION.

           DIMENSION D(3),B(3),C(3),BO(3),DLB(3),A(3)
           COMMON DELRMS,ACCEL,RHO,T
           READ(5,2) A(1),A(2),A(3),C(1),C(2),C(3)
     2     FORMAT(7F10.5)
     3     READ(5,5)T,RHO
     5     FORMAT(2F15.8)
           WRITE(6,200)
   200     FORMAT(104H1        T            RHO          A1    NATL FRQ (W) DA
          1MP RATIO (Z)  DELTA RMS   ACCEL RMS        FO    /)
C          SET UP INITIAL VALUES OF B(I), JUMP SIZE DLB(J), AND PARAMETER
C          D(J) WHICH IS USED TO INDICATE WHEN ALL VARIABLES ARE WITHIN ONE
C          JUMP OF THE OPTIMUM
           DO 6 J=1,3
           DLB(J) = 0.1*(A(J)-C(J))
           B(J) =0.5*(A(J)+C(J))
     6     CONTINUE
           CALL SHOOT(F,B)
           FO = F
C          INITIAL VALUES ARE SET UP. NOW GO THROUGH 8 ITERATIONS TO FIND
C          OPTIMUM B(I),F
     7     DO 95 L = 1,8
     8     DO 70 I = 1,3
           D(I) = 0.0
           BO(I) = B(I)
    10     B(I) = BO(I) + DLB(I)
C          KEEP B(I) WITHIN SPECIFIED RANGE
           IF(B(I)-A(I))15,12,12
    12     B(I) = A(I)
    15     CALL SHOOT(F,B)
```

```
        IF(F-FO)50,20,20
   20   B(I) = BO(I)-DLB(I)
C       KEEP B(I) WITHIN SPECIFIED RANGE
   21   IF(B(I)-C(I))22,22,25
   22   B(I) = C(I)
   25   CALL SHOOT(F,B)
        IF(F-FO)50,40,40
   40   B(I) = BO(I)
C       IF PROGRAM REACHES HERE THEN B(I) IS A LOCAL MINIMUM. IF THIS
C       HAPPENS FOR ALL B(I) THEN B(I) IS WITHIN ONE JUMP OF THE OPTIMUM
C       LET D(I)=1, RETAIN OLD VALUE OF FO (SKIP OVER FO=F)
        D(I) = 1.
        GO TO 70
   50   CONTINUE
C       WE HAVE A NEW VALUE OF B(I) AND F. NOW SEARCH IN ANOTHER DIRECTION
C       FROM THIS NEW POINT IN PARAMETER (B) SPACE
        FO = F
   70   CONTINUE
        SUMD = D(1) + D(2) + D(3)
C       WRITE PARAMETERS, ETC AFTER ALL PARAMETERS HAVE BEEN EXAMINED ONE
C       JUMP IN EACH DIRECTION
        WRITE(6,100)T,RHO,B(1),B(2),B(3),DELRMS,ACCEL,FO
  100   FORMAT(8F13.7)
C       IF ALL B(I) ARE WITHIN ONE JUMP OF OPTIMUM THEN REDUCE JUMP SIZE
        IF(SUMD-2.5)8,80,80
   80   DO 90 K=1,3
   90   DLB(K) = 0.1*DLB(K)
   95   CONTINUE
        GO TO 3
        END




        SUBROUTINE SHOOT(F,B)
C       ACCEL = RMS ACCELERATION/SQRT(2*PI*AV)
C       DELRMS = DELTA RMS/SQRT(2*PI*AV)
C       B(1)=ASUB1, B(2)=W(NATL FREQ), B(3)=Z(DAMPING RATIO)
        DIMENSION B(3)
        COMMON DELRMS,ACCEL,RHO,T
        S = SQRT(1. - B(3)**2)
        ACCEL=SQRT((B(2)**3*(B(1)**2 + ((1.-B(1))**2) + 2.*B(1)*(1.-B(1))*
       1(EXP(-B(3)*B(2)*T))*
       2(COS(S*B(2)*T) - (B(3)/S)*SIN(S*B(2)*T))))/(4.*B(3)))
        DELRMS =SQRT(((1. - 2.*(B(1) - 2.*(B(3)**2)) - 2.*(B(1)**2)*(4.*(B
       1(3)**2)- 1.) + 2.*B(1)*(1. - B(1) + 4.*(B(3)**2)*(1. + B(1)))*(EX
       2P(-B(3)*B(2)*T))*COS(S*B(2)*T)+ 2.*B(1)*B(3)*(-1.+4.*(B(3)**2)*(1.
       3+ B(1)) - 3.*B(1))*(EXP(-B(3)*B(2)*T))*(SIN(S*B(2)*T))/S)/(4.*B(3)
       4*B(2))) - 2.*B(1)*B(3)/B(2) + (B(1)**2)*T)
        F = RHO*ACCEL + DELRMS
        RETURN
        END
```

```
/*
//G.SYSIN   DD    *

C      DATA

/*
```

APPENDIX D

Evaluation of $I = \dfrac{1}{2\pi j} \displaystyle\int_{-j\infty}^{j\infty} \dfrac{\phi^n\, e^{\phi\sqrt{2}\,x}}{(\phi^4+1)^2}\, d\phi$

When the denominator of above equation for I is factored, I may be written as

$$I = \frac{1}{2\pi j} \int_{-j\infty}^{j\infty} \frac{\phi^n\, e^{\phi\sqrt{2}\,x}}{(\phi+\frac{1+j}{\sqrt{2}})^2(\phi+\frac{1-j}{\sqrt{2}})^2(\phi-\frac{1+j}{\sqrt{2}})^2(\phi-\frac{1-j}{\sqrt{2}})^2}\, d\phi \qquad (D.1)$$

The integration indicated by Equation (D.1) is carried out by evaluating the residues of the four poles that lie in the contour taken around the left half plane. Thus

$$\text{Res}[(-1+j)/\sqrt{2}] = \frac{d}{d\phi}\left[\frac{\phi^n\, e^{\phi\sqrt{2}\,x}}{(\phi+\frac{1+j}{\sqrt{2}})(\phi^2-\sqrt{2}\,\phi+1)^2}\right]_{\phi = \frac{-1+j}{\sqrt{2}}} \qquad (D.2)$$

When Equation (D.2) is evaluated, we find

$$\text{Res}[(-1+j)/\sqrt{2}] = \frac{1}{16}\left(\frac{-1+j}{\sqrt{2}}\right)^{n-1} e^{(-1+j)x}\, [x-j(n-x-3)] \qquad (D.3)$$

Similarly

$$\text{Res}[(-1-j)/\sqrt{2}] = \frac{1}{16}\left(\frac{-1-j}{\sqrt{2}}\right)^{n-1} e^{(-1-j)x}\, [x+j(n-x-3)] \qquad (D.4)$$

Since $I = \text{Res}[(-1+j)/\sqrt{2}] + \text{Res}[(-1-j)/\sqrt{2}]$, Equations (D.3) and (D.4) may be combined to give a general expression for I as

$$I = \frac{1}{16} e^{-x} [A \cos x + B \sin x] \qquad\qquad (D.5)$$

where the coefficients A and B are given in the following table for values
of n from 0 through 8.

n	A	B
0	$3\sqrt{2}$	$-\sqrt{2}(3+2x)$
1	$2x$	$-2(2+x)$
2	$-\sqrt{2}(1-2x)$	$\sqrt{2}$
3	$2x$	$2x$
4	$\sqrt{2}$	$\sqrt{2}(1-2x)$
5	$-2x$	$-2(2-x)$
6	$-\sqrt{2}(3-2x)$	$3\sqrt{2}$
7	$2(4-x)$	$-2x$
8	$-5\sqrt{2}$	$-5\sqrt{2}$

APPENDIX E

ANALOGY BETWEEN DETERMINISTIC AND RANDOM PROCESSES

$$\xrightarrow{X(s)} \boxed{H(s)} \xrightarrow{Y(s)}$$

$$Y(s) = H(s)X(s)$$

Deterministic	Random
Parsevals theorem [51]:	The mean squared value of y may be given by

$$\int_{-\infty}^{\infty} y^2(t)dt = \frac{1}{2\pi j}\int_{-j\infty}^{j\infty} Y(s)Y(-s)ds \qquad \frac{\overline{y^2}}{2\pi} = \frac{1}{2\pi j}\int_{-j\infty}^{j\infty} H(s)H(-s)\Phi_{xx}(s)ds$$

For the above system

$$\int_{-\infty}^{\infty} y^2(t)dt = \frac{1}{2\pi j}\int_{-j\infty}^{j\infty} H(s)H(-s)X(s)X(-s)ds$$

For $X(s) = a/s$ 　　　　　　For $\Phi_{xx}(s) = -AV/s^2$

$$\frac{1}{a^2}\int_{-\infty}^{\infty} y^2(t)dt = \frac{1}{2\pi j}\int_{-j\infty}^{j\infty} \frac{H(s)}{s}\frac{H(-s)}{-s}ds \qquad \frac{\overline{y^2}}{2\pi AV} = \frac{1}{2\pi j}\int_{-j\infty}^{j\infty} \frac{H(s)}{s}\frac{H(-s)}{-s}ds$$

Therefore

$$\frac{1}{a^2}\int_{-\infty}^{\infty} y^2(t)dt = \frac{\overline{y^2}}{2\pi AV}$$

$$\text{Evaluation} \atop \text{of} \quad I = \lim_{\epsilon \to 0} \int_{-j\infty}^{j\infty} \frac{\phi^n e^{\phi x}}{(\phi+\epsilon)(\phi^2+2\zeta\phi+1)(-\phi+\epsilon)(\phi^2+2\zeta\phi+1)} \, d\phi$$

The above integral may be evaluated by summing the residues of the three poles that lie within a contour taken around the left half plane. Thus

$$I = \text{Res } (-\epsilon) + \text{Res } (-\zeta+j\sqrt{1-\zeta^2}) + \text{Res } (-\zeta-j\sqrt{1-\zeta^2}) \qquad \text{(F.1)}$$

The residue at $-\epsilon$ is given by

$$\text{Res } (-\epsilon) = \frac{(-\epsilon)^n e^{-\epsilon x}}{2\epsilon} \qquad \text{(F.2)}$$

In the expression for $\delta_{p,rms}$ (Equation (94)) the numerator of one of the terms is of the form $1 - e^{\phi x}$. For this case

$$\text{Res}(-\epsilon)_{1-e^{\phi x}} = \frac{1}{2} x \qquad \text{(F.3)}$$

The residues at the poles $\phi = -\zeta \pm j\sqrt{1-\zeta^2}$ are

$$\text{Res}(-\zeta+j\sqrt{1-\zeta^2}) = \frac{(-\zeta+j\sqrt{1-\zeta^2})^{n-2} e^{(-\zeta+j\sqrt{1-\zeta^2}\, x)}}{8\zeta[1-\zeta^2+j\zeta\sqrt{1-\zeta^2}\,]} \qquad \text{(F.4)}$$

$$\text{Res}(-\zeta-j\sqrt{1-\zeta^2}) = \frac{(-\zeta-j\sqrt{1-\zeta^2})^{n-2} e^{(-\zeta-j\sqrt{1-\zeta^2}\, x)}}{8\zeta[1-\zeta^2-j\zeta\sqrt{1-\zeta^2}\,]} \qquad \text{(F.5)}$$

Thus I may be given in the following general form where the coefficients A, B, and C are listed below for several values of n:

$$I = \frac{e^{-\zeta x}}{4\zeta(1-\zeta^2)} [A \cos \sqrt{1-\zeta^2} + B \sin \sqrt{1-\zeta^2} \, x] + C \qquad \text{(F.6)}$$

n	A	B	C
0	$(4\zeta^2-1)(1-\zeta^2)$	$-\zeta\sqrt{1-\zeta^2}(3-4\zeta^2)$	See Equation (F.3)
1	$-2\zeta(1-\zeta^2)$	$\sqrt{1-\zeta^2}(1-2\zeta^2)$	$-1/2$
2	$(1-\zeta^2)$	$\zeta\sqrt{1-\zeta^2}$	0
4	$-(1-\zeta^2)$	$\zeta\sqrt{1-\zeta^2}$	0

BIOGRAPHICAL NOTE

After attending public schools in New York, the author entered M.I.T. in 1958 to obtain an engineering education. Summers were spent working at Grumman Aircraft Engineering Corporation where technical functions included programming numerically controlled milling machines as well as analysis and simulation of hydraulic servomechanisms. In 1962 he received the S.B. degree and returned to M.I.T. as a research assistant at the M.I.T. Instrumentation Laboratory. Upon receiving the S.M. degree from M.I.T. in 1963 he remained at the Instrumentation Laboratory as a staff engineer working on subjects related to inertial guidance and navigation. Primary areas of responsibility included the analysis, design, assembly and testing of a digital controller and of a unique inertial guidance subsystem. Research into the cause of gyro drift resulting from thermal gradients was also performed.

In 1965 the author began his doctoral thesis. While pursuing this investigation, an interest in system reliability and accuracy (begun as a Bachelor's thesis in 1961) led to a study of system improvement brought about by multiplexing redundant system outputs. In addition, various industrial consulting jobs were taken during this period.

Professional societies include ASME and Sigma Xi.

The following are the author's publications:

1. "Sampled-Data Velocity Vector Control of a Spacecraft", ASME Paper 63-WA-314, November, 1963.

2. "Multiple Sensors Boost Signal Quality" with D. C. Karnopp, Control Engineering, Vol. 13, No. 7, July, 1966.

3. "Multiplexing of Continuous Signals to Improve Accuracy and Reliability", with D. C. Karnopp, to be published in Regelungstechnik.

4. "Frequency Effects in Analog Channels Multiplexed for Reliability", with D. C. Karnopp, Proceedings of the 1967 Joint Automatic Controls Conference.

5. "Optimum Linear Random Vibration Isolation", Proceedings of the 1967 Joint Automatic Controls Conference.

6. "On the Optimization of Vehicle Suspensions Using Random Process Theory", with D. C. Karnopp and I. Paul, Proceedings of the 1967 Transportation Engineering Conference.